The Pennsylvania State University

The Graduate School

College of Engineering

ATTITUDE DYNAMICS AND CONTROL OF A SPACECRAFT USING SHIFTING MASS DISTRIBUTION

A Dissertation in

Aerospace Engineering

by

Young Tae Ahn

Submitted in Partial Fulfillment
of the Requirements
for the Degree of

Doctor of Philosophy

December 2012

The thesis of Young Tae Ahn was reviewed and approved* by the following:

David B. Spencer
Professor of Aerospace Engineering
Thesis Advisor
Chair of Committee

Robert G. Melton
Professor of Aerospace Engineering

Sven G. Bilén
Associate Professor of Engineering Design, Electrical Engineering, and Aerospace Engineering

Christopher D. Rahn
Professor of Mechanical Engineering

George A. Lesieutre
Professor of Aerospace Engineering
Head of the Department of Aerospace Engineering

*Signatures are on file in the Graduate School

ABSTRACT

Spacecraft need specific attitude control methods that depend on the mission type or special tasks. The dynamics and the attitude control of a spacecraft with a shifting mass distribution within the system are examined. The behavior and use of conventional attitude control actuators are widely developed and performing at the present time. However, the advantage of a shifting mass distribution concept can complement spacecraft attitude control, save mass, and extend a satellite's life. This can be adopted in practice by moving mass from one tank to another, similar to what an airplane does to balance weight. Using this shifting mass distribution concept, in conjunction with other attitude control devices, can augment the three-axis attitude control process. Shifting mass involves changing the center-of-mass of the system, and/or changing the moments of inertia of the system, which then ultimately can change the attitude behavior of the system.

This dissertation consists of two parts. First, the equations of motion for the shifting mass concept (also known as morphing) are developed. They are tested for their effects on attitude control by showing how shifting the mass changes the spacecraft's attitude behavior. Second, a method for optimal mass redistribution is shown using a combinatorial optimization theory under constraints. It closes with a simple example demonstrating an optimal reconfiguration.

The procedure of optimal reconfiguration from one mass distribution to another to accomplish attitude control has been demonstrated for several simple examples. Mass shifting could work as an attitude controller for fine-tuning attitude behavior in small

satellites. Various constraints can be applied for different situations, such as no mass shift between two tanks connected by a failed pipe or total amount of shifted mass per pipe being set for the time optimum solution. Euler angle changes influenced by the mass reconfiguration are accomplished while stability conditions are satisfied. In order to increase the accuracy, generally, more than two control systems are installed in a satellite. Combination with another actuator will be examined to fulfill the full attitude control maneuver. Future work can also include more realistic spacecraft design and operational considerations on the behavior of this type of control system.

TABLE OF CONTENTS

LIST OF FIGURES

LIST OF TABLES

NOMENCLATURE

d	radius of the imaginary sphere of the satellite system
$\overline{d}$	displacement vector from the origin center-of-mass to the new center-of-mass
dm	a small mass element in a body
$f(x)$	objective function
h	altitude of a satellite
m_i	mass of fuel in each tank (kg)
n	mean motion of the orbital reference frame
$\overline{r}$	position vector of the mass element *dm* or the control mass
$\overline{r}_c$	position vector of the composite mass center of the mass center of body G
$\overline{r}_0$	position vector of the mass center of body G
$\overline{x}$	state vector
$\overline{u}$	control vector
$\overline{y}$	observation vector
ϕ	latitude of a satellite
λ	longitude of a satellite
$\overline{\omega}$	angular velocity vector of a satellite with respect to the inertial coordinate system
$\overline{\varpi}$	angular velocity vector of a satellite with respect to the body fixed coordinate system
Ψ	roll angle (rad)
θ	pitch angle (rad)
φ	yaw angle (rad)
$\overline{\rho}$	position vector of the mass element *dm* from the center-of-mass of body G
$A^{M/N}$	transformation matrix converting the coordinate system from N to M
A, *B*, *C, I*	moments of inertia (kg m^2)
B	subscript for body fixed frame (e.g., $X_BY_BZ_B$)
D	the distance between two parallel axes (used in parallel axis theorem)
DCM	Direction Cosine Matrix
E	subscript for Earth-centered fixed frame (e.g., $X_EY_EZ_E$)
G	gravitational constant
$\overline{H}$	angular momentum of a rotating body
I	subscript for the inertial frame (e.g., $X_IY_IZ_I$)
I_r	moment of inertia along roll-axis (kg m^2)
I_p	moment of inertia along pitch-axis (kg m^2)
I_y	moment of inertia along yaw-axis (kg m^2)
L, M, N	arbitrary coordinate systems
M	total mass of the satellite system (kg)
M_{mass}	total mass of the moving masses (kg)
M_{sat}	mass of the dry satellite (kg)
$\overline{M}_G$	gravity gradient moment
R	subscript for the orbital reference coordinate system (e.g., $X_RY_RZ_R$)

R_e	the radius of the Earth
$\overline{R}_G$	vector to the composite center-of-mass of the system in the inertial coordinate system
$\overline{R}_0$	vector to the center-of-mass of an object in the inertial coordinate system
$\overline{\Omega}_{X_R Y_R Z_R}$	angular velocity vector of a orbital reference coordinate system with respect to the inertial coordinate system

ACKNOWLEDGMENTS

I would like to acknowledge a lot of people who helped me with this dissertation. I would never have been able to finish this work without the support from all of them.

I would like to express my sincere gratitude to my advisor, Dr. David B. Spencer, for his continuing attention, guidance, and support throughout this dissertation. His patience and consistent care helped keep me challenged and allowed me to achieve this personal milestone. Having him as an advisor for my both master's and doctoral degree is the best luck I ever had. Gratefulness is also extended to all other committee members for their advice where this dissertation should proceed and careful review, namely, Dr. Robert G. Melton, Dr. Sven G. Bilén, and Dr. Chris Rahn.

My special thanks must be given to my parents to whom I owe everything that I am today. Their encouragement and unconditional love helped me to overcome every crisis I have faced in my life. My brothers-in-law, sisters, nephews, and nieces are also cheering me all the time with their best wishes. Finally, I would like to thank all of my colleagues and friends who helped me relax and kept me fresh.

Chapter 1

INTRODUCTION

A general spacecraft attitude control system is composed of three major functions: sensors, controllers, and dynamic processes. The sensor detects the satellite's attitude and controllers adjust the system. The vehicle's dynamic rotational motion completes the attitude control system. The purpose of attitude control of a spacecraft is to change its orientation with respect to the defined frame of reference or to maintain a desired orientation in the presence of disturbance torque. To achieve a desired direction, a spacecraft needs specific attitude control methods that are dependent on its mission or special tasks, for example, weather forecasting, communications, or military observation. Attitude control methods are divided into two classes: active control and passive control. Distinction between active and passive is that active methods require expenditure of energy and passive ones do not.

The main contribution of this dissertation is to develop new control designs for satellite attitude dynamics. The dynamics and attitude control of a spacecraft using a shifting mass distribution within the system is investigated. The main advantage of a shifting mass distribution concept is that it may allow for completing attitude control and saving fuel and extending a satellite's life as well. This can be adopted in practice by moving mass such as a liquid fuel from one tank to another, similar to what an airplane does to balance its weight. Using this shifting mass distribution concept, when used in

conjunction with another attitude control system, can achieve a better attitude control process.

The procedure of optimal reconfiguration from one mass distribution to another to accomplish attitude control consists of two parts. First, the equations of motion for the shifting mass concept (also known as morphing) are developed. They are tested for their effects on the attitude control by showing how shifting the mass changes the spacecraft's attitude behavior. After verifying that mass shifting could work as an attitude controller for fine-tuning attitude behavior in a small satellite, Euler angle changes influenced by the mass reconfiguration are developed while stability conditions are satisfied. Extending this result, the ground coverage (pointing characteristics) change from a mass redistribution, which is a final goal of this research, is examined. In the meantime, the controllability is examined to see if this new concept can be applied as a sole controller. Due to the limited amount that mass can be shifted, the angular control range is calculated to establish the relationship between shifting mass and pointing angle range. With this range result, a simulation is performed under various constraints considering the practical applications. Since all masses are assumed to move instantaneously for the maneuver in this dissertation, continuous mass transfer case could be taken into account for further research.

Once the exact system dynamics and mathematical formulation methods are developed, the second part of the research developed the advanced optimization algorithm using different boundary conditions and physical characteristics. A method for optimal mass redistribution is shown using a combinatorial optimization theory under constraints. The optimization technique illustrated here focuses on both minimizing the

total optimal mass travel and distribution among the tanks. Various optimal solutions are also represented with different constraints. For instance, all tanks are available for mass transfer or limited mass shifting case is examined using MATLAB's Optimization Solvers. Moreover, various constraints can be applied for different situations, such as no mass shift between two tanks connected by a blocked path or total amount of shifted mass per pipe being set for the time optimal solution by modifying the solving algorithm. Thus, the modified objective function should be developed to increase the trustworthiness and expertise of this research.

The primary goals of this study are to examine a new way of control method by mass redistribution inside the system without other control methods by

⇒ developing a concept controlling the moment of inertia of the satellite and establishing a generalized solution as a single controller;

⇒ combining with other types of actuators to fulfill the full attitude control maneuver in order to increase the maneuver accuracy;

⇒ modeling the optimization algorithm, which is similar to network theory and under various cost functions;

⇒ examining the effects of shifting mass on ground coverage and other attitude accuracies; and

⇒ finding the optimal mass travelling and distributing of mass among the tanks.

The remaining chapters are organized as following: Chapter 2 contains brief reviews for satellite attitude control methods for both active and passive controllers. Additionally, basic control representatives used for this dissertation are introduced. In Chapter 3, a

specific design for this research has been defined and the related equations of motion are found. Compared with the general approach to the motion of gravity-gradient-stabilized satellites, a reverse approach to compute the moments of inertia with limited known conditions is developed. Once the minimum mass transfer mapping is obtained, the optimization process is characterized to find the optimal solution. Network theory is applied to define various objective functions. Chapter 4 shows the simulation results based on the equations developed in Chapter 3. Beginning with a simple case, which is the center-of-mass does not change after mass movement, examples for more complicated cases are illustrated. Moreover, restrictions such as a blocked pipe or an abandoned tank are tested. In addition to working as a sole control method, mass redistribution with an internal rotating device is added. Chapter 5 summarizes all the performed tasks, discusses the result and presents conclusions that can be drawn from the results. Suggestions for future work are also included.

Chapter 2

BACKGROUND

A spacecraft attitude control system, as seen in the block diagram in Figure 2.1, is composed of three major functions: sensor, controller, and dynamic process. The sensor detects the satellite's attitude and controllers operate the system to achieve the desired Euler angles and/or rates. The resulting dynamic rotating motion of the vehicle completes the closed loop of the attitude control system.

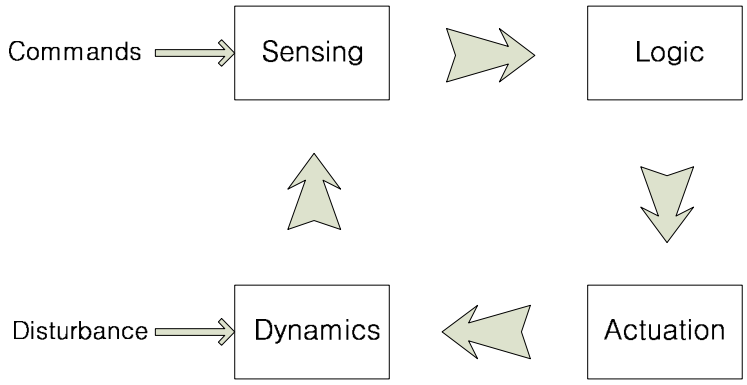

Figure 2.1: Diagram of Spacecraft Attitude Dynamics and Control [1]

2.1 Literature Review

Enormous amounts of research on attitude control methods have been published over the years. Consequently, the behavior and use of conventional attitude control actuators are very developed and heavily used at the present time. Studer [2] discusses the ACES (spacecraft attitude control and energy storage) system with a minimum of four

wheels operating for three-axis attitude control. An optimal design to generate control torque by wheels spinning at a high speed was investigated. Tsiotras [3] presents a satellite system with four or more momentum wheels and three thrusters. Momentum wheels are used as not only actuators but as a provider of power to the satellite from the stored energy. Thrusters accomplish quick and large maneuvers needed for orbit initialization or transfer phases and manage the momentum. A control law evaluates the torque, which was decomposed into two parts: tracking the power level of the wheels and controlling the attitude of satellite. Urakubo et al. [4] used two reaction wheels to investigate the satellite system under control while the angular momentum was fairly small. An extended Lyapunov control method was applied to derive a discontinuous state feedback law. Similarly, Krishnan [5] demonstrated attitude control of a satellite with two momentum wheels. Three wheels were initially installed but one of them failed. Two different control strategies were attempted for the uncontrollable satellite system. It was shown that a time-invariant continuous feedback control law could not stabilize the system successfully, but discontinuous feedback achieved stabilized equilibrium. Control momentum gyros were also analyzed by other researchers. Mapar [6] introduced a new approach to the CMG (Control Moment Gyro) applicable to the Space Station *Freedom* project. A torque equilibrium attitude was chosen for linearization of the nonlinear equations of motion instead of the local horizontal vertical frame since the latter was not suitable for linearization. Regional pole placement combined with the optimal control were used to stabilize an uncontrollable space station. A single gimbaled control moment gyro with some restriction was tested by Shi [7]. The applied restrictions helped to design the control system and to align the controller and the sensor axis, thus the torque could

remain almost constant. However, these active control devices are high-priced and have a penalty in fuel consumption if passive control methods are not applied. Zheng [8] presented an active optimal control for three-axis stabilized satellite by flywheels. A flexible spacecraft with vibrating solar array formed a nonlinear system and the second order terms were included in the equations. Linear quadratic regulators were used for approximation to satisfy the optimization.

Environmental forces such as solar radiation pressure, aerodynamic drag, gravity gradient torque, and magnetic torque are inevitable for a LEO satellite. Sometimes these forces act as a perturbation, but also can counteract as a controller. Shrivastava [9] provide a survey of satellite attitude dynamics and control under the influence of environmental torques. Park [10] presents a three-axis control scheme for a rigid satellite body with external disturbances. The minimax approach and the inverse optimal approach provided guidance for an optimal robust control law. Among these passive control methods, magnetic torque control is widely used, especially for small satellites in low Earth orbit (LEO). Lovera [11] used magnetic actuators to solve the inertial pointing problem by means of static attitude and rate feedback. Musser [12] presented an autonomous spacecraft attitude control method using a linear quadratic regulator algorithm. Since a satellite's orbit is not aligned with the geomagnetic field, the trajectory is time variant; therefore, the optimal feedback gain is time-varing as well and it is converted as a function of position not the simulation time. Ahsun [13] provided a control method for electromagnetic formation flying. High temperature superconducting wires acted as magnetic dipoles for the satellites' formation in LEO. Nonlinear dynamic equations were simulated under the closed loop control method. Psiaki [14] developed a

three-axis control method with magnetic torque rods to achieve nadir pointing accuracy on the order of 0.5 to 1.0 deg. Without any help from other actuators such as thrusters or reaction wheels, the simulation showed a robust closed-loop system. Alfriend [15] also used a closed-loop control law for a dual-spin satellite. The satellite spin axis is assumed to be parallel to the installed dipoles and the interaction with the geomagnetic field was considered. Both approximate and numerical solutions were found for comparison. Psiaki [16] discussed three-axis attitude stabilization of a nadir-pointing spacecraft in LEO controlled by aerodynamic magnetic torques. Yaw and pitch axes control was carried out by passive aerodynamic drag torques, whereas active magnetic control was responsible for the roll axis.

Gravity gradient attitude control is another consideration for a small satellite in LEO. It provides a long term control solution with small amount of force due to the gravitational difference around the center-of-mass of the whole system. Since the 1960s, gravity-gradient control has attracted attention due to its simplicity. Arduini [17] generated the general formulation of magnetic damping control for a gravity-gradient-stabilized satellite. The dynamics and control for a near polar orbit satellite subject to the gravity torque was analyzed by Wisniewski [18]. Contrary to its simple design, the relationship between the Earth's magnetic field and the magnetic torque from coils were expressed in nonlinear equations. It was shown that the magnetorquers could work as a sole three-axis actuator for gravity-gradient-stabilized satellite. Martel [19] found a control algorithm to utilize a magnetic control system, eliminating the need for a damper system. Three magnetic torquers and one three-axis magnetometer were used for stability

of a gravity-gradient-stabilized system. Kalman filtering provided the results for satellite attitude angles and their rates.

In addition, satellite systems with appendages or interconnected systems were investigated using several approaches. Modi [20] reviewed the attitude dynamics of spacecraft with flexible parts and Lips [21] found a general formulation for a satellite with arbitrary number of flexible appendages. The location and shape of the appendages were not restricted. Governing coupled nonlinear equations for vibration from appendages were examined for practical applications. The center-of-mass of the whole system was important with the existence of individual appendages. Ng [22] developed further a formulation of an interconnected flexible body system. Shifting center-of-mass and slewing of independent bodies were associated for a large scale spacecraft application. A satellite system with two beam-type appendages was implemented for feasibility. The general approach was to calculate the center-of-mass by the location of arbitrary appendages and the equations of motion were analyzed to provide the dynamics and attitude control for a multi-body system. Kang [23, 24] used a liquid fuel tank for angular momentum exchange. A single movable mass control system was introduced by Childs [25]. An active control system by momentum exchange for an artificial-*g* space station was developed. Kumar [26] also applied one movable mass to the miniature satellite. The single mass was restricted to move along one axis and the related equations of motion were derived through a Lagrangian approach. For the control strategy, a linear quadratic regulator was chosen.

Among the extensive ongoing research, the consideration of center-of-mass shifting under the influence of the gravitational force is the motivation for this

dissertation. Since relocating the center-of-mass is applicable for attitude control by changing the rotation angles and rates, this new concept may work as a controller for a multi-body satellite system in LEO. Control can be accomplished by mass redistribution in a satellite system using the gravity-gradient technique. Shifting mass involves changing the center-of-mass of the system, and/or changing the moments of inertia of the system, which then ultimately can change the attitude behavior of the system.

2.2 Coordinate System

A coordinate system is a convention to express a unique position of a point in n-th order space. Each position is composed of a series of scalar values. Three mutually orthogonal vectors can define one coordinate system, i.e., a reference frame. Three vectors for a random coordinate system $\mathbf{Z}$ are denoted as $\mathbf{X_Z}$, $\mathbf{Y_Z}$, and $\mathbf{Z_Z}$, respectively, and will be used in this dissertation. All coordinate systems in this research are assumed to be right-handed orthonormal systems. Thus, the following equations are satisfied for any case:

$$\hat{\mathbf{v}}_\mathbf{Z} \cdot \hat{\mathbf{w}}_\mathbf{Z} = \begin{pmatrix} 1, & \hat{\mathbf{v}} = \hat{\mathbf{w}} \\ 0, & \hat{\mathbf{v}} \neq \hat{\mathbf{w}} \end{pmatrix} \quad \text{for } \forall\ \hat{\mathbf{v}}, \hat{\mathbf{w}} \in \{\hat{\mathbf{X}}, \hat{\mathbf{Y}}, \hat{\mathbf{Z}}\} \tag{2.1}$$

$$\hat{\mathbf{X}}_\mathbf{Z} \times \hat{\mathbf{Y}}_\mathbf{Z} = \hat{\mathbf{Z}}_\mathbf{Z} \tag{2.2}$$

$$\hat{\mathbf{Y}}_\mathbf{Z} \times \hat{\mathbf{Z}}_\mathbf{Z} = \hat{\mathbf{X}}_\mathbf{Z} \tag{2.3}$$

$$\hat{\mathbf{Z}}_\mathbf{Z} \times \hat{\mathbf{X}}_\mathbf{Z} = \hat{\mathbf{Y}}_\mathbf{Z} \tag{2.4}$$

In this dissertation, the several coordinate systems are introduced based on different interests. One position in two different coordinate systems can be transferred easily by a direction cosine matrix without changing its original characteristic. By extending this through a chain rule, any transition can be performed. Some problems can be set up in one coordinate system and be solved in a different system. The following coordinate systems are generally used for satellite attitude control systems.

2.2.1 The Inertial Coordinate System

The inertial coordinate system denoted by the letter **I** is the system in which the origin is located at the Earth's center. In this system, $\hat{\mathbf{X}}_\mathbf{I}$ is defined as the unit vector form the Earth's center to the first point of Aries. The unit vector $\hat{\mathbf{Z}}_\mathbf{I}$ is chosen from the Earth's center to the North Pole. The vector $\hat{\mathbf{Y}}_\mathbf{I}$ is chosen to complete the right-handed system. Figure 2.2 shows a diagram for the inertial coordinate system.

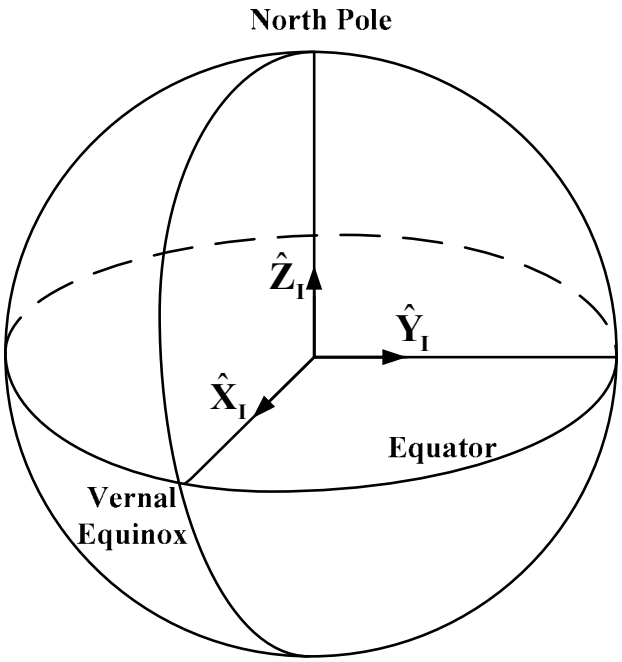

Figure 2.2: The Inertial Coordinate System

2.2.2 The Earth-Centered Fixed Coordinate System

The Earth-centered fixed coordinate system denoted by the letter **E** is illustrated in Figure 2.3. Compared with the inertial coordinate system, this reference frame is fixed to the Earth, thus it rotates at the same speed as the Earth's rotation with the origin located at the Earth's center. In this system, $\hat{\mathbf{X}}_\mathbf{E}$ is defined as the unit vector from the Earth's center to the Prime Meridian and the Equator. The unit vector $\hat{\mathbf{Z}}_\mathbf{E}$ is chosen from the Earth's center to the North Pole. The vector $\hat{\mathbf{Y}}_\mathbf{E}$ is chosen to complete the right-handed system pointing from the center of the Earth to the 90th meridian east.

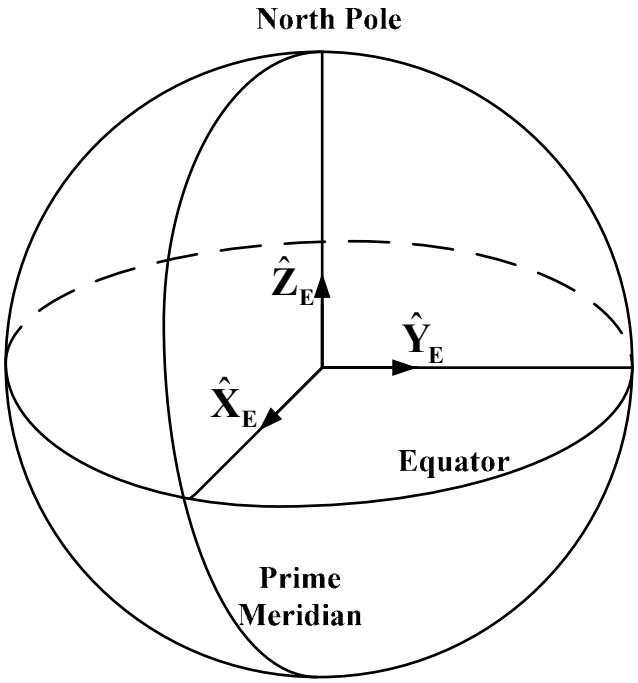

Figure 2.3: The Earth-Centered Fixed Coordinate System

2.2.3 The Body-Fixed Coordinate System

The body-fixed coordinate system, denoted with the letter **B**, is the system in which its origin is generally located at the center-of-mass of a satellite. As its name suggests, this reference coordinate system is defined in relation to the satellite itself. This orthnormal system can be chosen to point any direction. Figure 2.4 shows one example of the body-fixed coordinate system.

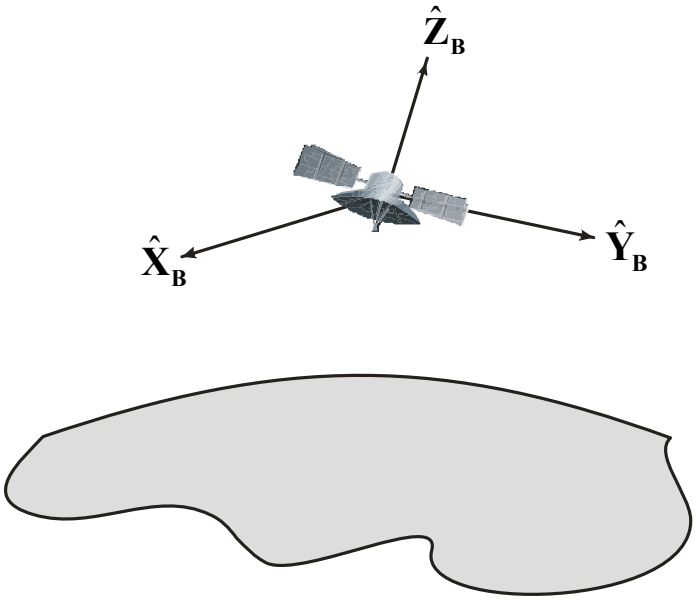

Figure 2.4: The Body-fixed Coordinate System

2.2.4 The Orbital Reference Coordinate System

The orbital reference coordinate system, which is denoted by the letter **R**, is the fundamental coordinate system for satellite attitude control maneuvers. Since attitude control occurs around the center-of-mass of a satellite, this coordinate system must always be taken into account. The satellite's center-of-mass is the origin of this coordinate system. The unit vector $\hat{\mathbf{Z}}_R$ points radially from the Earth's center to the satellite. The unit vector $\hat{\mathbf{X}}_R$ is defined in the tangential direction of the satellite in an orbit. From Equation (2.4), $\hat{\mathbf{Y}}_R$, which is normal to both $\hat{\mathbf{X}}_R$ and $\hat{\mathbf{Z}}_R$, completes the orbital reference coordinate system pointing out of the page. A simplified orbital

reference coordinate system is shown in Figure 2.5. Appendix A shows several examples of how different coordinate systems can be converted between each other.

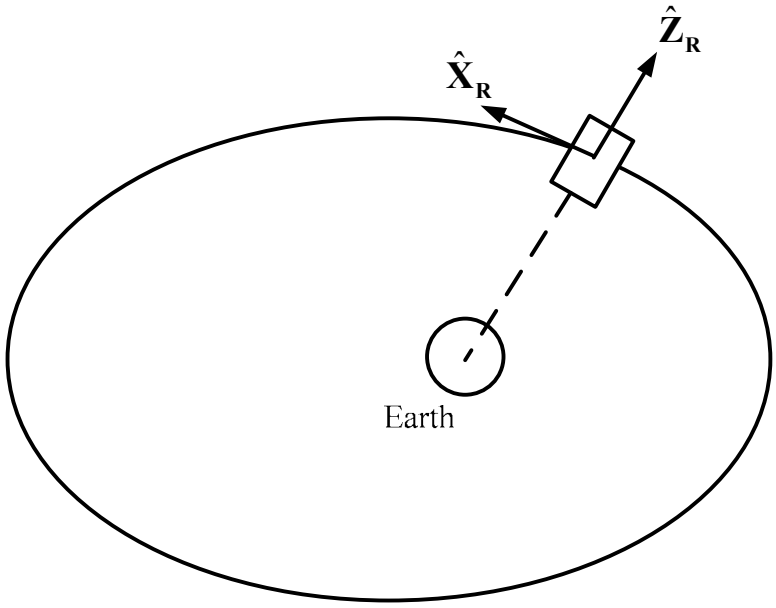

Figure 2.5: The Orbital Reference Coordinate System

2.3 Attitude Representations

Four different coordinate systems are defined in the previous sections. The next step is to establish the transition relationships between these systems. The fundamental concept of this procedure is to explain one coordinate system in terms of another system. Sometimes it is necessary to extend from a small motion change in a satellite to the groundtrack on the Earth. To achieve this maneuver the attitude change must be considered in the orbital reference coordinate system first and the resulting effect in an inertial coordinate system can be found by applying the relationship between those two

coordinate systems. However, it is more intuitive if this process goes through the body-fixed coordinate system since the relationship between the body-fixed coordinate system and the inertial coordinate system is readily known. Also, the small difference can be seen more easily than connecting the orbital reference coordinate system to the inertial coordinate system directly. The transition process can be combined by applying the chain rule through direction cosine matrices. Assume two unit vectors $\left[\hat{\mathbf{x}}_\mathbf{M} \quad \hat{\mathbf{y}}_\mathbf{M} \quad \hat{\mathbf{z}}_\mathbf{M}\right]$ and $\left[\hat{\mathbf{x}}_\mathbf{N} \quad \hat{\mathbf{y}}_\mathbf{N} \quad \hat{\mathbf{z}}_\mathbf{N}\right]$ for two arbitrary coordinate systems **M** and **N**, respectively, and the relationship developed in next section can be applied for any transformation.

2.3.1 Direction Cosine Matrix

As the two vectors $\left[\hat{\mathbf{x}}_\mathbf{M} \quad \hat{\mathbf{y}}_\mathbf{M} \quad \hat{\mathbf{z}}_\mathbf{M}\right]$ and $\left[\hat{\mathbf{x}}_\mathbf{N} \quad \hat{\mathbf{y}}_\mathbf{N} \quad \hat{\mathbf{z}}_\mathbf{N}\right]$ are unit vectors, each can be expressed with vectors of the other system following the simple rule of linear algebra. For example, $\hat{\mathrm{x}}_\mathbf{M}$ may be written as

$$\hat{\mathrm{x}}_\mathbf{M} = x_x\hat{\mathbf{x}}_\mathbf{N} + x_y\hat{\mathbf{y}}_\mathbf{N} + x_z\hat{\mathbf{z}}_\mathbf{N} = \begin{bmatrix} x_x & x_y & x_z \end{bmatrix} \begin{bmatrix} \hat{\mathbf{x}}_\mathbf{N} \\ \hat{\mathbf{y}}_\mathbf{N} \\ \hat{\mathbf{z}}_\mathbf{N} \end{bmatrix} \tag{2.5}$$

Likewise, both $\hat{\mathrm{y}}_\mathbf{M}$ and $\hat{\mathrm{z}}_\mathbf{M}$ have similar expressions and these equations may be merged into one matrix as following:

$$\begin{bmatrix} \hat{\mathbf{x}}_{\mathbf{M}} \\ \hat{\mathbf{y}}_{\mathbf{M}} \\ \hat{\mathbf{z}}_{\mathbf{M}} \end{bmatrix} = \begin{bmatrix} x_x & x_y & x_z \\ y_x & y_y & y_z \\ z_x & z_y & z_z \end{bmatrix} \begin{bmatrix} \hat{\mathbf{x}}_{\mathbf{N}} \\ \hat{\mathbf{y}}_{\mathbf{N}} \\ \hat{\mathbf{z}}_{\mathbf{N}} \end{bmatrix} = \mathrm{DCM}^{\mathbf{M/N}} \begin{bmatrix} \hat{\mathbf{x}}_{\mathbf{N}} \\ \hat{\mathbf{y}}_{\mathbf{N}} \\ \hat{\mathbf{z}}_{\mathbf{N}} \end{bmatrix} \tag{2.6}$$

The matrix $\mathrm{DCM}^{\mathbf{M/N}}$ is the direction cosine matrix that relates the **M**-frame to the **N**-frame. The $\mathrm{DCM}^{\mathbf{M/N}}$ has nine elements for three-dimensional space representing the base unit vector of system **M** with respect to the system **N**. With the benefit of the characteristics of base unit vectors, which are orthonormal, additional constraint relationships for the elements of the $\mathrm{DCM}^{\mathbf{M/N}}$ can be derived from Equation (2.1). For instances, all nine elements are not required to describe the satellite's attitude. Also, there are six possible constraint equations with the elements of the $\mathrm{DCM}^{\mathbf{M/N}}$ and those constraints can yield the useful properties explained in Appendix B.

2.3.2 Euler Angles

Leonhard Euler (1707-83) claimed that any two different coordinate systems sharing the same origin, but with different orientations, might be aligned to each other by three successive rotations. The order of the rotation is not necessarily limited, but any one axis cannot be used twice in a row. One possible rotation order is that the first angle rotation is about the z-axis, the second angle rotation about the changed y-axis, and the last rotation angle about the changed x-axis. Now, it is guaranteed that there are always three angles used to complete the required maneuver, which are generally called Euler

angles. More details for this sequence and the rotation matrix calculation are explained in Appendix C.

There are two types of transformation from one coordinate system to the other. The first type is a rotation completed by all three different axes. This type provides six rotation sets. The second type is when the first and third angles rotate around the same axis and yield six transformation cases. Consequently, 12 possible instances of rotation result 12 combinations of Euler angle rotation sets.

Euler angles are fairly intuitive to understand. No further constraints or conditions are required. This characteristic may be useful for the intuitive transformation between the body-fixed coordinate system and the orbital reference coordinate system. Also, an alternative method, roll-pitch-yaw rotation for small angle changes, which has been applied for this research, could also be used.

There are a number of ways to describe the mapping sequences that exist for different situations. All those methods are used for the same purpose with various circumstances and it is also possible to convert between methods. Detailed conversion between direction cosine matrix and Euler angles are presented in Appendix D. Table 2.1 summarizes both advantages and disadvantages of each attitude mapping computation.

Table 2.1: Advantages and Disadvantages of Each Attitude Representation [27]

Parameterization	Advantages	Disadvantages
Direction Cosine Matrix	- No singularities - No trigonometric Functions - Clear physical interpretation - Convenient product rule for successive rotations	- Six redundant parameters
Euler Angles	- No redundant parameters - Clear physical interpretation	- Singularities at some angles - Trigonometric functions - No convenient product rule for successive rotations

2.4 Basic Representations in Angular Motion and Rotational Dynamics

There are several representations to be introduced to describe the angular motion in a rotating system. From the definitions of the moment of inertia and the parallel axis theorem, properties of the angular momentum are now presented. For example, other properties such as the conservation of angular momentum, are widely used through this research.

2.4.1 Moment of Inertia

The moment of inertia is defined as a measure of how difficult it is to change the rotational motion of an object around its rotating axis. This concept in angular dynamics is analogous to the role mass plays in linear dynamics. Likewise, mass is one of the most essential properties in a linear system, so angular quantities using moments of inertia in an angular system are unavoidable. Note that the moment of inertia is calculated not only from how the mass of the object is distributed but also how far the differential element of

mass is located from the axis. Thus, the moment of inertia can be changed if one of those or both changes. The equation for the moment of inertia is

$$I = \int_m d^2 dm \tag{2.7}$$

where I is the moment of inertia, m is the total mass of an object, dm is the differential element of mass, and d is the distance of dm from the rotating axis.

2.4.2 Parallel Axis Theorem

The parallel axis theorem is used for calculating of the moment of inertia of an object about any axis. If a certain axis does not pass through its center-of-mass with a given the moment of inertia of a body, then there must be another axis passing through the center-of-mass and is parallel to the axis. Under those circumstances, the following equation holds

$$I = I_{\text{center\_of\_mass}} + M_{\text{total\_mass}} D^2 \tag{2.8}$$

where $I_{\text{center\_of\_mass}}$ is the moment of inertia of the object about an axis passing through its center-of-mass, $M_{\text{total\_mass}}$ is the total mass of the object, and D is the distance between two axes.

2.4.3 Angular Momentum

A set of governing equations for the rotating system results in the differential equations of the angular momentum about the center-of-mass. Suppose two coordinate systems, the inertial coordinate system with a subscript I and the body-fixed coordinate system with a subscript B. Let $\bar{R}$ be a random vector, then the derivatives of $\bar{R}$ in each coordinate system can be related by

$$\left[\frac{d\bar{R}}{dt}\right]_{\mathrm{I}} = \left[\frac{d\bar{R}}{dt}\right]_{\mathrm{B}} + \bar{\omega}\times\bar{R} \tag{2.9}$$

where $\left[\frac{d\bar{R}}{dt}\right]_{\mathrm{I}}$, $\left[\frac{d\bar{R}}{dt}\right]_{\mathrm{B}}$ are derivatives in the inertial coordinate system and the body-fixed coordinate system, respectively, and $\bar{\omega}$ is the angular velocity of the body-fixed coordinate system relative to the inertial coordinate system.

Two coordinate systems, the inertial coordinate system $\hat{\mathbf{X}}_{\mathbf{I}}\hat{\mathbf{Y}}_{\mathbf{I}}\hat{\mathbf{Z}}_{\mathbf{I}}$ with the origin at $\mathrm{O}_{\mathbf{I}}$ and the body-fixed coordinate system $\hat{\mathbf{X}}_{\mathbf{B}}\hat{\mathbf{Y}}_{\mathbf{B}}\hat{\mathbf{Z}}_{\mathbf{B}}$ with the origin $\mathrm{O}_{\mathbf{B}}$ located at the center-of-mass of the body, are illustrated in Figure 2.6. Both $\left[\hat{\mathrm{X}}_{\mathbf{I}} \quad \hat{\mathrm{Y}}_{\mathbf{I}} \quad \hat{\mathrm{Z}}_{\mathbf{I}}\right]$ and $\left[\hat{\mathrm{X}}_{\mathbf{B}} \quad \hat{\mathrm{Y}}_{\mathbf{B}} \quad \hat{\mathrm{Z}}_{\mathbf{B}}\right]$ are assumed to be corresponding unit vectors without loss of generality. Then, for any arbitrary small mass m_s in the body **B**, $\bar{R}_i = \bar{R}_o + \bar{r}_i$. Substituting into Equation (2.9) results

$$\dot{\bar{R}}_i = \dot{\bar{R}}_o + \dot{\bar{r}}_i + \bar{\omega} \times \bar{r}_i = \bar{v}_o + \bar{v}_i + \bar{\omega} \times \bar{r}_i \tag{2.10}$$

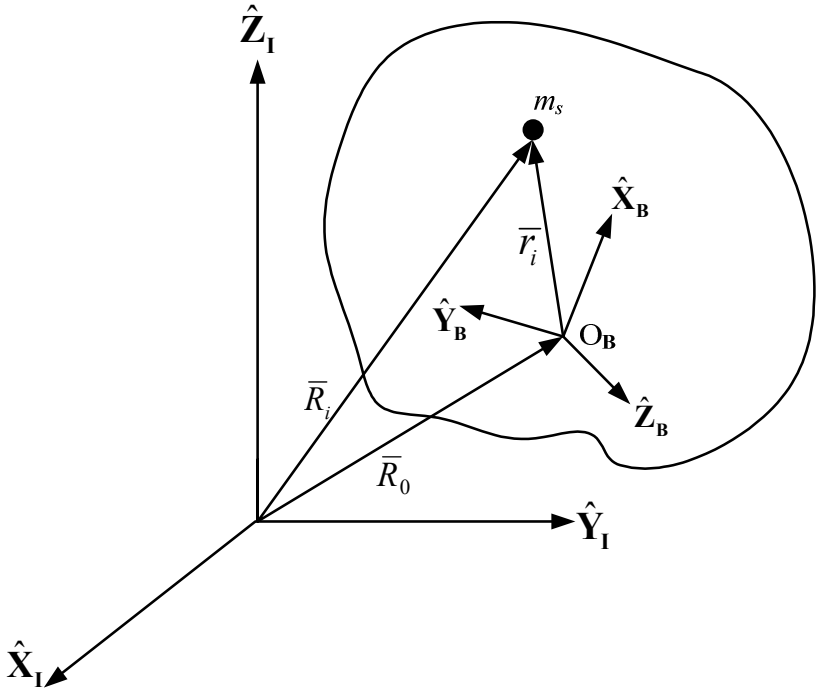

Figure 2.6: Rigid Body Diagram

Inserting Equation (2.10) into the definition of the angular momentum equation, the following equation is obtained,

$$\dot{\bar{H}}_i = \bar{r}_i \times m_s \dot{\bar{R}}_i = m_s \bar{r}_i \times \left(\dot{\bar{R}}_o + \dot{\bar{r}}_i + \bar{\omega} \times \bar{r}_i \right) \tag{2.11}$$

where $\dot{\bar{H}}_i$ is the derivative of the angular momentum vector of a rigid body about its center-of-mass. By assuming the body as a rigid body, $\dot{\bar{r}}_i = 0$ satisfies and it follows that

$$\dot{\bar{H}}_i = m_i \bar{r}_i \times \left(\dot{\bar{R}}_o + \dot{\bar{r}}_i + \bar{\omega} \times \bar{r}_i \right) = -\bar{v}_0 \times m_i \bar{r}_i + m_i \bar{r}_i \times \left(\bar{\omega} \times \bar{r}_i \right) \tag{2.12}$$

Then, the angular momentum of the entire body is calculated by the summation of the small mass over the whole body

$$\dot{\bar{H}} = \sum_i \dot{\bar{H}}_i = -\bar{v}_0 \times \sum_i m_i \bar{r}_i + \sum_i m_i \bar{r}_i \times \left(\bar{\omega} \times \bar{r}_i \right) \tag{2.13}$$

Since the origin of body **B**, $O_{\mathbf{B}}$, is assumed to be located at the center-of-mass of the body, it follows that

$$\sum_i m_i \bar{r}_i = 0 \tag{2.14}$$

Equation (2.13) then reduces to

$$\dot{\bar{H}} = \sum_i m_i \bar{r}_i \times \left(\bar{\omega} \times \bar{r}_i \right) \tag{2.15}$$

Equation (2.15) can be used to find Euler's equation describing the dynamics of a rigid body in a rotating system. A detailed derivation of Equation (2.16) is found in Hibbeler [28]. In Equation (2.16), it is presented that the change of angular momentum in an inertial coordinate system is the summation of the angular momentum change in the body coordination system plus the cross product of the angular velocity of the body coordinate system with respect to the inertial coordinate system and angular momentum of the body, i.e.,

$$\bar{M}_{\text{external}} = \dot{\bar{H}} = \left[\frac{d\bar{H}}{dt}\right]_{\text{I}} = \left[\frac{d\bar{H}}{dt}\right]_{\text{B}} + \bar{\omega}^{\text{B/I}} \times \bar{H} \tag{2.16}$$

where $\bar{M}_{\text{external}}$ is the external moment acting on the body about its mass center.

2.5 Sensors and Controllers for Satellite Attitude Dynamics

In order to perform the mission of the satellite successfully, the satellite's orbit and attitude control system is essential. With more accurate and efficient measurement and maneuvering, better performance of the satellite's duties may be expected. As illustrated in Figure 2.1, the first step in the attitude control starts by observing the satellite's attitude. This observation is performed by various sensors installed in a satellite system. Sensor modeling and attitude determination for satellite has been well organized by Sunde [29]. Chobotov [1] shows the torque ranges of several control actuators in Table 2.2.

Table 2.2: Torque Range of Control Actuators [1]

Control Actuators	Torque Range (N·m)
Reaction Wheel	10^{-1} to 1
Moment Gyro	10^{-2} to 10^{3}
Magnetic Torquer	10^{-2} to 10^{-1}
Aerodynamic	10^{-5} to 10^{-3}
Gravity Gradient	10^{-6} to 10^{-3}

Active control is used for maneuvers that require high accuracy. The downside of these systems is that they need more power or consume fuel, which shortens the life of a spacecraft. On the converse, passive control is attractive for its low cost, simplicity, and decreased power usage.

2.5.1 Gravity Gradient

The gravity gradient torque is one of the environmental torques of important applicability to the attitude control of a satellite. This torque by the Earth can be used to stabilize satellites in a nadir pointing attitude and can act on two axes of the orbital reference coordinate system. In orbit, a non-symmetric mass distribution of the satellite performs as a torque due to the Earth's gravity.

When the motion of a satellite is described, it is common to express the motion of a satellite in orbital reference coordinate system defined in Section 2.2.4. In Figure 2.7, the coordinate system $\hat{\mathbf{X}}_\mathbf{R}\hat{\mathbf{Y}}_\mathbf{R}\hat{\mathbf{Z}}_\mathbf{R}$ is the orbital reference coordinate system. The orbit is circular and n is the mean motion. The origin of this right-handed, orthogonal frame is at

the center-of-mass of the satellite with the $\hat{\mathbf{Z}}_{\mathbf{R}}$ axis directed radially outward from the center of the Earth, the $\hat{\mathbf{X}}_{\mathbf{R}}$ axis in the direction of velocity, and the $\hat{\mathbf{Y}}_{\mathbf{R}}$ axis completing the right-hand system by pointing normal to the orbital plane. This orbital reference coordinate system $\hat{\mathbf{X}}_{\mathbf{R}}\hat{\mathbf{Y}}_{\mathbf{R}}\hat{\mathbf{Z}}_{\mathbf{R}}$ is also referred to as the Clohessy-Wiltshire [30] coordinate system. The roll, pitch, and yaw axes are defined such that the principal body-fixed coordinate system $\hat{\mathbf{X}}_{\mathbf{P}}\hat{\mathbf{Y}}_{\mathbf{P}}\hat{\mathbf{Z}}_{\mathbf{P}}$ is aligned with the $\hat{\mathbf{X}}_{\mathbf{R}}\hat{\mathbf{Y}}_{\mathbf{R}}\hat{\mathbf{Z}}_{\mathbf{R}}$ axes, respectively. When the $\hat{\mathbf{X}}_{\mathbf{P}}$ axis is aligned with $\hat{\mathbf{X}}_{\mathbf{R}}$ it is defined as the roll axis. Similarly, the pitch and yaw axes are defined from the relations between $\hat{\mathbf{Y}}_{\mathbf{P}}$ and $\hat{\mathbf{Y}}_{\mathbf{R}}$, and $\hat{\mathbf{Z}}_{\mathbf{P}}$ and $\hat{\mathbf{Z}}_{\mathbf{R}}$, respectively. If the principal body-fixed coordinate system $\hat{\mathbf{X}}_{\mathbf{P}}\hat{\mathbf{Y}}_{\mathbf{P}}\hat{\mathbf{Z}}_{\mathbf{P}}$ and the orbital reference frame $\hat{\mathbf{X}}_{\mathbf{R}}\hat{\mathbf{Y}}_{\mathbf{R}}\hat{\mathbf{Z}}_{\mathbf{R}}$ are slightly misaligned, then three angles, the roll, pitch and yaw angles, are defined as the angular differences between each other. By observing the behavior of these angles, the satellite's attitude can be explained. The roll, pitch, and yaw angles are illustrated in Figure 2.8.

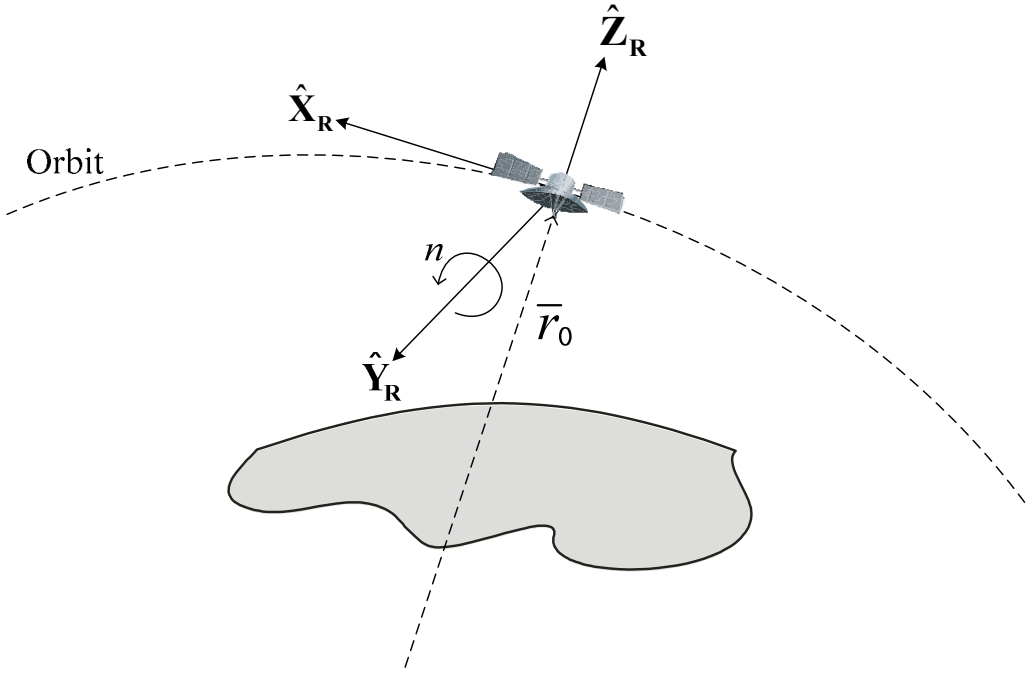

Figure 2.7: Orbital Reference Coordinate System in a Circular Orbit [31]

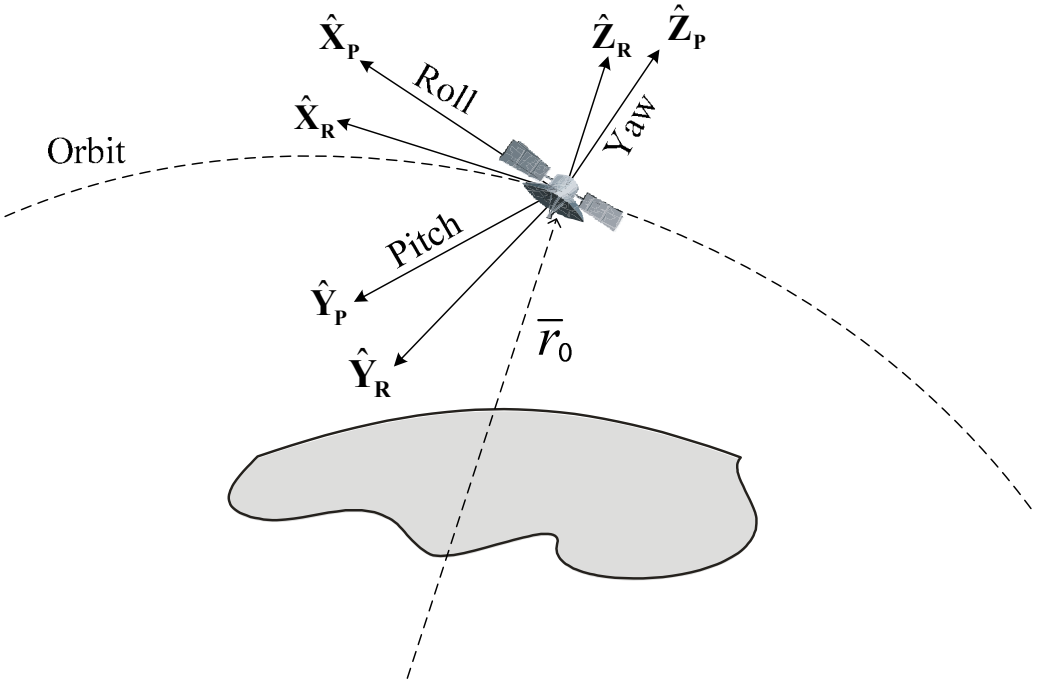

Figure 2.8: Diagram of Roll, Pitch, and Yaw Angles [31]

The Euler equations of motion under the gravity-gradient torque derived by Curtis [31] with consideration of the net torque acting over the body G by the Earth's gravity are:

$$\begin{aligned} A\dot{\omega}_x + (C-B)\omega_y\omega_z &= \frac{3\mu r_{0_y} r_{0_z}}{r_0^5}(C-B) \\ B\dot{\omega}_y + (A-C)\omega_z\omega_x &= \frac{3\mu r_{0_x} r_{0_z}}{r_0^5}(A-C) \\ C\dot{\omega}_x + (B-A)\omega_x\omega_y &= \frac{3\mu r_{0_x} r_{0_y}}{r_0^5}(B-A) \end{aligned} \tag{2.17}$$

where $A = \int_m y^2 + z^2 dm$, $B = \int_m x^2 + z^2 dm$, and $C = \int_m x^2 + y^2 dm$, respectively, and $\bar{r}_0 = \begin{bmatrix} r_{0_x} & r_{0_y} & r_{0_z} \end{bmatrix}^T$.

To investigate the relationship between two coordinate systems, the position vector $\bar{r}_0$ and the angular velocity is $\bar{\omega}$ can be expressed as:

$$\bar{r}_0 = \begin{bmatrix} 0 & 0 & r_0 \end{bmatrix}^T \tag{2.18}$$

$$\bar{\omega} = \begin{bmatrix} 0 & n & 0 \end{bmatrix}^T \tag{2.19}$$

Substituting Equations (2.18) and (2.19) into (2.17) yields

$$\dot{\omega}_x = \dot{\omega}_y = \dot{\omega}_z = 0 \tag{2.20}$$

It is implied that the principal body-fixed coordinate system remains aligned with the orbital reference coordinate system from Equation (2.20). In other words, this satellite system is gravity-gradient stabilized. The gravity-gradient stabilization is a convenient method for a small angle rotation and the main interest of this dissertation.

In Figure 2.7, the angular velocity, $\bar{\omega}$, of the satellite in the inertial coordinate system is composed of two parts.

$$\bar{\omega} = \bar{\Omega} + \bar{\omega}_{\text{rel}} \tag{2.21}$$

where $\bar{\Omega}$ is the angular velocity of the orbital reference coordinate system with respect to the inertial coordinate system and $\bar{\omega}_{\text{rel}}$ is the relative angular velocity of the satellite with respect to the orbital reference coordinate system. It is noted that the summation cannot be computed because two vectors on the right side do not belong to the same coordinate system. Since the orbit is assumed to be circular, the following vector is found:

$$\bar{\Omega} = \begin{bmatrix} 0 \\ n \\ 0 \end{bmatrix} \tag{2.22}$$

$\bar{\omega}_{\text{rel}}$ in terms of pitch and yaw angles is expressed as:

$$\bar{\omega}_{\text{rel}} = \begin{bmatrix} \omega_{\text{roll}} - \omega_{\text{yaw}} \sin\theta \\ \omega_{\text{yaw}} \cos\theta \sin\psi + \omega_{\text{pitch}} \cos\psi \\ \omega_{\text{yaw}} \cos\theta \cos\psi - \omega_{\text{pitch}} \sin\psi \end{bmatrix} \tag{2.23}$$

where ψ, θ, and φ are roll, pitch, and yaw angles. Note that the roll, pitch and yaw angles are small, hence the small angle approximation ($\sin x \approx x$ and $\cos x \approx 1$) can be applied. In addition, neglecting the higher order terms in Equation (2.23) results

$$\bar{\omega}_{\text{rel}} = \begin{bmatrix} \dot{\psi} \\ \dot{\theta} \\ \dot{\varphi} \end{bmatrix} \tag{2.24}$$

where $\dot{\psi}$, $\dot{\theta}$, and $\dot{\varphi}$ are angular rates. Since Equations (2.22) and (2.24) are not in the same coordinate system, three rotations must be carried out and Equation (C.5) implements the successive rotation $\varphi - \theta - \psi$ in order. Equation (2.25) is an alternative form of Equation (C.5) after the approximation for small angles and higher order terms are neglected.

$$\begin{bmatrix} 1 & \varphi & -\theta \\ -\varphi & 1 & \psi \\ \theta & -\psi & 1 \end{bmatrix} \tag{2.25}$$

Then, $\bar{\Omega}$ is rotated by Equation (2.25) as following:

$$\bar{\Omega} = \begin{bmatrix} 1 & \varphi & -\theta \\ -\varphi & 1 & \psi \\ \theta & -\psi & 1 \end{bmatrix} \begin{bmatrix} 0 \\ n \\ 0 \end{bmatrix} = \begin{bmatrix} n\varphi \\ n \\ -n\psi \end{bmatrix} \tag{2.26}$$

and substituting Equations (2.24) and (2.26) into (2.21) yields

$$\bar{\omega} = \begin{bmatrix} \dot{\psi} + n\varphi \\ \dot{\theta} + n \\ \dot{\varphi} - n\psi \end{bmatrix} \tag{2.27}$$

Now, the angular velocity in the inertial coordinate system is described with roll, pitch, and yaw angles. Similar mathematics for the position vector $\bar{r}_0$ delivers

$$\bar{r}_0 = \begin{bmatrix} -r_0\theta \\ r_0\psi \\ r_0 \end{bmatrix} \tag{2.28}$$

By substituting the equations obtained into Equation (2.17), Euler's equations of motion of the satellite including gravity-gradient terms are computed

$$I_y\ddot{\varphi} + (I_p - I_r)n^2\varphi + (I_p - I_r - I_y)n\dot{\psi} = 0 \tag{2.29}$$

$$I_r\ddot{\psi} + (I_r - I_p + I_y)n\dot{\varphi} + 4(I_p - I_y)n^2\psi = 0 \tag{2.30}$$

$$I_p\ddot{\theta} + 3(I_r - I_y)n^2\theta = 0 \tag{2.31}$$

where I_r, I_p, and I_y are the roll, pitch, and yaw moments of inertia of the spacecraft, respectively. With these governing differential equations, Equations (2.29), (2.30), and (2.31), gravity-gradient torque effects can be analyzed for small angles between the body-fixed coordinate system and the orbital reference coordinate system.

It is noted that Equation (2.31) is a second-order differential equation that is uncoupled to the other two variables, ψ and φ. Thus, the classical solutions for the Equation (2.31) have the form of

$$\theta = P_1 e^{p_1 t} + P_2 e^{p_2 t} \tag{2.32}$$

where

$$p_{1,2} = \pm i \sqrt{\frac{3\left(I_r - I_y\right) n^2}{I_p}} \tag{2.33}$$

For the pitch angle in Equation (2.32) to be stable, both p_1 and p_2 must be imaginary in Equation (2.33). Otherwise, the solution increases as time increases, which means the satellite rotates about the pitch axis in an unstable manner. Therefore, the inside of the root in Equation (2.33) must be positive to be stable. The following inequality must be satisfied at any time to be gravity-gradient stabilized.

$$I_r > I_y \tag{2.34}$$

When the pitch motion is stabilized, the pitch frequency is given by

$$\omega_{f_{\text{pitch}}} = n\sqrt{\frac{3\left(I_r - I_y\right)}{I_p}} \tag{2.35}$$

For an elliptical orbit with small eccentricity e_{orbit}, Kaplan [32] showed that only the pitch angle is affected. The additional term to Equation (2.32) is presented as:

$$\theta_e = P_1 e^{p_1 t} + P_2 e^{p_2 t} + \frac{2e_{\text{orbit}} \sin nt}{\frac{3\left(I_r - I_y\right)}{I_p} - 1} \tag{2.36}$$

Curtis [31] also showed that the roll and yaw angles have the same frequency and are given by

$$\omega_{f_{\text{roll/yaw}}} = n\sqrt{\frac{1}{2}\left(b \pm \sqrt{b^2 - 4c}\right)} \tag{2.37}$$

where $b = 3\left(\frac{I_p - I_y}{I_r}\right) + \left(\frac{I_p - I_r}{I_y}\right)\left(\frac{I_p - I_y}{I_r}\right) + 1$ and $c = 4\left(\frac{I_p - I_r}{I_y}\right)\left(\frac{I_p - I_y}{I_r}\right)$, respectively.

With all solutions and inequalities for the three angles of a satellite, it is found that there are two inequalities must be satisfied to be stable, $I_r > I_y > I_p$ or $I_p > I_r > I_y$.

Case 1 $I_r > I_y > I_p$

As stated earlier, the satellite is rotating at the speed of mean motion about the pitch axis under the influence of a gravity-gradient torque. This means that the satellite rotates about the minor axis of inertia, not about the roll axis, which is the major axis of the inertia. Then, the satellite is not stable eventually due to the energy dissipation.

Case 2 $I_p > I_r > I_y$

Contrary to the Case 1, the satellite rotates about the major axis of the inertia, the pitch axis. This implies that the axis of rotation by the gravity-gradient torque coincides with the major axis of inertia, which is desired for stable motion. Thus, this criterion will be applied for the optimization in the next chapter.

2.6 Controllability and Observability

Controllability and observablility were first introduced by Kalman [33] for control theory. Those two concepts are roughly defined as:

Controllability indicates how well the system's state containing the system's variables can be changed from the adjusting an external input. A state is said to be controllable if it can be changed by an external input.

Observability indicates how well the system's state containing the system's variables can be determined from the known output. A state is said to be observable if it can be determined from the known output.

Both controllability and observability can give a better understanding from the linear time-invariant system as follows

$$\begin{aligned} \dot{\bar{x}}(t) &= A\bar{x}(t) + B\bar{u}(t) \\ \bar{y}(t) &= C\bar{x}(t) + D\bar{u}(t) \end{aligned} \tag{2.38}$$

where the state vector $\bar{x}(t)$ is an *m*-vector, the control vector $\bar{u}(t)$ is a *n*-vector, and the observation vector $\bar{y}(t)$ is an *l*-vector. Then, the controllability matrix is defined as:

$$M_C = \begin{bmatrix} B & AB & A^2B & \cdots & A^{m-1} \end{bmatrix} \tag{2.39}$$

If $\text{rank}\left(M_C^{-1}\right) = m$, this system is called controllable. The observability matrix is defined as:

$$M_o = \begin{bmatrix} C \\ CA \\ CA^2 \\ \vdots \\ CA^{m-1} \end{bmatrix} \tag{2.40}$$

If $\text{rank}\left(M_o^{-1}\right) = m$, this system is called observable. Those two representations may be extended to the system expressed in a differential equation form as:

$$\frac{d^m \bar{y}(t)}{dt^m} + a_{m-1}\frac{d^{m-1}\bar{y}(t)}{dt^{m-1}} + \cdots + a_1\frac{d\bar{y}(t)}{dt} + a_0\bar{y}(t) = b_{m-1}\frac{d^{m-1}\bar{u}(t)}{dt^{m-1}} + b_{m-2}\frac{d^m\bar{u}(t)}{dt^m} + \cdots + b_1\frac{d\bar{u}(t)}{dt} + b_0\bar{u}(t) \tag{2.41}$$

If this system is controllable, it can be written as:

$$\dot{\bar{x}}(t) = \begin{bmatrix} 0 & 1 & 0 & \cdots & 0 \\ 0 & 0 & 1 & \cdots & 0 \\ \vdots & \vdots & \vdots & \ddots & \vdots \\ -a_0 & -a_1 & -a_2 & \cdots & -a_{m-1} \end{bmatrix}\bar{x}(t) + \begin{bmatrix} 0 \\ 0 \\ \vdots \\ 1 \end{bmatrix}\bar{u}(t) \tag{2.42}$$

$$\bar{y}(t) = \begin{bmatrix} b_0 & b_1 & \cdots & b_{m-2} & b_{m-1} \end{bmatrix}\bar{x}(t) \tag{2.43}$$

Equations (2.42) and (2.43) are called the controllable canonical form. Similarly, if the system is also observable, the differential Equation (2.41) can be written as:

$$\dot{\bar{x}}(t) = \begin{bmatrix} 0 & 0 & \cdots & 0 & -a_0 \\ 0 & 0 & \cdots & 0 & -a_1 \\ \vdots & \vdots & \ddots & \vdots & \vdots \\ 0 & 0 & \cdots & 1 & -a_{m-1} \end{bmatrix}\bar{x}(t) + \begin{bmatrix} b_0 \\ b_1 \\ \vdots \\ b_{m-1} \end{bmatrix}\bar{u}(t) \tag{2.44}$$

$$\bar{y}(t) = \begin{bmatrix} 0 & 0 & \cdots & 1 \end{bmatrix}\bar{x}(t) \tag{2.45}$$

Equations (2.44) and (2.45) are called the observable canonical form.

2.7 Ground Track / Ground Coverage

For many satellites, the information of geodetic data is needed and those data are the well-known concepts of longitude (λ), latitude (ϕ), and altitude (h). If the position vector in the inertial coordinate system is provided, those values can be computed and vice versa without knowing the orbital element values. If the Earth is a perfect sphere, then the conversion is a simple calculation. However, the longitude and latitude are defined based on the Earth's elliptical shape, the difference between geodetic and geocentric system should be considered for exact values. Figure 2.9 illustrates how those two systems are related each other.

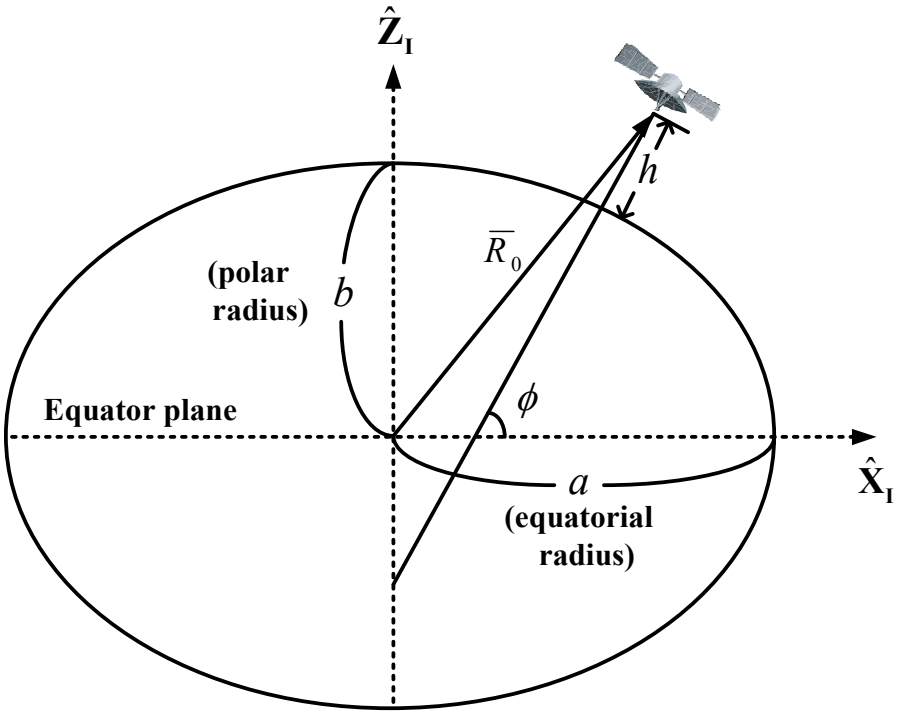

Figure 2.9: Diagram of Geodetic and Geocentric System

Because of the need to convert from the position vector to the latitude and longitude values taking into account the elliptical shape of the Earth is nonlinear, a large number of different conversion methods have been derived. Bowring [34, 35] and Jones [36] presented the conversion from inertial to geodetic system through Newton's iterative technique. Vermeille [37, 38] found the closed form solution for non-iterative method and the geodetic coordinate (λ , ϕ , h) are computed as

$$\lambda = 2\tan^{-1}\left(\frac{y}{x+\sqrt{x^2+y^2}}\right) \tag{2.46}$$

$$\phi = 2\tan^{-1}\left(\frac{z}{D+\sqrt{D^2+z^2}}\right) \tag{2.47}$$

$$h = \frac{k+e^2-1}{k}\sqrt{D^2+z^2} \tag{2.48}$$

where

$$D = \frac{k\sqrt{x^2+y^2}}{k+e^2} \qquad k = \sqrt{u+v+w^2}-w \qquad w = \frac{e^2}{2v}\left(u+v-\frac{1-e^2}{a^2}z^2\right)$$

$$v = \sqrt{u^2+e^4\left(\frac{1-e^2}{a^2}z^2\right)} \qquad u = r\left(1+t+\frac{1}{t}\right) \qquad t = \sqrt[3]{1+s+\sqrt{s(2+s)}}$$

$$s = \frac{e^4}{4r^3}\left(\frac{x^2+y^2}{a^2}\right)\left(\frac{1-e^2}{a^2}z^2\right) \qquad r = \frac{1}{6}\left(\frac{x^2+y^2}{a^2}+\frac{1-e^2}{a^2}z^2-e^4\right)$$

From Equations (2.46)-(2.48), the ground track of a satellite can be expressed via latitude and longitude. When a satellite moves along its orbit without roll, pitch, and yaw oscillation, the ground coverage forms a straight line along where the ground track passes the center of ground coverage area. If a satellite has small angles for roll, pitch, or yaw motions, then the ground coverage changes into a periodic curve on the ground. In Figure 2.10, the roll motion is around the $\hat{\mathbf{X}}_\mathbf{B}$ axis, the pitch motion is around the $\hat{\mathbf{Y}}_\mathbf{B}$ axis and the yaw motion is around the $\hat{\mathbf{Z}}_\mathbf{B}$ axis, respectively. The amplitude of the periodic curve is a function of latitude and longitude. It is noted that the ΔLat and ΔLong are function of the Euler's angles and the frequency is also the function of the Euler angle's frequencies.

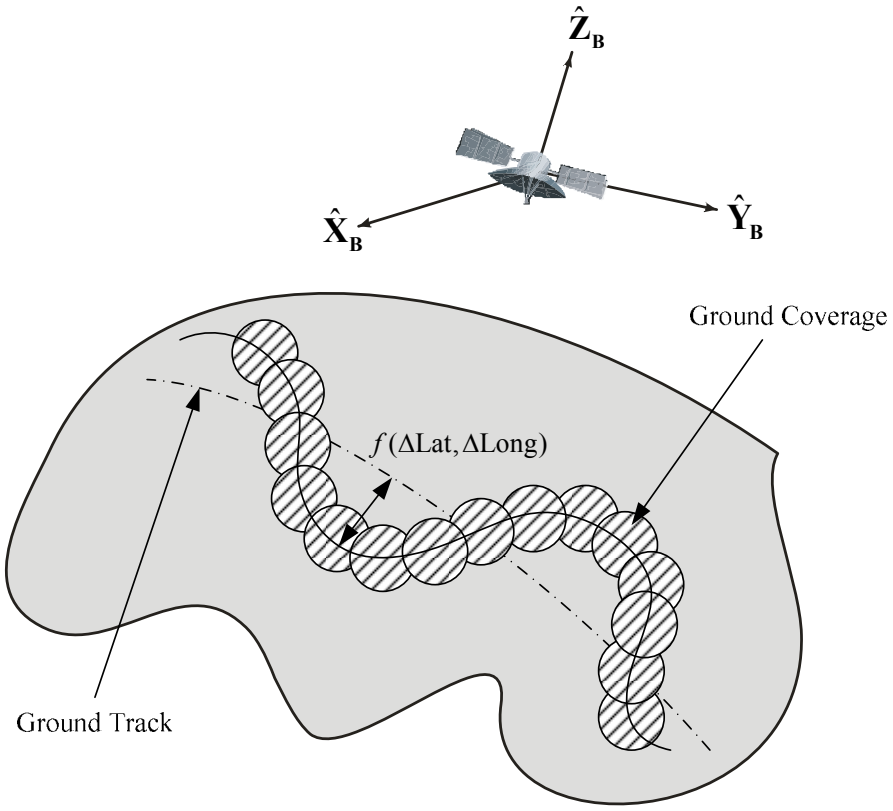

Figure 2.10: Diagram of Trace of Ground Coverage Due to the Satellite Attitude Motion

Thus, if a specific task related to the ground coverage is given to the satellite, the approach used for this research can be applied. One example is simulated for a map-making mission with camera point at the ground on Earth. If the body coordinate system and orbital reference coordinate system are aligned, then there are no Euler angles motions observed and the ground coverage is a straight line with thickness of the image circle depending on the camera's performance. High frequency oscillations provide more coverage on the ground.

Chapter 3

ANALYSIS

3.1 Governing Equations of Motion for a Satellite with Movable Mass

An internal moving mass of a LEO (Low Earth Orbit) satellite under the influence of the Earth's gravity may cause an unexpected attitude change should the mass distribution change. The magnitude of the gravity-gradient torque is small and this environmental disturbance is inevitable in LEO, but this can be used as a passive control method for long term attitude control. A satellite is assumed to be a rigid body for attitude dynamics in most cases, as is the assumption in this research. The system is composed of two parts: the main satellite which is rigid, and a movable mass or masses. This approach expects a more complex computation as a result of the additional terms in the equations. A correct equation must be derived for the internal mass distribution to accommodate the gravity-gradient torque properly.

Both Roberson [39] and Grubin [40] developed the governing equations of motions of a satellite vehicle bearing movable masses. Roberson selected the mass center at the composite center-of-mass of the system. This reference point expects the center-of-mass changes as the mass parts move. Grubin avoided the mass center wandering by locating the reference point of the system at the center-of-mass of the satellite.

The equations of motion of the satellite system with an attached moving mass are developed by Kunciw [41] and Edwards [42]. A brief development is presented below.

In Figure 3.1, $\overline{R}_C$ is the position vector to the composite center-of-mass and $\overline{R}_0$ is to the center-of-mass of the satellite from the inertial coordinate system origin. $\overline{r}_C$ and $\overline{r}$ are vectors to the composite center-of-mass and to the control mass, respectively. The body fixed coordinate system, $\hat{\mathbf{X}}_\mathbf{B}\hat{\mathbf{Y}}_\mathbf{B}\hat{\mathbf{Z}}_\mathbf{B}$, is located at the center-of-mass of the satellite.

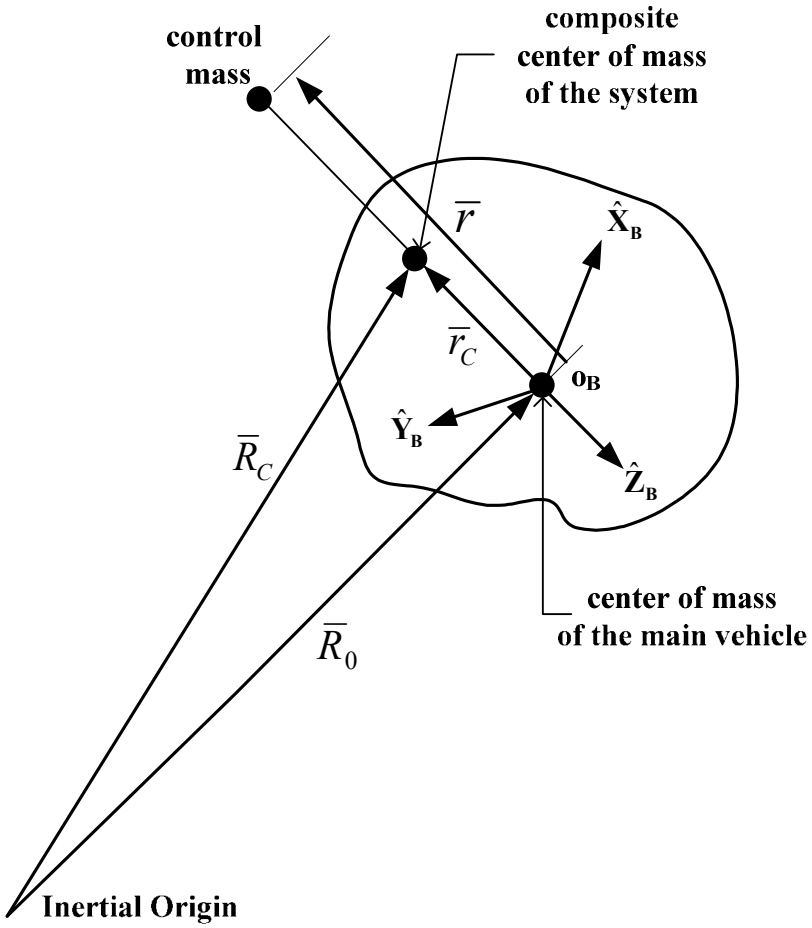

Figure 3.1: Diagram of a Vehicle with a Movable Mass

The equations of motion of the system are given by Edwards [42] as

$$\begin{aligned}&\left[I_x+\mu_C(y^2+z^2)\right]\dot{\varpi}_x+\left[I_z-I_y+\mu_C(y^2-z^2)\right]\varpi_y\varpi_z\\&+\mu_C\left[-xy\dot{\varpi}_y-xz\dot{\varpi}_z+2(y\dot{y}+z\dot{z})\varpi_x+yz(\varpi_z^2-\varpi_y^2)\right.\\&\left.-2\dot{x}y\varpi_y-2\dot{x}z\varpi_z-xz\varpi_x\varpi_y+xy\varpi_x\varpi_z+y\ddot{z}-z\ddot{y}\right]=0\end{aligned}\tag{3.1}$$

$$\begin{aligned}&\left[I_y+\mu_C(z^2+x^2)\right]\dot{\varpi}_y+\left[I_x-I_z+\mu_C(z^2-x^2)\right]\varpi_z\varpi_x\\&+\mu_C\left[-yz\dot{\varpi}_z-yx\dot{\varpi}_x+2(z\dot{z}+x\dot{x})\varpi_y+zx(\varpi_x^2-\varpi_z^2)\right.\\&\left.-2\dot{y}z\varpi_z-2\dot{y}x\varpi_x-yx\varpi_y\varpi_z+yz\varpi_y\varpi_x+z\ddot{x}-x\ddot{z}\right]=0\end{aligned}\tag{3.2}$$

$$\begin{aligned}&\left[I_z+\mu_C(x^2+y^2)\right]\dot{\varpi}_z+\left[I_y-I_x+\mu_C(x^2-y^2)\right]\varpi_x\varpi_y\\&+\mu_C\left[-zx\dot{\varpi}_x-zy\dot{\varpi}_y+2(x\dot{x}+y\dot{y})\varpi_z+xy(\varpi_y^2-\varpi_x^2)\right.\\&\left.-2\dot{z}x\varpi_x-2\dot{z}y\varpi_y-zy\varpi_z\varpi_x+zx\varpi_z\varpi_y+x\ddot{y}-y\ddot{x}\right]=0\end{aligned}\tag{3.3}$$

where $\begin{bmatrix}I_x & I_y & I_z\end{bmatrix}^T$ are the principal moments of inertia of the satellite without the movable mass, $\bar{\varpi}=\begin{bmatrix}\varpi_x & \varpi_y & \varpi_z\end{bmatrix}^T$ are the angular rates, $\begin{bmatrix}x & y & z\end{bmatrix}^T$ is the position vector of the movable mass, and $\begin{bmatrix}\dot{x} & \dot{y} & \dot{z}\end{bmatrix}^T$ and $\begin{bmatrix}\ddot{x} & \ddot{y} & \ddot{z}\end{bmatrix}^T$ are the velocity and the acceleration of the movable mass, respectively. Note that all these quantities are with respect to the body fixed coordinate system. The parameter $\mu_C=\dfrac{M_{\text{mass}}M_{\text{sat}}}{M_{\text{mass}}+M_{\text{sat}}}$ where M_{mass} and M_{sat} are the mass of the movable mass and the satellite's mass, respectively, is used to simplify the equations.

Equations (3.1), (3.2), and (3.3) are the general equations with the assumption of no external torque with continuous mass movement considered. Appendix E presents the

approximate equations after some assumptions are applied such as neglecting the higher order terms and the position of the movable mass is fixed. Starting from this model, a new mass shifting model is designed in next section.

3.2 Mass Shifting Method

Equations (3.1)-(3.3) describe the motion of a satellite with a moving mass without external torque. Since the gravitational force acts as the passive controller, it is necessary to develop equations of motion including torque from environmental torque, which is the gravity gradient. This computation gives the fundamental idea of attitude control by shifting masses of the system.

The governing equations under the influence of the Earth's gravitational force are already given in Equations (2.29)-(2.31). It is known that the roll, pitch, and yaw angles are functions of the moments of inertia of the satellite and mean motion, which is constant for a circular orbit. This means the attitude of a satellite can be changed by changing the moments of inertia of the satellite.

To find the relationship between the moments of inertia and the Euler angles, each component of the moments of inertia and Euler angles can be expressed by two elements, an initial value and a small deviation caused by mass redistribution. Note that the assumptions used for the Equations (2.29)-(2.31) are that the body-fixed coordinate system coincides with the principal axes and the orbit is circular. Then, moments of inertia and Euler angles can be described by:

$$\begin{aligned} I_r &= I_{r_0} + \Delta I_r \\ I_p &= I_{p_0} + \Delta I_p \\ I_y &= I_{y_0} + \Delta I_y \end{aligned} \tag{3.4}$$

$$\begin{aligned} \psi &= \psi_0 + \Delta\psi \\ \theta &= \theta_0 + \Delta\theta \\ \varphi &= \varphi_0 + \Delta\varphi \end{aligned} \tag{3.5}$$

The angular rates of the Euler angles in Equation (3.5) are

$$\begin{aligned} \dot{\psi} &= \dot{\psi}_0 + \Delta\dot{\psi} \\ \dot{\theta} &= \dot{\theta}_0 + \Delta\dot{\theta} \\ \dot{\varphi} &= \dot{\varphi}_0 + \Delta\dot{\varphi} \end{aligned} \tag{3.6}$$

The state vector, $\bar{x}$, is defined as

$$\bar{x} = \begin{bmatrix} \Delta\psi \\ \Delta\theta \\ \Delta\varphi \\ \Delta\dot{\psi} \\ \Delta\dot{\theta} \\ \Delta\dot{\varphi} \end{bmatrix} \tag{3.7}$$

In addition, $\bar{u}$, the control vector, is defined as

$$\bar{u} = \begin{bmatrix} \Delta I_r \\ \Delta I_p \\ \Delta I_y \end{bmatrix} \tag{3.8}$$

The equations of motion can be found by substituting Equations (3.4), (3.5), and (3.6) into Equations (2.29), (2.30), and (2.31) with higher-order terms neglected. All the intermediate steps are found in Appendix F. Those equations can be written in the linearized state space form as:

$$\dot{\bar{x}} = A\bar{x} + B\bar{u} \tag{3.9}$$

Substituting Equations (3.7) and (3.8) into Equations (2.29) - (2.31), yields

$$\dot{\bar{x}} = \begin{bmatrix} \Delta\dot{\psi} \\ \Delta\dot{\theta} \\ \Delta\dot{\varphi} \\ \Delta\ddot{\psi} \\ \Delta\ddot{\theta} \\ \Delta\ddot{\varphi} \end{bmatrix} = \begin{bmatrix} A_{11} & A_{12} \\ A_{21} & A_{22} \end{bmatrix} \begin{bmatrix} \Delta\psi \\ \Delta\theta \\ \Delta\varphi \\ \Delta\dot{\psi} \\ \Delta\dot{\theta} \\ \Delta\dot{\varphi} \end{bmatrix} + \begin{bmatrix} B_{11} \\ B_{21} \end{bmatrix} \begin{bmatrix} \Delta I_r \\ \Delta I_p \\ \Delta I_y \end{bmatrix} \tag{3.10}$$

where

$$A_{11} = \begin{bmatrix} 0 & 0 & 0 \\ 0 & 0 & 0 \\ 0 & 0 & 0 \end{bmatrix}, \qquad A_{12} = \begin{bmatrix} 1 & 0 & 0 \\ 0 & 1 & 0 \\ 0 & 0 & 1 \end{bmatrix}$$

$$A_{21} = \begin{bmatrix} \dfrac{4n^2\left(I_{y_0} - I_{p_0}\right)}{I_{r_0}} & 0 & 0 \\ 0 & \dfrac{3n^2\left(I_{y_0} - I_{r_0}\right)}{I_{p_0}} & 0 \\ 0 & 0 & \dfrac{n^2\left(I_{r_0} - I_{p_0}\right)}{I_{y_0}} \end{bmatrix}$$

$$A_{22}=\begin{bmatrix} 0 & 0 & \dfrac{n\left(I_{p_0}-I_{r_0}-I_{y_0}\right)}{I_{r_0}} \\ 0 & 0 & 0 \\ \dfrac{n\left(I_{r_0}+I_{y_0}-I_{p_0}\right)}{I_{y_0}} & 0 & 0 \end{bmatrix}$$

$$B_{11}=\begin{bmatrix} 0 & 0 & 0 \\ 0 & 0 & 0 \\ 0 & 0 & 0 \end{bmatrix}$$

$$B_{21}=\begin{bmatrix} \dfrac{4n^2\left(I_{p_0}-I_{y_0}\right)\psi_{r_0}+n\left(-I_{p_0}+I_{r_0}\right)\dot{\varphi}_{y_0}}{I_{r_0}^2} & \dfrac{4n^2\psi_{r_0}+n\dot{\varphi}_{y_0}}{I_{r_0}} & \dfrac{4n^2\psi_{r_0}-n\dot{\varphi}_{y_0}}{I_{r_0}} \\ -\dfrac{3n^2\theta_{y_0}}{I_{p_0}} & \dfrac{3n^2\left(I_{r_0}-I_{y_0}\right)\theta_{p_0}}{I_{p_0}^{\ 2}} & \dfrac{3n^2\theta_{p_0}}{I_{p_0}} \\ \dfrac{n\dot{\psi}_{r_0}+n^2\varphi_{y_0}}{I_{y_0}} & -\dfrac{n\dot{\psi}_{r_0}+n^2\varphi_{y_0}}{I_{y_0}} & \dfrac{n\left(I_{p_0}-I_{r_0}\right)\dot{\psi}_{r_0}+n^2\left(I_{p_0}-I_{r_0}\right)\varphi_{y_0}}{I_{y_0}^2} \end{bmatrix}$$

Equation (3.10) presents the change of the Euler angles affected by the change of the principal moments of inertia subject to gravity-gradient torque. However, the body-fixed coordinate system is not always aligned with the principal axis. Thus, the products of inertia terms are not zeros. The control vector can be defined as $\bar{u}=\begin{bmatrix}\Delta I_r & \Delta I_p & \Delta I_y & \Delta I_{rp} & \Delta I_{py} & \Delta I_{ry}\end{bmatrix}^T$. The linearized state space form is developed in Appendix G.

Similarly, the full linearized Euler equations including the gravity gradient, wheel devices, and external moment are given by Sidi [43] as:

$$I_r\ddot{\psi}+4n^2(I_p-I_y)\psi-n(I_p-I_y-I_r)\dot{\varphi}+\dot{h}_{wx}+nh_{wz} \\ -\dot{\varphi}-I_{rp}\ddot{\theta}-I_{ry}\ddot{\varphi}-I_{ry}n^2\varphi-2I_{py}n\dot{\theta}=M_{dr}+M_{cr} \tag{3.11}$$

$$I_p\ddot{\theta}+3n^2(I_r-I_y)\theta+\dot{h}_{wy}-I_{rp}(\ddot{\psi}+2n\dot{\varphi}-n^2\psi) \\ +I_{py}(-\ddot{\varphi}+2n\dot{\psi}+n^2\varphi)=M_{dp}+M_{cp} \tag{3.12}$$

$$I_y\ddot{\varphi}-n(I_y+I_r-I_p)\dot{\psi}+n^2(I_p-I_r)\varphi+\dot{h}_{wz}-nh_{wx} \\ -I_{py}\ddot{\theta}-I_{ry}\ddot{\psi}+2nI_{rp}\dot{\theta}-n^2I_{ry}\psi=M_{dy}+M_{cy} \tag{3.13}$$

In Equations (3.11)-(3.13), $\bar{H}_w=\begin{bmatrix}h_{wx} & h_{wy} & h_{wz}\end{bmatrix}^T$ is the momentum vector of any wheels while the rotating axes are aligned with the body axes. Thus, $h_{wx}=I_{wx}\omega_{wx}$, $h_{wy}=I_{wy}\omega_{wy}$, and $h_{wz}=I_{wz}\omega_{wz}$, where I_{wx}, I_{wy}, and I_{wz} are the principal moments of inertia of the wheel and $\begin{bmatrix}\omega_{wx} & \omega_{wy} & \omega_{wz}\end{bmatrix}^T$ is the angular velocity vector of the wheel with respect to the body. The angular momentum vector generated by the wheel to the satellite body along the body-fixed coordinate system is $\begin{bmatrix}\dot{h}_{wx} & \dot{h}_{wy} & \dot{h}_{wz}\end{bmatrix}^T$. $\bar{M}_c$ and $\bar{M}_d$ represent the control moment from other control actuators and the environmental disturbance, respectively. Differential equations for small angle changes with respect to the control moments and related linearized state equation are presented in Appendix H.

3.3 Mass Distribution System Design

It is found that the moments of inertia change affects the rotating angles and their rates. This means mass shifting inside a satellite system can convert the environmental disturbance into the passive control mechanism. The approach is to find mass distribution

with several movable masses that will change the center-of-mass and moments of inertia affecting the satellite's attitude behavior. This method can be used for controlling the angular velocity and accelerations. Starting from known values of the moments of inertia and angular velocity of the satellite system at stage 1 (before mass shift), a different mass distribution can be calculated for stage 2 (after mass shift) that produces the desired angular behavior.

To examine this concept, six mass tanks are equally distributed along the imaginary sphere illustrated in Figure 3.2. All tanks are assumed to be connected by massless pipes, so the contributions of the pipes to the moments of inertia are ignored. Two imaginary planes are placed on this sphere (analogous to the Earth's equator and the plane separating the eastern and western hemispheres). Tanks are placed 90 degrees apart on each plane, with tanks located at the intersection of these two planes. Each tank is assumed to have the same capacity, all have the same dry mass, and all are located at the same distance from the center of the spacecraft. Adjacent tanks can transfer mass through the massless pipes connecting each other. It is also assumed that the mass shifting occurs instantaneously. Thus the angular momentum is conserved without applied external torque and the angular velocity immediately before the mass transfer is the initial angular velocity immediately after transfer completion.

From this fundamental model, a more complicated model with other control actuators can be developed and the related governing equations of motion and control laws would need to be derived. Also, the feasibility of this system to achieve both attitude maneuvers and maintain stability is important for actual application. Comparing the

values from position sensors with data after maneuvering may be repeated until its task is satisfied. Finally, an optimal solution can be computed for attitude determination.

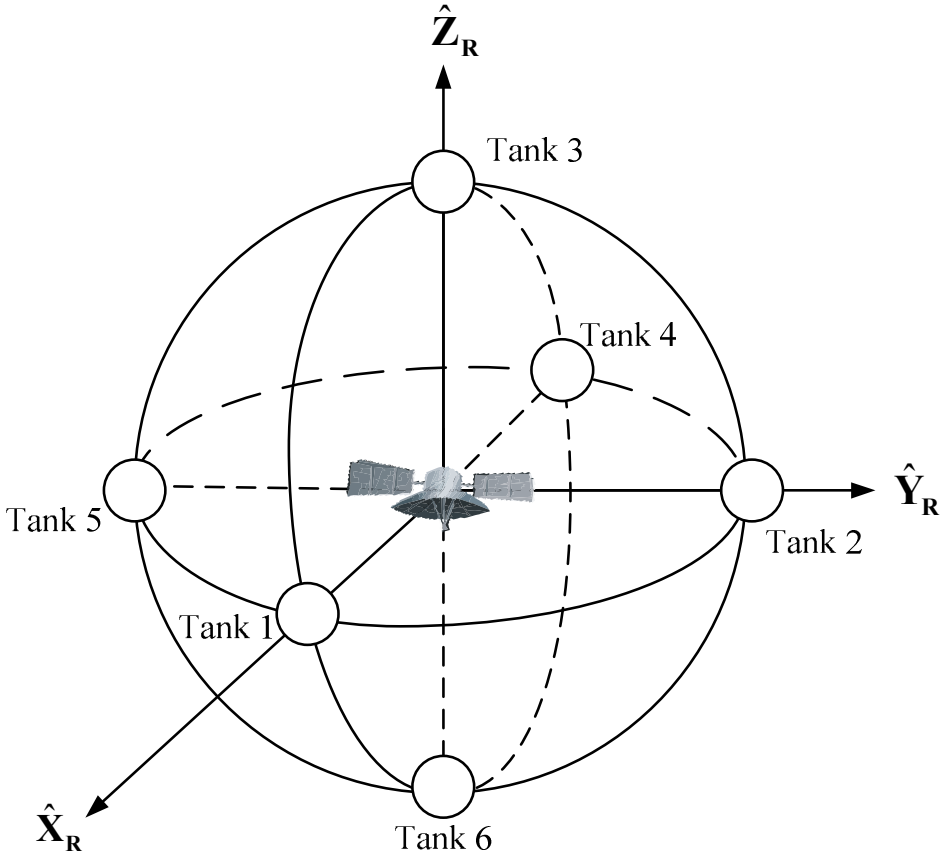

Figure 3.2: Configuration of the Satellite System with 6 Mass Tanks

To evaluate this problem, two models are developed. The first model analyzes the rotational motion using Euler's equations of motion for a rotating system. In these equations of motion, the contribution to the moments of inertia is broken down between the "dry" satellite and the liquid that is available for transfer between the tanks. The second model solves the optimal mass transfer problem by determining how to shift mass

from one configuration to another. Given an initial configuration and a final desired configuration, the optimal path to shift mass from one configuration to another is demonstrated.

3.4 Developing Dynamic and Control Equations

The moments of inertia of the whole system consists of two parts, the satellite's moment of inertia, I_{sat}, which is not changing over time; and the mass system operated by moving mass in order to change its own moments of inertia, I_{mass}. By assuming the body fixed axes of the dry satellite to be aligned with the principal axes, the moment of inertia matrix for the satellite is given by

$$I_{\text{sat}} = \begin{bmatrix} I_{\text{sat}_r} & 0 & 0 \\ 0 & I_{\text{sat}_p} & 0 \\ 0 & 0 & I_{\text{sat}_y} \end{bmatrix} \tag{3.14}$$

where the subscriptions r, p, and y represent the roll, pitch, and yaw axes, respectively. From the definition of the moment of inertia matrix, Equation (3.15) is calculated for this design with the assumption of the location of tanks.

$$I_{\text{mass}} = \begin{bmatrix} \sum_{k=1}^{6} m_k (y_k^2 + z_k^2) & -\sum_{k=1}^{6} m_k x_k y_k & -\sum_{k=1}^{6} m_k x_k z_k \\ -\sum_{k=1}^{6} m_k x_k y_k & \sum_{k=1}^{6} m_k (x_k^2 + z_k^2) & -\sum_{k=1}^{6} m_k y_k z_k \\ -\sum_{k=1}^{6} m_k x_k z_k & -\sum_{k=1}^{6} m_k y_k z_k & \sum_{k=1}^{6} m_k (x_k^2 + y_k^2) \end{bmatrix} \tag{3.15}$$
$$= \begin{bmatrix} I_{\text{mass}_r} & 0 & 0 \\ 0 & I_{\text{mass}_p} & 0 \\ 0 & 0 & I_{\text{mass}_y} \end{bmatrix}$$

where I_{mass_r}, I_{mass_p}, and I_{mass_y} are computed as:

$$\begin{aligned} I_{\text{mass}_r} &= d^2 (m_2 + m_3 + m_5 + m_6) \\ I_{\text{mass}_p} &= d^2 (m_1 + m_3 + m_4 + m_6) \\ I_{\text{mass}_y} &= d^2 (m_1 + m_2 + m_4 + m_5) \end{aligned} \tag{3.16}$$

where *d* is radius of the sphere. All products of inertia vanish with the assumption that each tank lies along a principal axis. In general, the total principal moments of inertia are simply found by adding Equations (3.14) and (3.15). However, the center-of-mass changes as mass moves, thus the new center-of-mass must be updated after every mass shift. The new center-of-mass in the body coordinate system in Figure 3.2 at each time when the mass moves from one tank to another is

$$d \begin{bmatrix} \frac{m_1 - m_4}{m_1 + m_4} & \frac{m_2 - m_5}{m_2 + m_5} & \frac{m_3 - m_6}{m_3 + m_6} \end{bmatrix} \tag{3.17}$$

Equation (3.18) represents the amount of changed moment of inertia after the mass redistribution. Since it is a symmetric matrix, three real eigenvalues exist and the corresponding eigenvectors compose an orthogonal basis. In addition, the three eigenvalues are the principal moments of inertia, and the eigenvectors form the direction cosine matrix that relates the new reference frame to the old reference frame.

From the definition of the moment of inertia, the controllable amount of moment of inertia by adding mass to the tanks or changing the location of the tanks are calculated by substituting $I = I_0 + \Delta I$, $m = m_0 + \Delta m$, $x = x_0 + \Delta x$, $y = y_0 + \Delta y$, $z = z_0 + \Delta z$.

$$I_{\text{mass}} + \Delta I_{\text{mass}} = \begin{bmatrix} I_{11} & I_{12} & I_{13} \\ I_{21} & I_{22} & I_{23} \\ I_{31} & I_{32} & I_{33} \end{bmatrix} \tag{3.18}$$

where

$$I_{11} = \sum_{k=1}^{6} (m_k + \Delta m_k)\left[(y_k + \Delta y_k)^2 + (z_k + \Delta z_k)^2 \right]$$

$$I_{22} = \sum_{k=1}^{6} (m_k + \Delta m_k)\left[(x_k + \Delta x_k)^2 + (z_k + \Delta z_k)^2 \right]$$

$$I_{33} = \sum_{k=1}^{6} (m_k + \Delta m_k)\left[(x_k + \Delta x_k)^2 + (y_k + \Delta y_k)^2 \right]$$

$$I_{12} = I_{21} = -\sum_{k=1}^{6} (m_k + \Delta m_k)(x_k + \Delta x_k)(y_k + \Delta y_k)$$

$$I_{13} = I_{31} = -\sum_{k=1}^{6} (m_k + \Delta m_k)(x_k + \Delta x_k)(z_k + \Delta z_k)$$

$$I_{23} = I_{32} = -\sum_{k=1}^{6} (m_k + \Delta m_k)(y_k + \Delta y_k)(z_k + \Delta z_k)$$

Finally, the control moment of inertia is occurred only on the mass system and is given as:

$$\Delta I = \Delta I_{\text{mass}} = \begin{bmatrix} \Delta I_r & \Delta I_{rp} & \Delta I_{ry} \\ \Delta I_{pr} & \Delta I_p & \Delta I_{py} \\ \Delta I_{yr} & \Delta I_{yp} & \Delta I_y \end{bmatrix} \tag{3.19}$$

where

$$\Delta I_r \cong \sum_{k=1}^{6} \left[2m_k (y_k \Delta y_k + z_k \Delta z_k) + \Delta m_k (y_k^2 + z_k^2) \right]$$

$$\Delta I_p \cong \sum_{k=1}^{6} \left[2m_k (x_k \Delta x_k + z_k \Delta z_k) + \Delta m_k (x_k^2 + z_k^2) \right]$$

$$\Delta I_y \cong \sum_{k=1}^{6} \left[2m_k (x_k \Delta x_k + y_k \Delta y_k) + \Delta m_k (x_k^2 + y_k^2) \right]$$

$$\Delta I_{rp} = \Delta I_{pr} \cong -\sum_{k=1}^{6} (\Delta m_k x_k y_k + m_k \Delta x_k y_k + m_k x_k \Delta y_k)$$

$$\Delta I_{ry} = \Delta I_{yr} \cong -\sum_{k=1}^{6} (\Delta m_k x_k z_k + m_k \Delta x_k z_k + m_k x_k \Delta z_k)$$

$$\Delta I_{py} = \Delta I_{yp} \cong -\sum_{k=1}^{6} (\Delta m_k y_k z_k + m_k \Delta y_k z_k + m_k y_k \Delta z_k)$$

(This is an approximated solution since higher-order terms are dropped).

Recall that the total moments of inertia are the summation of the satellite's moment of inertia and moving masses' moments of inertia. Since the satellite's moment of inertia remains unchanged, the moment of inertia change comes from the change in moments of inertia of moving masses.

$$\begin{aligned} I &= I_{\text{sat}} + I_{\text{mass}} \\ I + \Delta I &= I_{\text{sat}} + (I_{\text{mass}} + \Delta I_{\text{mass}}) \end{aligned} \tag{3.20}$$

Note that no external torque acts during the mass shifting, thus the angular momentum is conserved, as seen in Equation (3.21).

$$\left(I_{\text{sat}} + I_{\text{mass}}\right)\bar{\omega}_1 = \left(I_{\text{sat}} + I_{\text{mass}} + \Delta I_{\text{mass}}\right)\bar{\omega}_2 \tag{3.21}$$

where $\bar{\omega}_1$ and $\bar{\omega}_2$ are the angular velocities at stage 1 and stage 2, respectively.

Coinciding the origin of two different systems, a dry satellite and a tank system, helps avoid the appearance of the products of inertia. This assumption can be easily made by the center-of-mass of the tank system staying at the center of the satellite which is Equation (3.17) and is equal to the zero vector. Starting from a simple design (case 1 through case 4) without changing the center-of-mass of the tank system, a general equation (case 4) including the mass center change is developed.

Case 1 Each tank is moving along each axis without mass transfer;

Conditions: $\Delta m_k = 0 \;\; (k = 1,...,6)$

Since the moment of inertia is a function of the mass and the distance from the reference point, this property introduces case 1, which is each tank moves along each axis without changing its amount of mass. This means that if any pair of tanks (tank1 and tank 4, tank 2 and tank 5, tank 3 and tank 6) are located on the one straight line with same

distance from the origin but in the opposite direction, both center-of-mass principal axes remain unchanged. Thus, the constraints for case 1 is that mass 1 and mass 4 move only along the roll axis, mass 2 and mass 5 along the pitch axis, and mass 3 and mass 6 along the yaw axis. Equation (3.22) presents the total moments of inertia at stage 1.

$$
\begin{aligned}
I &= I_{\text{sat}} + I_{\text{mass}} \\
&= \begin{bmatrix} I_{\text{sat}_r} & 0 & 0 \\ 0 & I_{\text{sat}_p} & 0 \\ 0 & 0 & I_{\text{sat}_y} \end{bmatrix} + \begin{bmatrix} I_{\text{mass}_r} & 0 & 0 \\ 0 & I_{\text{mass}_p} & 0 \\ 0 & 0 & I_{\text{mass}_y} \end{bmatrix} \\
&= \begin{bmatrix} I_{\text{sat}_r} + 4d(m_2 y + m_3 z) & 0 & 0 \\ 0 & I_{\text{sat}_p} + 4d(m_1 x + m_3 z) & 0 \\ 0 & 0 & I_{\text{sat}_y} + 4d(m_1 x + m_2 y) \end{bmatrix}
\end{aligned}
\tag{3.22}
$$

The controllable moment of inertia of is computed by (3.19):

$$
\Delta I = \begin{bmatrix} 4d(m_2 \Delta y + m_3 \Delta z) & 0 & 0 \\ 0 & 4d(m_1 \Delta x + m_3 \Delta z) & 0 \\ 0 & 0 & 4d(m_1 \Delta x + m_2 \Delta y) \end{bmatrix} \tag{3.23}
$$

Case 2 Masses are moving while the tank locations are fixed;

Conditions: $\Delta x = \Delta y = \Delta z = 0$, $m_1 = m_4$, $m_2 = m_5$, $m_3 = m_6$

As stated in case 1, the moment of inertia is the function of the mass and the distance from the reference point which is the location of each tank. Contrary to case 1, the constraint for case 2 is to change the mass in each tank while the tank location is fixed.

For the same reason as in case 1, the mass pairs of tank 1 and tank 4, tank 2 and tank 5, tank 3 and tank 6 must be the same amount after mass shifting. Then the change of moment of inertia is computed in Equation (3.24). Compared with Equation (3.23), mass changes terms are presented instead of tank location changes.

$$\Delta I = \begin{bmatrix} 2d^2(\Delta m_2 + \Delta m_3) & 0 & 0 \\ 0 & 2d^2(\Delta m_1 + \Delta m_3) & 0 \\ 0 & 0 & 2d^2(\Delta m_1 + \Delta m_2) \end{bmatrix} \tag{3.24}$$

Case 3 Mass locations move along each axis and the masses are changing;

Conditions: $m_1 = m_4$, $m_2 = m_5$, $m_3 = m_6$

Case 3 is a combination of case 1 and case 2. If one component of the moment of inertia needs to be increased, three options are available: moving pair masses away from the origin (case 1), increasing mass (case 2), or performing both at the same time (case 3). Then ΔI is the summation of Equations (3.23) and (3.24).

$$\Delta I = \begin{bmatrix} 2d^2(\Delta m_2 + \Delta m_3) + 4d(m_2\Delta y + m_3\Delta z) & 0 & 0 \\ 0 & 2d^2(\Delta m_1 + \Delta m_3) + 4d(m_1\Delta x + m_3\Delta z) & 0 \\ 0 & 0 & 2d^2(\Delta m_1 + \Delta m_2) + 4d(m_1\Delta x + m_2\Delta y) \end{bmatrix} \tag{3.25}$$

Case 4 Tank locations are moving in any direction and masses are changing;

Conditions: $m_1 = m_4$, $m_2 = m_5$, $m_3 = m_6$

A complete controllable moment of inertia for any location of masses without changing the center-of-mass after mass shifting can be calculated by computing Equation (3.19). Two restrictions must be considered. The mass pair must have same amount mass in each tank and lie in the same straight line with same distance from the origin but in opposite directions. If the position vector of mass 1 is $\begin{bmatrix} x_1 & y_1 & z_1 \end{bmatrix}^T$, then the location of mass 4 is automatically determined as $\begin{bmatrix} -x_1 & -y_1 & -z_1 \end{bmatrix}^T$.

Cases 1 through 3 keep the center-of-mass at the same center-of-mass of the satellite with strict restrictions to avoid the appearance of products of inertia. However, case 4 considers masses that are allowed to move free of the rotating axis, thus the products of inertia terms are shown in this case. Bang [44] used a product of inertia to control for a bias momentum in a spacecraft. With this restriction, Equation (3.19) results.

$$\Delta I = \begin{bmatrix} 4[m_1(y_1\Delta y_1 + z_1\Delta z_1) + \\ m_2(y_2\Delta y_2 + z_2\Delta z_2) + \\ m_3(y_3\Delta y_3 + z_3\Delta z_3)] + \\ 2[\Delta m_1(y_1^2 + z_1^2) + \\ \Delta m_2(y_2^2 + z_2^2) + \\ \Delta m_3(y_3^2 + z_3^2)] \end{bmatrix} & \begin{bmatrix} -2(\Delta m_1 x_1 y_1 + m_1 \Delta x_1 y_1 \\ + m_1 x_1 \Delta y_1 + \Delta m_2 x_2 y_2 \\ + m_2 \Delta x_2 y_2 + m_2 x_2 \Delta y_2 \\ + \Delta m_3 x_3 y_3 + m_3 \Delta x_3 y_3 \\ + m_3 x_3 \Delta y_3) \end{bmatrix} & \begin{bmatrix} -2(\Delta m_1 x_1 z_1 + m_1 \Delta x_1 z_1 \\ + m_1 x_1 \Delta z_1 + \Delta m_2 x_2 z_2 \\ + m_2 \Delta x_2 z_2 + m_2 x_2 \Delta z_2 \\ + \Delta m_3 x_3 z_3 + m_3 \Delta x_3 z_3 \\ + m_3 x_3 \Delta z_3) \end{bmatrix} \\ \begin{bmatrix} -2(\Delta m_1 x_1 y_1 + m_1 \Delta x_1 y_1 \\ + m_1 x_1 \Delta y_1 + \Delta m_2 x_2 y_2 \\ + m_2 \Delta x_2 y_2 + m_2 x_2 \Delta y_2 \\ + \Delta m_3 x_3 y_3 + m_3 \Delta x_3 y_3 \\ + m_3 x_3 \Delta y_3) \end{bmatrix} & \begin{bmatrix} 4[m_1(x_1\Delta x_1 + z_1\Delta z_1) + \\ m_2(x_2\Delta x_2 + z_2\Delta z_2) + \\ m_3(x_3\Delta x_3 + z_3\Delta z_3)] + \\ 2[\Delta m_1(x_1^2 + z_1^2) + \\ \Delta m_2(x_2^2 + z_2^2) + \\ \Delta m_3(x_3^2 + z_3^2)] \end{bmatrix} & \begin{bmatrix} -2(\Delta m_1 y_1 z_1 + m_1 \Delta y_1 z_1 \\ + m_1 y_1 \Delta z_1 + \Delta m_2 y_2 z_2 \\ + m_2 \Delta y_2 z_2 + m_2 y_2 \Delta z_2 \\ + \Delta m_3 y_3 z_3 + m_3 \Delta y_3 z_3 \\ + m_3 y_3 \Delta z_3) \end{bmatrix} \\ \begin{bmatrix} -2(\Delta m_1 x_1 z_1 + m_1 \Delta x_1 z_1 \\ + m_1 x_1 \Delta z_1 + \Delta m_2 x_2 z_2 \\ + m_2 \Delta x_2 z_2 + m_2 x_2 \Delta z_2 \\ + \Delta m_3 x_3 z_3 + m_3 \Delta x_3 z_3 \\ + m_3 x_3 \Delta z_3) \end{bmatrix} & \begin{bmatrix} -2(\Delta m_1 y_1 z_1 + m_1 \Delta y_1 z_1 \\ + m_1 y_1 \Delta z_1 + \Delta m_2 y_2 z_2 \\ + m_2 \Delta y_2 z_2 + m_2 y_2 \Delta z_2 \\ + \Delta m_3 y_3 z_3 + m_3 \Delta y_3 z_3 \\ + m_3 y_3 \Delta z_3) \end{bmatrix} & \begin{bmatrix} 4[m_1(x_1\Delta x_1 + y_1\Delta y_1) + \\ m_2(x_2\Delta x_2 + y_2\Delta y_2) + \\ m_3(x_3\Delta x_3 + y_3\Delta y_3)] + \\ 2[\Delta m_1(x_1^2 + y_1^2) + \\ \Delta m_2(x_2^2 + y_2^2) + \\ \Delta m_3(x_3^2 + y_3^2)] \end{bmatrix} \end{bmatrix} \tag{3.26}$$

From Equation (3.26), a general equation for *n* pairs of masses can be computed. Suppose 2*n* masses are arbitrarily distributed satisfying the two conditions: (1) the masses m_a (a=1, 2,…, n) and m_{n+a} are the pair masses and their corresponding locations are expressed by $\begin{bmatrix} x_a & y_a & z_a \end{bmatrix}^T$ and $\begin{bmatrix} -x_a & -y_a & -z_a \end{bmatrix}^T$, respectively; (2) m_a has same mass as m_{n+a}. Then, Equation (3.27) is computed.

$$\Delta I = \begin{bmatrix} \Delta I_{11} & \Delta I_{12} & \Delta I_{13} \\ \Delta I_{21} & \Delta I_{22} & \Delta I_{23} \\ \Delta I_{31} & \Delta I_{32} & \Delta I_{33} \end{bmatrix} \tag{3.27}$$

where

$$\Delta I_{11} \cong 4\sum_{i=1}^{n}(m_i y_i \Delta y_i + z_i \Delta z_i) + 2\sum_{i=1}^{n}\Delta m_i (y_i^2 + z_i^2)$$

$$\Delta I_{22} \cong 4\sum_{i=1}^{n}(m_i x_i \Delta x_i + z_i \Delta z_i) + 2\sum_{i=1}^{n}\Delta m_i (x_i^2 + z_i^2)$$

$$\Delta I_{33} \cong 4\sum_{i=1}^{n}(m_i x_i \Delta x_i + y_i \Delta y_i) + 2\sum_{i=1}^{n}\Delta m_i (x_i^2 + y_i^2)$$

$$\Delta I_{13} = \Delta I_{31} \cong -2\sum_{i=1}^{n}(\Delta m_i x_i z_i + m_i \Delta x_i z_i + m_i x_i \Delta z_i)$$

$$\Delta I_{12} = \Delta I_{21} \cong -2\sum_{i=1}^{n}(\Delta m_i x_i y_i + m_i \Delta x_i y_i + m_i x_i \Delta y_i)$$

$$\Delta I_{23} = \Delta I_{32} \cong -2\sum_{i=1}^{n}(\Delta m_i y_i z_i + m_i \Delta y_i z_i + m_i y_i \Delta z_i)$$

Case 5 Center-of-mass is changing due to the moving masses;

Condition: no restriction

To take an advantage of not moving the center-of-mass, all previous cases used different restrictions such as mass can move only in one direction except for case 4 or the positions of a pair of masses must be symmetric to the origin. These restrictions require less computational time than the case considering center of mass change.

To investigate a general case while masses are distributed arbitrary, thus affecting center of mass shifting, the configuration of the six tanks is considered. The locations of the six tanks are fixed but the liquid mass can travel to any adjacent tank. This mass transfer may cause an asymmetric mass distribution and result a center of mass shift. Once the center of mass has been changed, the moment of inertia of both satellite system

and tank system must be recalculated. The parallel axis theorem is useful to compute the new moment of inertia matrix of the satellite. With a known new center-of-mass, the moment of inertia of the mass system can be calculated from the new mass distribution.

The change of moment of inertia of the satellite must be added to Equation (3.20). That is, the inertia tensor becomes

$$\begin{aligned} I &= I_{\text{sat}} + I_{\text{mass}} \\ I + \Delta I &= (I_{\text{sat}} + \Delta I_{\text{sat}}) + (I_{\text{mass}} + \Delta I_{\text{mass}}) \\ \Delta I &= \Delta I_{\text{sat}} + \Delta I_{\text{mass}} \end{aligned} \tag{3.28}$$

No external torque is applied during the mass shifting, thus the angular momentum is conserved as seen in Equation (3.29).

$$\left(I_{\text{sat}_1} + I_{\text{mass}_1}\right)\bar{\omega}_1 = \left(I_{\text{sat}_2} + I_{\text{mass}_2}\right)\bar{\omega}_2 \tag{3.29}$$

where the subscripts 1 and 2 represents stage 1 and stage 2, respectively.

The new center-of-mass for a random mass distribution is computed in Equation (3.17) as $d\begin{bmatrix} \frac{m_1 - m_4}{m_1 + m_4} & \frac{m_2 - m_5}{m_2 + m_5} & \frac{m_3 - m_6}{m_3 + m_6} \end{bmatrix}$ and both I_{sat_2} and I_{mass_2} must be calculated from this reference point. Define a vector, $\bar{d}$, a displacement vector from the center-of-mass at stage 1 to the center-of-mass at stage 2. Then, the parallel axis theorem can be expressed as:

$$I_{\text{sat}_2} = I_{\text{sat}_1} + M_{\text{sat}}[(\bar{d} \cdot \bar{d})I_{3\times 3} - \bar{d} \otimes \bar{d}] \tag{3.30}$$

where M_{sat} is the mass of the dry satellite and $I_{3\times3}$ is 3×3 identity matrix and $\otimes$ denotes the outer product. Substituting $\bar{d} = d\begin{bmatrix} \frac{m_1 - m_4}{m_1 + m_4} & \frac{m_2 - m_5}{m_2 + m_5} & \frac{m_3 - m_6}{m_3 + m_6} \end{bmatrix}^T$ into Equation (3.30) yields

$$
\begin{aligned}
I_{\text{sat}_2} &= I_{\text{sat}_1} + M_{\text{sat}}[(\bar{d}\cdot\bar{d})I_{3\times3} - \bar{d}\otimes\bar{d}] \\
&= I_{\text{sat}_1} + M_{\text{sat}}d^2\left[\left(\left(\frac{m_1 - m_4}{m_1 + m_4}\right)^2 + \left(\frac{m_2 - m_5}{m_2 + m_5}\right)^2 + \left(\frac{m_3 - m_6}{m_3 + m_6}\right)^2\right)\begin{bmatrix} 1 & 0 & 0 \\ 0 & 1 & 0 \\ 0 & 0 & 1 \end{bmatrix}\right. \\
&\left. - \begin{bmatrix} \left(\frac{m_1 - m_4}{m_1 + m_4}\right)^2 & \left(\frac{m_1 - m_4}{m_1 + m_4}\right)\left(\frac{m_2 - m_5}{m_2 + m_5}\right) & \left(\frac{m_1 - m_4}{m_1 + m_4}\right)\left(\frac{m_3 - m_6}{m_3 + m_6}\right) \\ \left(\frac{m_2 - m_5}{m_2 + m_5}\right)\left(\frac{m_1 - m_4}{m_1 + m_4}\right) & \left(\frac{m_2 - m_5}{m_2 + m_5}\right)^2 & \left(\frac{m_2 - m_5}{m_2 + m_5}\right)\left(\frac{m_3 - m_6}{m_3 + m_6}\right) \\ \left(\frac{m_3 - m_6}{m_3 + m_6}\right)\left(\frac{m_1 - m_4}{m_1 + m_4}\right) & \left(\frac{m_3 - m_6}{m_3 + m_6}\right)\left(\frac{m_2 - m_5}{m_2 + m_5}\right) & \left(\frac{m_3 - m_6}{m_3 + m_6}\right)^2 \end{bmatrix}\right]
\end{aligned}
\tag{3.31}
$$

The moment of inertia matrix of the moving mass for stage 2, I_{mass_2}, is computed by the definition of the moment of inertia given in Equation (3.15) with respect to the new center-of-mass and computed as:

$$
I_{\text{mass}_2} = \begin{bmatrix} I_{\text{mass}_r} & I_{\text{mass}_{rp}} & I_{\text{mass}_{ry}} \\ I_{\text{mass}_{pr}} & I_{\text{mass}_p} & I_{\text{mass}_{py}} \\ I_{\text{mass}_{yr}} & I_{\text{mass}_{yp}} & I_{\text{mass}_y} \end{bmatrix} \tag{3.32}
$$

where

$$I_{\text{mass}_r} =$$
$$d^2\left[m_1\left[\left(0-\frac{m_2-m_5}{m_2+m_5}\right)^2+\left(0-\frac{m_3-m_6}{m_3+m_6}\right)^2\right]+m_2\left[\left(1-\frac{m_2-m_5}{m_2+m_5}\right)^2+\left(0-\frac{m_3-m_6}{m_3+m_6}\right)^2\right]\right.$$
$$+m_3\left[\left(0-\frac{m_2-m_5}{m_2+m_5}\right)^2+\left(1-\frac{m_3-m_6}{m_3+m_6}\right)^2\right]+m_4\left[\left(0-\frac{m_2-m_5}{m_2+m_5}\right)^2+\left(0-\frac{m_3-m_6}{m_3+m_6}\right)^2\right]$$
$$\left.+m_5\left[\left(-1-\frac{m_2-m_5}{m_2+m_5}\right)^2+\left(0-\frac{m_3-m_6}{m_3+m_6}\right)^2\right]+m_6\left[\left(0-\frac{m_2-m_5}{m_2+m_5}\right)^2+\left(-1-\frac{m_3-m_6}{m_3+m_6}\right)^2\right]\right]$$

$$I_{\text{mass}_p} =$$
$$d^2\left[m_1\left[\left(1-\frac{m_1-m_4}{m_1+m_4}\right)^2+\left(0-\frac{m_3-m_6}{m_3+m_6}\right)^2\right]+m_2\left[\left(0-\frac{m_1-m_4}{m_1+m_4}\right)^2+\left(0-\frac{m_3-m_6}{m_3+m_6}\right)^2\right]\right.$$
$$+m_3\left[\left(0-\frac{m_1-m_4}{m_1+m_4}\right)^2+\left(1-\frac{m_3-m_6}{m_3+m_6}\right)^2\right]+m_4\left[\left(-1-\frac{m_1-m_4}{m_1+m_4}\right)^2+\left(0-\frac{m_3-m_6}{m_3+m_6}\right)^2\right]$$
$$\left.+m_5\left[\left(0-\frac{m_1-m_4}{m_1+m_4}\right)^2+\left(0-\frac{m_3-m_6}{m_3+m_6}\right)^2\right]+m_6\left[\left(0-\frac{m_1-m_4}{m_1+m_4}\right)^2+\left(-1-\frac{m_3-m_6}{m_3+m_6}\right)^2\right]\right]$$

$$I_{\text{mass}_y} =$$
$$d^2\left[m_1\left[\left(1-\frac{m_1-m_4}{m_1+m_4}\right)^2+\left(0-\frac{m_2-m_5}{m_2+m_5}\right)^2\right]+m_2\left[\left(0-\frac{m_1-m_4}{m_1+m_4}\right)^2+\left(1-\frac{m_2-m_5}{m_2+m_5}\right)^2\right]\right.$$
$$+m_3\left[\left(0-\frac{m_1-m_4}{m_1+m_4}\right)^2+\left(0-\frac{m_2-m_5}{m_2+m_5}\right)^2\right]+m_4\left[\left(-1-\frac{m_1-m_4}{m_1+m_4}\right)^2+\left(0-\frac{m_2-m_5}{m_2+m_5}\right)^2\right]$$
$$\left.+m_5\left[\left(0-\frac{m_1-m_4}{m_1+m_4}\right)^2+\left(-1-\frac{m_2-m_5}{m_2+m_5}\right)^2\right]+m_6\left[\left(0-\frac{m_1-m_4}{m_1+m_4}\right)^2+\left(0-\frac{m_2-m_5}{m_2+m_5}\right)^2\right]\right]$$

$$I_{\text{mass}_{rp}} = -d^2\left[m_1\left(1-\frac{m_1-m_4}{m_1+m_4}\right)\left(0-\frac{m_2-m_5}{m_2+m_5}\right)+m_2\left(0-\frac{m_1-m_4}{m_1+m_4}\right)\left(1-\frac{m_2-m_5}{m_2+m_5}\right)\right.$$
$$m_3\left(0-\frac{m_1-m_4}{m_1+m_4}\right)\left(0-\frac{m_2-m_5}{m_2+m_5}\right)+m_4\left(-1-\frac{m_1-m_4}{m_1+m_4}\right)\left(0-\frac{m_2-m_5}{m_2+m_5}\right)$$
$$\left. m_5\left(0-\frac{m_1-m_4}{m_1+m_4}\right)\left(-1-\frac{m_2-m_5}{m_2+m_5}\right)+m_6\left(0-\frac{m_1-m_4}{m_1+m_4}\right)\left(0-\frac{m_2-m_5}{m_2+m_5}\right)\right]$$

$$I_{\text{mass}_{ry}} = -d^2\left[m_1\left(1-\frac{m_1-m_4}{m_1+m_4}\right)\left(0-\frac{m_3-m_6}{m_3+m_6}\right)+m_2\left(0-\frac{m_1-m_4}{m_1+m_4}\right)\left(0-\frac{m_3-m_6}{m_3+m_6}\right)\right.$$
$$m_3\left(0-\frac{m_1-m_4}{m_1+m_4}\right)\left(1-\frac{m_3-m_6}{m_3+m_6}\right)+m_4\left(-1-\frac{m_1-m_4}{m_1+m_4}\right)\left(0-\frac{m_3-m_6}{m_3+m_6}\right)$$
$$\left. m_5\left(0-\frac{m_1-m_4}{m_1+m_4}\right)\left(0-\frac{m_3-m_6}{m_3+m_6}\right)+m_6\left(0-\frac{m_1-m_4}{m_1+m_4}\right)\left(-1-\frac{m_3-m_6}{m_3+m_6}\right)\right]$$

$$I_{\text{mass}_{py}} = -d^2\left[m_1\left(0-\frac{m_2-m_5}{m_2+m_5}\right)\left(0-\frac{m_3-m_6}{m_3+m_6}\right)+m_2\left(1-\frac{m_2-m_5}{m_2+m_5}\right)\left(0-\frac{m_3-m_6}{m_3+m_6}\right)\right.$$
$$m_3\left(0-\frac{m_2-m_5}{m_2+m_5}\right)\left(1-\frac{m_3-m_6}{m_3+m_6}\right)+m_4\left(0-\frac{m_2-m_5}{m_2+m_5}\right)\left(0-\frac{m_3-m_6}{m_3+m_6}\right)$$
$$\left. m_5\left(-1-\frac{m_2-m_5}{m_2+m_5}\right)\left(0-\frac{m_3-m_6}{m_3+m_6}\right)+m_6\left(0-\frac{m_2-m_5}{m_2+m_5}\right)\left(-1-\frac{m_3-m_6}{m_3+m_6}\right)\right]$$

As expected from case 4, the products of inertia components in both matrices appear. This implies that the control vector has six elements instead of three. Equations (3.31) and (3.32) may be used for a system equipped with other actuators, environmental disturbances, or external torques combined as given in Equation (H.4) in Appendix H.

Once the state vector, $\bar{x}(t)$, is obtained, then the observation vector can be determined as necessary. For this dissertation, the deviation of latitude and longitude due to the satellite's Euler angles is examined. When a satellite is pointing at a target that is

not in the nadir direction, the deviation angle, $\Delta\sigma$, from the satellite can be expressed by the Earth's central angle, $\Delta\lambda$. A diagram for the angular relationship between the satellite and the Earth is illustrated in Figure 3.3.

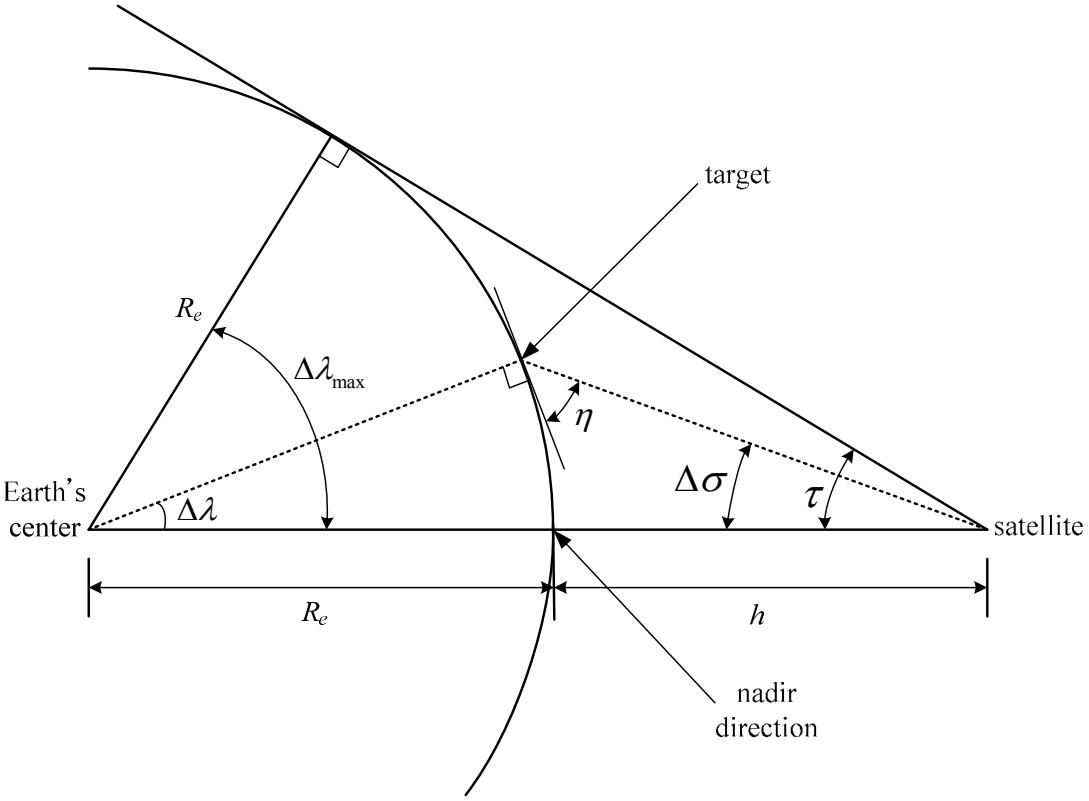

Figure 3.3: Angular Relationships between Satellite and Earth [45]

Then the following equations are satisfied with known value of $\Delta\sigma$.

$$\sin\tau = \cos\Delta\lambda_{\max} = \frac{R_e}{R_e + h} \tag{3.33}$$

$$\cos\eta = \frac{\sin\Delta\sigma}{\sin\tau} \tag{3.34}$$

where η is the satellite elevation angle. Then, the Earth's central angle, $\Delta\lambda$, is computed from

$$\Delta\lambda = \frac{\pi}{2} - \eta - \Delta\sigma \tag{3.35}$$

Note that $\Delta\lambda$ is a function of both latitude and longitude and the equations for conversion are given by Larson [45].

$$\cos\left[\frac{\pi}{2} - \left(\mathrm{Lat}_0 - \Delta\mathrm{Lat}\right)\right] = \cos\Delta\lambda \sin\mathrm{Lat}_0 + \sin\Delta\lambda \cos\mathrm{Lat}_0 \cos\Phi \tag{3.36}$$

$$\cos\Delta\mathrm{Long} = \frac{\cos\Delta\lambda - \sin\mathrm{Lat}_0 \sin(\mathrm{Lat}_0 + \Delta\mathrm{Lat})}{\cos\mathrm{Lat}_0 \cos(\mathrm{Lat}_0 + \Delta\mathrm{Lat})} \tag{3.37}$$

where Lat_0 is the latitude of the nadir location and Φ is the azimuth of the target. Simplifying Equations (3.36) and (3.37) with respect to the deviations in latitude and longitude using the small angle approximation yields

$$\Delta\mathrm{Lat} = \frac{-1}{\cos\mathrm{Lat}_0}\left[\cos\Delta\lambda \sin\mathrm{Lat}_0 + \sin\Delta\lambda \cos\mathrm{Lat}_0 \cos\Phi - \sin\mathrm{Lat}_0\right] \tag{3.38}$$

$$\Delta\mathrm{Long} = \cos^{-1}\left[\frac{\cos\Delta\lambda - \sin\mathrm{Lat}_0 \sin(\mathrm{Lat}_0 + \Delta\mathrm{Lat})}{\cos\mathrm{Lat}_0 \cos(\mathrm{Lat}_0 + \Delta\mathrm{Lat})}\right] \tag{3.39}$$

Finally, Equations (3.38) and (3.39) can be used to find the relationship between the state and the observation, which is the matrix C in Equation (2.38).

3.5 Finding the Moments of Inertia Changes from Stage 1 to Stage 2

Figure 3.4 summarizes the process to find the change in the moments of inertia from stage 1 to stage 2. The initial mass distribution and initial angles for roll, pitch, and yaw are known at stage 1. Then, the moments of inertia of stage 1 can be computed easily. Using the governing equations of motion for a gravity-gradient-stabilized satellite, Euler angles can be calculated as a periodic function of time. Also roll, pitch, and yaw oscillation frequencies are found as a function of the moments of inertia. From the known position vector of the satellite in the inertial coordinate system, the latitude and longitude of the ground location are obtained. Since the satellite is oscillating around the groundtrack due to the Euler angles, ground coverage may be determined depending on the type of ground-observing sensor. The first goal of this research is to find the change in the moments of inertia from the given conditions. Since the mass distribution of stage 2 is unknown, moments of inertia and roll, pitch, and yaw angles cannot be computed.

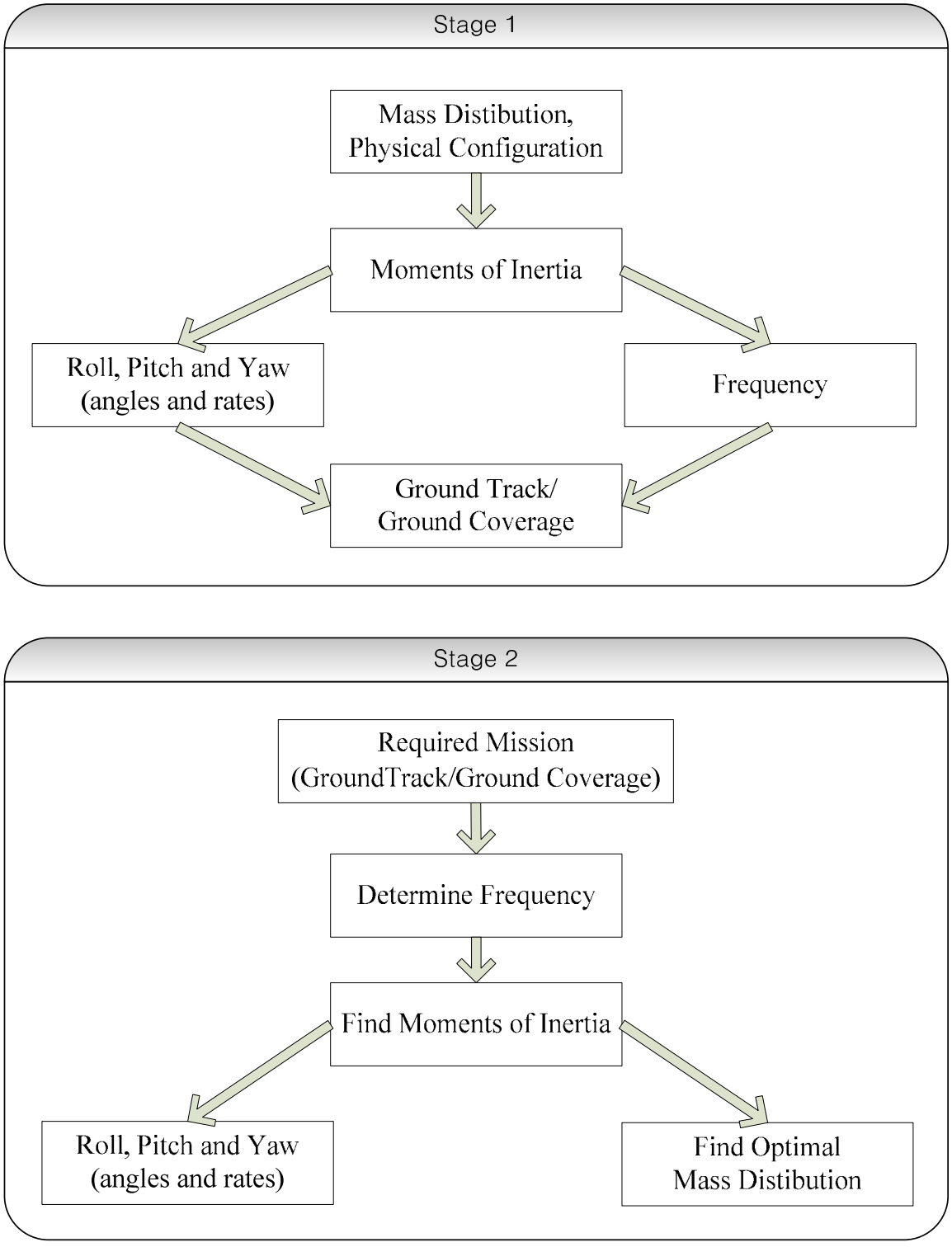

Figure 3.4: Summary of Finding the Moments of Inertia Change

Instead, the starting point is to determine the roll, pitch, and yaw oscillation frequencies for stage 2.

As seen in Equations (2.35) and (2.37), the roll/yaw oscillation frequency and the pitch oscillation frequency is function of the moments of inertia. Then, the frequency ratio of stage 1 to stage 2 is related to the moments of inertia at stage 1 and their changes and are computed in Equations (3.40) and (3.41):

$$\frac{\text{pfr}}{100} = \frac{\sqrt[n]{\dfrac{3(I_{r_2} - I_{y_2})}{I_{p_2}}}}{\sqrt[n]{\dfrac{3(I_{r_1} - I_{y_1})}{I_{p_1}}}} = \frac{\sqrt[n]{\dfrac{3(I_{r_1} + \Delta I_r) - (I_{y_1} + \Delta I_y)}{(I_{p_1} + \Delta I_p)}}}{\sqrt[n]{\dfrac{3(I_{r_1} - I_{y_1})}{I_{p_1}}}} \tag{3.40}$$

$$\frac{\text{ryfr}}{100} = \frac{\sqrt[n]{\dfrac{1}{2}\left(b_2 \pm \sqrt{b_2^2 - 4c_2}\right)}}{\sqrt[n]{\dfrac{1}{2}\left(b_1 \pm \sqrt{b_1^2 - 4c_1}\right)}} \tag{3.41}$$

where

$$b_2 = 3\left(\frac{I_{p_1} + \Delta I_p - (I_{y_1} + \Delta I_y)}{I_{r_1} + \Delta I_r}\right) + \left(\frac{I_{p_1} + \Delta I_p - (I_{r_1} + \Delta I_r)}{I_{y_1} + \Delta I_y}\right)\left(\frac{I_{p_1} + \Delta I_p - (I_{y_1} + \Delta I_y)}{I_{r_1} + \Delta I_r}\right) + 1$$

$$c_2 = 4\left(\frac{I_{p_1} + \Delta I_p - (I_{r_1} + \Delta I_r)}{I_{y_1} + \Delta I_y}\right)\left(\frac{I_{p_1} + \Delta I_p - (I_{y_1} + \Delta I_y)}{I_{r_1} + \Delta I_r}\right)$$

and pfr (%, pitch frequency ratio) is the pitch frequency ratio of stage 1 to stage 2. For example, pfr = 200 doubles the pitch frequency at stage 2. ryfr (%, roll/yaw frequency

ratio) can be determined in the same manner or a certain value can be provided. However, it is important that it is not always possible to complete the maneuver satisfying all restrictions. Therefore, the range for attitude change should be evaluated by trial and error. Equations (3.40) and (3.41) are simplified as follows.

$$(\text{pfr})^2(I_r - I_y)\Delta I_p + 100^2 I_p(\Delta I_y - \Delta I_r) = I_p(I_r - I_y)(100^2 - (\text{pfr})^2) \tag{3.42}$$

$$\left(\frac{\text{ryfr}}{100}\right)^2 = \frac{\left(b_2 \pm \sqrt{b_2^2 - 4c_2}\right)}{\left(b_1 \pm \sqrt{b_1^2 - 4c_1}\right)} \tag{3.43}$$

Recall that roll and yaw have same oscillation frequency, whereas the pitch oscillation frequency is independent of the other two. These two equations find the moments of inertia for stage 2 by determining the adequate frequencies for a specific mission and the ground map-making task is selected here. Note that the stability condition, $I_y < I_r < I_p$, must also be satisfied. Since the given conditions and the inequality are not enough to compute the unknown variables, there are huge number of combinations of solutions that exist and the minimum of the total mass transfer case will be chosen as the minimum mass mapping. However, the selected minimum mass mapping needs to be an optimal mass mapping; hence an optimization process must be added. The optimization computation is explained in next section.

3.6 Optimization Process

The optimization procedure is presented in this section. First, the objective of this simulation is stated. Next, the network theory is introduced to develop the objective function to meet the goal of this research and the most appropriate model is used to set up the objective functions. Finally, the optimal solution solver is chosen to find the optimal solution for the problem.

3.6.1 Optimal Mass Distribution

The objectives of this simulation are both to minimize the total mass transfer and to find the balanced mass distribution after mass mapping subject to the given roll/yaw oscillation frequency and pitch oscillation frequency under the gravity-gradient torque. Although how to transfer mass between tanks is not defined specifically, the usage of power is inevitable to perform this maneuver and eventually affects the operation lifetime of a satellite.

If the location of a tank is changed without mass movement, it plays the same role as mass transfer. Thus, minimizing the relocation distance of each tank can be substituted for minimizing the total mass movement. Also, both minimizing mass transfer and tank location change can be substituted for the objective of this dissertation.

Not only minimizing the total mass transfer, but well-balanced mass mapping for the maneuver is also important. For a series of mass transfers (or relocating each tank's position or both), a more balanced mass distribution among tanks yields less total mass transfer for next stage. Similarly, fewer tank location changes anticipates a shorter

journey for the following stage. In summary, the optimal mass transfer or tank relocation for this dissertation is to find the minimum mass transfer or minimum tank relocation (or both) and equally distribute each mass transfer or tank relocation.

3.6.2 Combinatorial Optimization

The mass shifting problem can be modeled in a similar manner to the combinatorial optimization problem. Cook [46] introduced several types of network models applicable to this dissertation such as minimum spanning tree, shortest path problem, maximum flow problems and minimum cost problem.

Generally, a network model is expressed by a diagram consisting of two characteristics: nodes and arcs. The nodes are usually represented by a circle, which means the beginning or completion of an operation, and the arc is represented by lines connecting the nodes. The arc can have direction whereas the nodes do not. Arcs expressed by arrows on the network indicate that flows can be moved only in the specified direction. A path is defined as a series of connections among nodes and, if it returns to the starting node, it is call a cycle type. If some nodes are connected without being included in a cycle, it is named as a tree structure.

1. **Minimum Spanning Tree**

This model designs that all network nodes are to be connected to each other while the total length of the extension is to be minimized; for example, computer networks that

connect all the computers in the most efficient problem, or the best way to supply water/electricity to each household. The solution process is as follows.

① Select one random node and connect it to the nearest node.

② Continue connecting nodes within the shortest distance that are not yet connected to any other.

③ Repeat until all nodes are connected.

2. Shortest Path Problem

This type of problem is to find the minimum distance between two nodes on the path to obtain the shortest path connecting all nodes. Case 1 (the location of tanks change without mass transfer) in Section 3.4 can be modeled as this type. Also, the well-known TSP (Travelling Salesman Problem) belongs to this type. Whereas the problem is fairly straightforward, many techniques to minimize the model have been and currently are being developed.

Dijkstra's algorithm [47] is one of the most widely used due to its simplicity and robustness. From the starting point of a given network, the following step is to connect to the nearest node until the whole connected path is found.

The shortest path problem is regarded as a special case of minimum cost flow problem, which is used for this research because the distance from the shortest-path problem corresponds to the cost for the minimum cost flow problem. Thus, the minimization of distance is that it is the minimization of the total cost. This process is solved as follows.

① Connect the node closest to the starting point.

② Next, connect to the closest node from the starting point.

③ Repeat until the entire network is connected.

3. Maximum Flow Problem

This problem is to maximize the flow rate between two points. Before applying this model, whether the flow rate has only one direction or both directions should be determined. This model can solve problems such as complex city traffic flow at intersections, or the flow of rush-hour subway passengers. Typically, there are flow capacity constraints for each arc that determine the maximum amount of flow. On the other hand, there is no capacity constraint for each node on the network. Thus, the intermediate transit nodes that pass through a node have no restriction on the amount of flow. Each intermediate node works as a transit node such that the flow quantities coming into that node exits. This process is solved as follows.

① Select an arbitrary path from the starting point to the final destination.

② Once the path is determined, allot the maximum amount of flow for that path. (Note that the maximum flow is automatically given by the minimum flow among all paths).

③ If it is possible to move flow in both directions, switch the path to see if the maximum volume is bigger.

④ Repeat until the volume of flow from the starting point to the final point is impossible.

4. Minimum Cost Flow Problem

The minimum cost flow problem deals with the case when the maximum flow capacity along each arc is limited and the cost accrued is proportional to the flow. Usually the minimum cost flow problem is similar to the transportation problem with small differences. In the former, a transit node exists, the latter does not have a transit node. Therefore, only one direct connection from the starting point to the final point exists for the transportation problem. On the contrary, the minimum cost flow problem can travel via the transit nodes. There is a simple solution method, similar to the transportation problem, using simplex algorithm widely applied for most large-scale cases.

The simplex algorithm is a powerful method for a linear programming and helps find the minimum solutions with provided conditions. The simplex algorithm can be summarized briefly as follows:

$$
\begin{aligned}
&\text{Min } F = c_1X_1 + c_2X_2 + c_3X_3 + \cdots + c_nX_n \\
&\text{such that} \\
&\quad a_{11}X_1 + a_{12}X_2 + a_{13}X_3 + \cdots + a_{1n}X_n \le b_1 \\
&\quad a_{21}X_1 + a_{22}X_2 + a_{23}X_3 + \cdots + a_{2n}X_n \le b_2 \\
&\qquad\qquad \vdots \\
&\quad a_{m1}X_1 + a_{m2}X_2 + a_{m3}X_3 + \cdots + a_{mn}X_n \le b_m \\
&\quad X_1,\ X_2,\ \cdots X_n \ge 0
\end{aligned}
\tag{3.44}
$$

where $c_i (i = 1, \cdots, n)$ are the weighting coefficients and $X_i (i = 1, \cdots, n)$ are the cost per each function, and $a_{ij} (i = 1, \cdots, m,\ j = 1, \cdots, n)$ and $b_j (i = 1, \cdots, m)$ are computed by the restrictions on the problem.

In Figure 3.5, for five destinations, there are 5! possible routes. Analytic solutions can be found by comparing all the possible costs, but it takes considerable time as more cities are included. To apply minimum cost flow problem methods to the mass shifting attitude problem, analogous representations can be made. A city represents a tank and the cost between two cities is the amount of mass moving through the massless pipe. The minimum cost for the entire system is same as the minimum amount of mass travelling throughout the whole satellite system. However, the direction of the mass travelling results in an opposite solution, thus the mass distribution problem is an asymmetric minimum cost flow problem requiring more variables in the equations. The optimal solution for minimum cost flow problem automatically satisfies the minimum amount of mass passing through the pipes, which is the goal of this research.

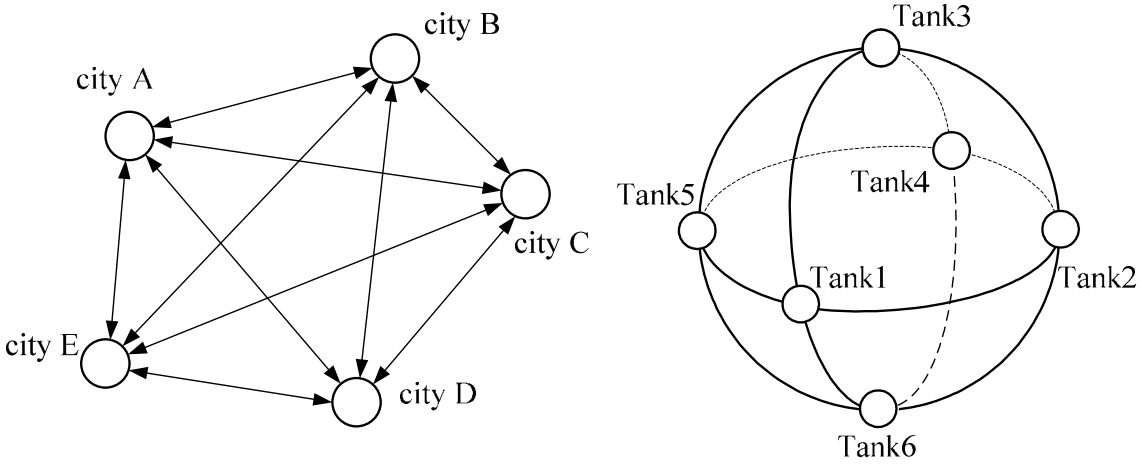

Figure 3.5: Minimum Cost Problem vs. Mass Distribution

To set up the objective function, two objectives are considered. The first objective is to minimize the total amount of mass that is transferred and the other objective is to balance the mass movement of the entire system. Based on the simplex algorithm, all possible mass transfer between any two tanks can be expressed by

$$\begin{aligned}\min f(x) = {} & |\text{Pipe\_12}| + |\text{Pipe\_21}| + |\text{Pipe\_13}| + |\text{Pipe\_31}| + 2|\text{Pipe\_14}| + 2|\text{Pipe\_41}| \\ & + |\text{Pipe\_15}| + |\text{Pipe\_51}| + |\text{Pipe\_16}| + |\text{Pipe\_61}| + |\text{Pipe\_23}| + |\text{Pipe\_32}| \\ & + |\text{Pipe\_24}| + |\text{Pipe\_42}| + 2|\text{Pipe\_25}| + 2|\text{Pipe\_52}| + |\text{Pipe\_16}| + |\text{Pipe\_62}| \\ & + |\text{Pipe\_34}| + |\text{Pipe\_43}| + |\text{Pipe\_35}| + |\text{Pipe\_53}| + 2|\text{Pipe\_36}| + 2|\text{Pipe\_63}| \\ & + |\text{Pipe\_45}| + |\text{Pipe\_54}| + |\text{Pipe\_46}| + |\text{Pipe\_64}| + |\text{Pipe\_56}| + |\text{Pipe\_65}|\end{aligned} \tag{3.45}$$

where Pipe_12 represents the mass amount moving through the pipe from tank 1 to tank 2. Therefore, Pipe_12 and Pipe_21 must have same magnitude, but with opposite signs. Note that a multiplicand 2 is included with Pipe_14 (also Pipe_41), Pipe_25 (also Pipe_52), and Pipe_36 (also Pipe_63) because the distance for those pairs of tanks is two units. However, Equation (3.45) only finds the minimum solution not considering the balanced mass distribution. Therefore, a modification is needed to satisfy both minimal mass transfer and balanced mass distribution. Equation (3.46) represents the modified objective function, $f(x)$, defined as the sum of the p-power ($p > 1$) of each mass moving through the connecting pipes. Also, no mass transfer through Pipe_14 (also Pipe_41), Pipe_25 (also Pipe_52), and Pipe_36 (also Pipe_63) is assumed since they are not directly connected, so the objective function reduces to

$$\begin{aligned}\min f(x) = {} & |\text{Pipe\_12}|^p + |\text{Pipe\_21}|^p + |\text{Pipe\_13}|^p + |\text{Pipe\_31}|^p + |\text{Pipe\_15}|^p + |\text{Pipe\_51}|^p \\ & + |\text{Pipe\_16}|^p + |\text{Pipe\_61}|^p + |\text{Pipe\_23}|^p + |\text{Pipe\_32}|^p + |\text{Pipe\_24}|^p + |\text{Pipe\_42}|^p \\ & + |\text{Pipe\_26}|^p + |\text{Pipe\_62}|^p + |\text{Pipe\_34}|^p + |\text{Pipe\_43}|^p + |\text{Pipe\_35}|^p + |\text{Pipe\_53}|^p \\ & + |\text{Pipe\_45}|^p + |\text{Pipe\_54}|^p + |\text{Pipe\_46}|^p + |\text{Pipe\_64}|^p + |\text{Pipe\_56}|^p + |\text{Pipe\_65}|^p\end{aligned} \tag{3.46}$$

where $p > 1$.

A similar process can be applied to find the objective function for optimal relocation of each tank. The shortest path problem only finds the shortest distance, but optimal relocation of each tank also requires a balanced displacement. Equation (3.47) is the objective function considering both minimizing the tank relocation distance and balancing the tank shift without changing mass in it.

$$\begin{aligned}\min f(x) = \Big(& |\text{tank 1 location change in x direction}|^p + |\text{tank 1 location change in y direction}|^p \\ & + |\text{tank 1 location change in z direction}|^p + |\text{tank 2 location change in x direction}|^p \\ & + |\text{tank 2 location change in y direction}|^p + |\text{tank 2 location change in z direction}|^p \\ & + |\text{tank 3 location change in x direction}|^p + |\text{tank 3 location change in y direction}|^p \\ & + |\text{tank 3 location change in z direction}|^p + |\text{tank 4 location change in x direction}|^p \\ & + |\text{tank 4 location change in y direction}|^p + |\text{tank 4 location change in z direction}|^p \\ & + |\text{tank 5 location change in x direction}|^p + |\text{tank 5 location change in y direction}|^p \\ & + |\text{tank 5 location change in z direction}|^p + |\text{tank 6 location change in x direction}|^p \\ & + |\text{tank 6 location change in y direction}|^p + |\text{tank 6 location change in z direction}|^p \Big)^{\frac{1}{2}}\end{aligned} \tag{3.47}$$

where $p > 1$.

3.6.3 Optimization Solver

Though the objective function is obtained using the simplex algorithm, the solution method cannot be applied since the objective function is not a linear equation. MATLAB's optimization toolbox [48] provides various optimization solvers for different objective functions and are selected based on the function and constraint type. These solvers are generally divided into two classes.

One group (fmincon, fminunc, fseminf, lsqcurvefit, etc.) use a gradient-based algorithm. The others (GA, pattern search, simulated annealing, etc.) are based on the probabilistic characteristics of the problem. A preferable solver may find the best solution quickly and efficiently, whereas an inappropriate solver may take a longer processing time or fail. Table 3.1 suggests the preferred optimal solvers for different types of problems. Although '*fmincon*' is missing from several selections in the table, it still can be used to solve most smooth objective functions with smooth constraints. To be eligible for a smooth constraint, the constraint must be differentiable at all points. All simulations for this research contain two equality constraints from roll/yaw and pitch oscillation frequency ratios and two inequality constraints from gravity-gradient stabilization ($I_y < I_r < I_p$). All the equality constraints for case 1 through case 4 are linear if $2n$ is chosen for the roll/yaw oscillation frequency. Otherwise, the constraint from different choice of the roll/yaw oscillation frequency becomes nonlinear but still differentiable at any point. The inequality constraints are always linear regardless of the roll/yaw and pitch oscillation frequencies at stage 2. For case 5, both equality and inequality

constraints are nonlinear all the time but all the constraints are also differentiable everywhere. Thus, '*fmincon*' is selected for the simulation results in Chapter 4.

Table 3.1: Suggested Optimization Decision Table by Objective Type and Constraint (http://www.mathworks.com/help/toolbox/optim/ug/brhkghv-18.html#brhkghv-21, date accessed 5/10/12)

Constraint Type	**Objective Type**				
	Linear	Quadratic	Least Squares	Smooth nonlinear	Nonsmooth
None	n/a (f = const or min = $-\infty$)	quadprog	lsqcurvefit lsqnonlin	fminsearch fminunc	fminsearch others
Bound	linprog	quadprog	lsqcurvefit lsqlin lsqnonlin lsqnonneg	fminbnd fmincon fseminf	fminbnd others
Linear	linprog	quadprog	lsqlin	fmincon fseminf	others
General smooth	fmincon	fmincon	fmincon	fmincon fseminf	others
Discrete	bintprog others	others	others	others	others

Chapter 4

SIMULATION RESULTS

Using the governing equations of motion for various types of mass distribution, Euler angles and their rate changes are examined by shifting the moment of inertia of the whole system. Starting from a simple example, different constraints are applied to see how different mass distributions affect the roll, pitch, and yaw angles and the ground coverage. The physical parameters of the problem are presented in Table 4.1.

Table 4.1: Physical Parameters of the System

Mass of the Satellite	100 kg
Number of Tanks	6
Total mass in tanks (10 kg each initially)	60 kg
Principal roll moment of inertia of the dry satellite	75 kg·m^2
Principal pitch moment of inertia of the dry satellite	100 kg·m^2
Principal yaw moment of inertia of the dry satellite	60 kg·m^2
Semi major axis (Circular Orbit)	7,000 km
Inclination	90 degree
Radius of the sphere (the locations of tanks from the origin)	1 m
Initial roll angle	0 rad
Initial pitch angle	0 rad
Initial yaw angle	0 rad
Initial roll rate	-0.00001 rad/sec
Initial pitch rate	0.00004 rad/sec
Initial yaw rate	-0.00006 rad/sec
Each stage lasts for 50,000 seconds	

First, several simulations present the optimal mass transfer or tank relocation satisfying all the constraints under the different designs for a polar orbit satellite with a map-making mission. Once the optimal solution is found, it is illustrated how the ground coverage can be affected by the roll frequency change. It is expected that the roll frequency should be increased to enlarge the ground coverage area per one track of the satellite cycle. However, it reduces the possibility of feasible mass distribution at stage 2 if the roll frequency at stage 2 is changed too much or too many additional restrictions are applied.

From Table 4.1, the roll frequency at stage 1 is 0.001506 Hz. The roll frequency at stage 2 can be determined from the roll frequency ratio relationship, Equation (3.43), or a certain value can be specified if necessary. It is found that Equation (3.43) becomes a linear constraint only if the roll frequency at stage 2 is $2n$ regardless of the roll frequency at stage 1. Except for this case, Equation (3.43) is always a nonlinear constraint. Compared with the roll frequency at stage 1, the roll frequency is increased around 43% when the roll/yaw frequency at stage 2 is $2n$ while the pitch frequency remains unchanged. These two frequency constraints and the inequality constraint for stability, $I_y < I_r < I_p$, are used as the general constraints for case 1 through case 4. Recall that the optimal solution does not exist if the roll/yaw or pitch frequency changes dramatically or any additional constraints due to the design are hard to achieve.

After several simple cases are examined, case 4, which is the general design with the center-of-mass unchanged, and case 5, which is the practical design with moving center-of-mass, are applied under various constraints.

Case 1 Tank locations are changing along each axis with fixed masses

Conditions

$\Delta m_k = 0 \ \ (k = 1,...,6)$

Roll frequency at stage 2: $2n$

Pitch frequency at stage 2: unchanged

pitch frequency constraint (Equation (3.42))

$$m_1(I_r - I_y + I_p)\Delta x + m_3(I_r - I_y - I_p)\Delta z = 0 \tag{4.1}$$

roll/yaw frequency constraint (Equation (3.43))

$$\Delta y = \frac{1}{8dm_2}(I_p - I_r - I_y) \tag{4.2}$$

stability constraint ($I_y < I_r < I_p$)

$$\begin{aligned} m_1\Delta x - m_3\Delta z &< \frac{1}{4d}(I_r - I_y) \\ m_2\Delta y - m_1\Delta x &< \frac{1}{4d}(I_p - I_r) \end{aligned} \tag{4.3}$$

objective function

$$\begin{aligned}\min f(x) = \Big(& \left|\text{tank 1 location change along x-axis}\right|^2 \\ & + \left|\text{tank 2 location change along y-axis}\right|^2 \\ & + \left|\text{tank 3 location change along z-axis}\right|^2 \Big)^{\frac{1}{2}}\end{aligned} \tag{4.4}$$

Equation (3.47) with p=2 is reduced to Equation (4.4) for the optimal location of each tank satisfying all four constraints, Equations (4.1)-(4.3). Each tank is limited to move up to 2m away from the origin. The roll, pitch, and yaw frequencies for stage 1 and stage 2 are presented in Table 4.2. Here, pitch frequency remains unchanged and roll/yaw frequencies are twice the mean motion of the satellite.

Table 4.2: Roll/Yaw and Pitch Frequencies at Each Stage for Case 1 (Hz)

Parameters	Stage 1	Stage 2
Pitch frequency	0.000611	0.000611
Roll / Yaw frequency	0.001506	0.002156

Table 4.3 presents the locations of each tank without mass movement to complete the attitude change. Note that the locations of the pair tank are symmetric with respect to the origin and tank 2 and tank 5 are located near the center-of-mass. On the other hand, all the other tanks remain near their original location. Although the optimal solution is to find the minimum movement of tank location and to distribute the shift, the shift is concentrated into only two tanks unless all constraints are not met.

Table 4.3: Tank location for Stage 1 and Stage 2 for Case 1 (m)

	Stage 1	Stage 2
Tank 1	[1, 0, 0]	[1.0000, 0, 0]
Tank 2	[0, 1, 0]	[0, 0.0625, 0]
Tank 3	[0, 0, 1]	[0, 0, 1.0000]
Tank 4	[-1, 0, 0]	[-1.0000, 0, 0]
Tank 5	[0, -1, 0]	[0, -0.0625, 0]
Tank 6	[0, 0, -1]	[0, 0, -1.0000]

Figure 4.1 illustrates the tank distribution for each stage. The circle on the diagram indicates the amount of mass. At stage 1, six tanks have the same amount of mass and are equally distributed on a sphere of radius 1. Tank 2 and tank 5 are located only 6 cm away from the center-of-mass. Since there is no mass change, the size of each tank at stage 2 is the same.

The amount of principal moment of inertia change from stage 1 to stage 2 is obtained as follows.

$$\Delta I = \begin{bmatrix} -37.498 & 0 & 0 \\ 0 & 0.00352 & 0 \\ 0 & 0 & -37.498 \end{bmatrix} (\mathrm{kg} \cdot \mathrm{m}^2) \tag{4.5}$$

Figure 4.2 shows the inequality, $I_y < I_r < I_p$, is satisfied for stability during the morphing. Roll and yaw moments of inertia are decreased while the pitch moment of inertia is almost the same as stage 1. With known values of principal moments of inertia at stage 2, three attitude angles and their rates can be computed. In Figure 4.3, it is easily noticed

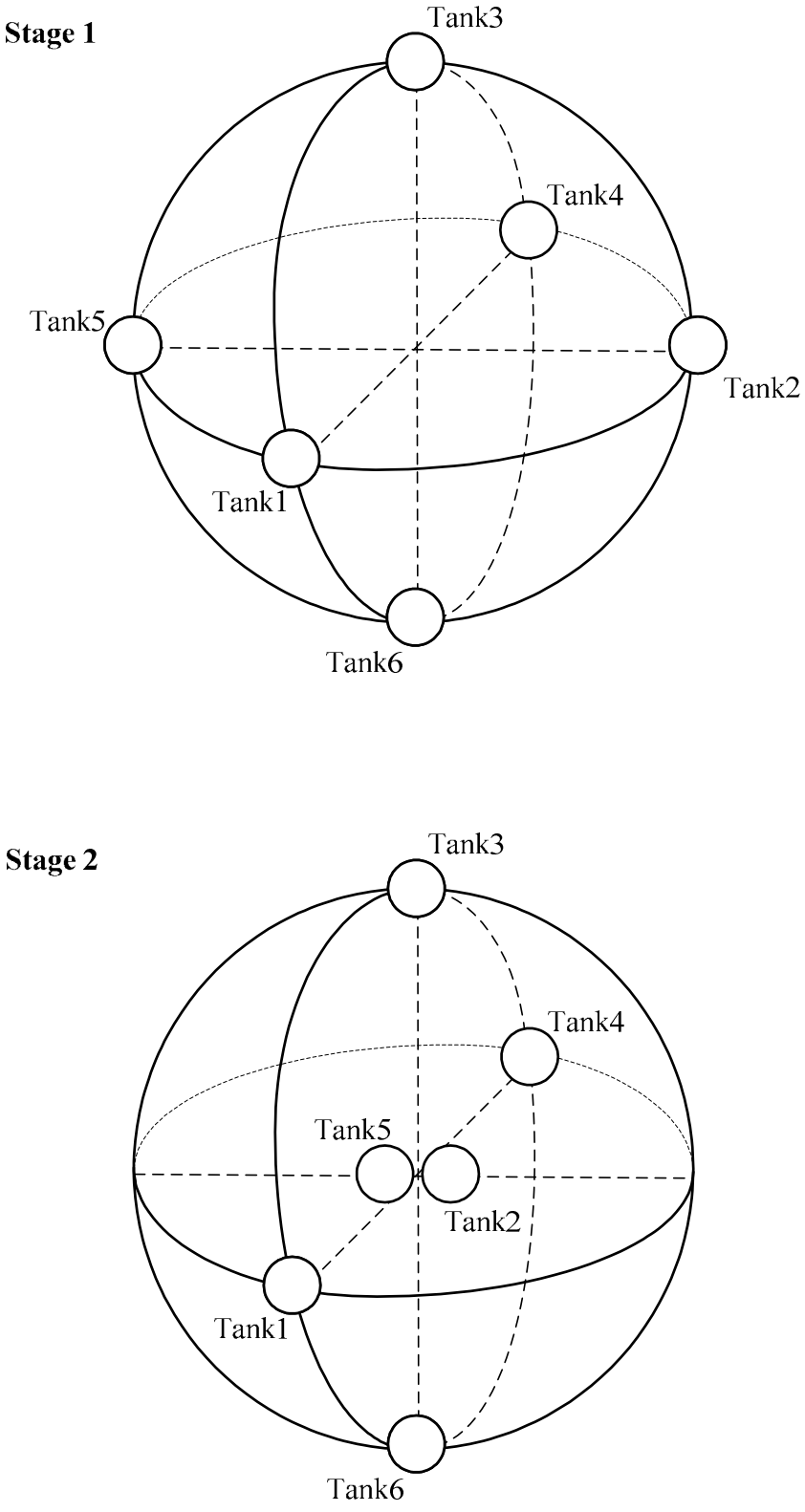

Figure 4.1: Diagram of Tank Distribution for Each Stage for Case 1

that the pitch frequency at stage 2 is unchanged subject to the constraint, whereas roll and yaw frequency change is noticeable due to small change from 0.001506 to 0.002156 (about a 43% increase).

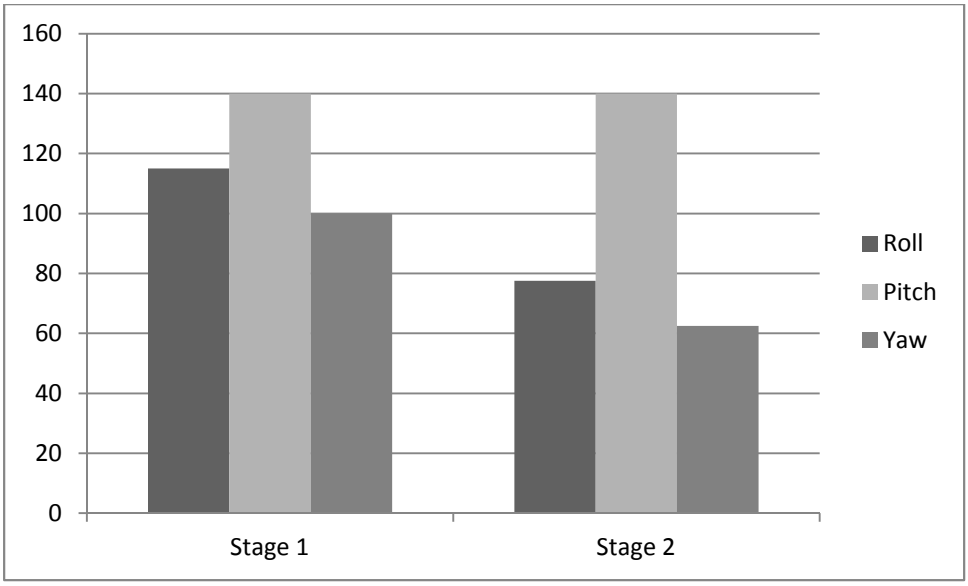

Figure 4.2: Principal Moments of Inertia for Each Stage for Case 1 ($kg \cdot m^2$)

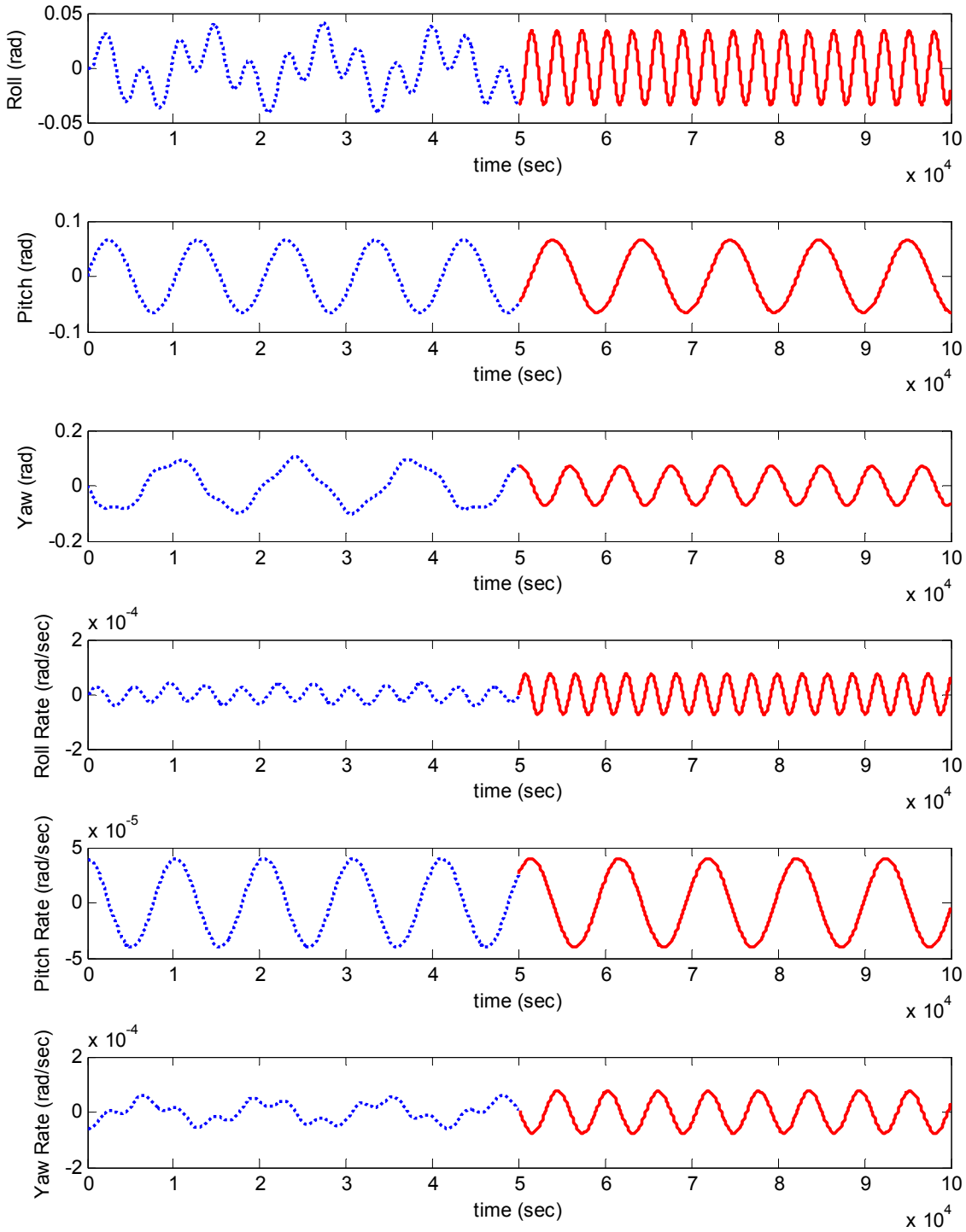

Figure 4.3: Roll, Pitch and Yaw Angles and Their Rates for Stage 1 and Stage 2 for Case 1 (stage 2 begins at 5×10^4 sec)

The series of image circles observed by ground-observing device such as a camera to make a satellite map-making mission is illustrated in Figure 4.4. It is observed for a polar orbiting satellite that the swept area at stage 2 shows enhanced ground coverage due to an increase in roll frequency. The longitude deviation range is increased from -0.061 to 0.061 degree at stage 1 to -0.186 to 0.186 degree, and this means around -20.78 to 20.78 km near the equator. As seen, the swept area is more uniformly covered.

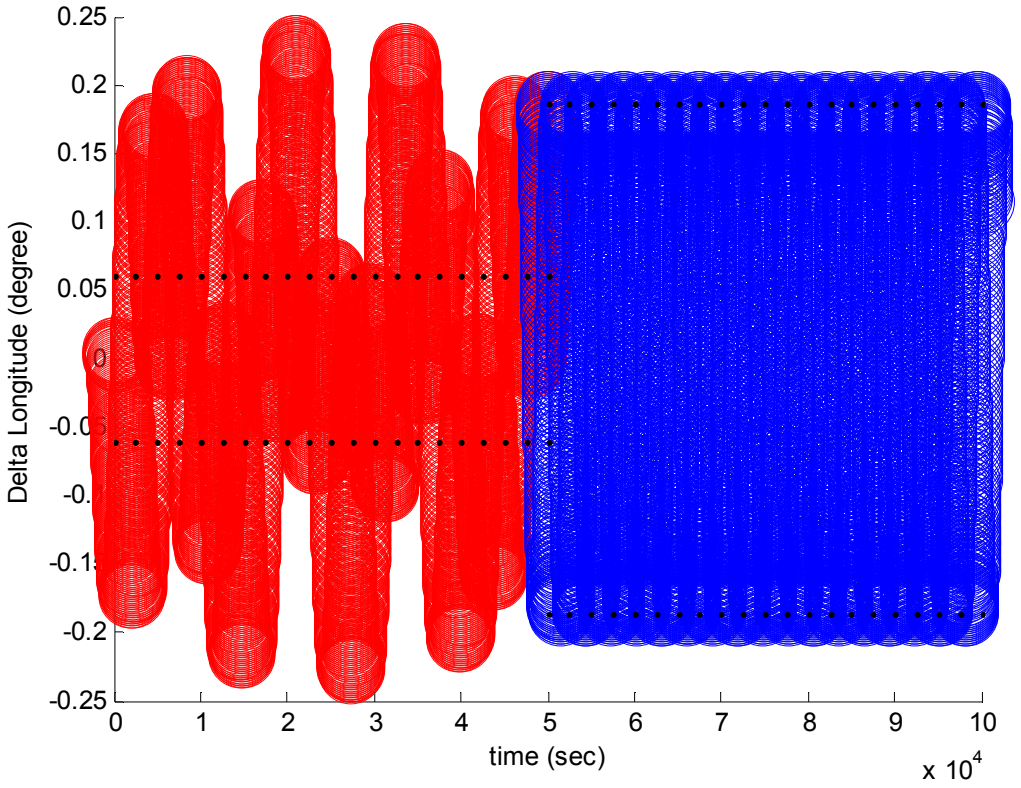

Figure 4.4: Ground Coverage Change between Stage 1 and Stage 2 for Case 1 (stage 2 begins at 5×10^4 sec)

Case 2 Masses are moving while the tank locations are fixed

Conditions

$\Delta x = \Delta y = \Delta z = 0$, $m_1 = m_4$, $m_2 = m_5$, $m_3 = m_6$

Roll frequency at stage 2: $2n$

Pitch frequency at stage 2: unchanged

pitch frequency constraint (Equation (3.42))

$$(I_r - I_y + I_p)\Delta m_1 + (I_r - I_y - I_p)\Delta m_3 = 0 \tag{4.6}$$

roll/yaw frequency constraint (Equation (3.43))

$$\Delta m_2 = \frac{1}{4d}(I_p - I_r - I_y) \tag{4.7}$$

stability constraint ($I_y < I_r < I_p$)

$$\begin{aligned} \Delta m_1 - \Delta m_3 &< \frac{1}{2d^2}(I_r - I_y) \\ \Delta m_2 - \Delta m_1 &< \frac{1}{2d^2}(I_p - I_r) \end{aligned} \tag{4.8}$$

objective function

$$\begin{aligned}\min f(x) = {} & |\text{Pipe\_12}|^2 + |\text{Pipe\_21}|^2 + |\text{Pipe\_13}|^2 + |\text{Pipe\_31}|^2 + |\text{Pipe\_15}|^2 + |\text{Pipe\_51}|^2 \\ & + |\text{Pipe\_16}|^2 + |\text{Pipe\_61}|^2 + |\text{Pipe\_23}|^2 + |\text{Pipe\_32}|^2 + |\text{Pipe\_24}|^2 + |\text{Pipe\_42}|^2 \\ & + |\text{Pipe\_26}|^2 + |\text{Pipe\_62}|^2 + |\text{Pipe\_34}|^2 + |\text{Pipe\_43}|^2 + |\text{Pipe\_35}|^2 + |\text{Pipe\_53}|^2 \\ & + |\text{Pipe\_45}|^2 + |\text{Pipe\_54}|^2 + |\text{Pipe\_46}|^2 + |\text{Pipe\_64}|^2 + |\text{Pipe\_56}|^2 + |\text{Pipe\_65}|^2\end{aligned} \tag{4.9}$$

Equation (4.9) is the same as Equation (3.46) with p=2 and used to find the optimal mass transfer while the tank location is fixed. Additional constraints for this case are that each pipe is allowed to transfer mass up to 10 kg, and each tank's capacity is up to 20 kg.

MATLAB's optimization solver results in no feasible solution satisfying all of the constraints. This means any mass distribution at stage 2 never achieves the roll frequency of 2n under this design.

Removing one of the constraints, which is that the mass of each tank can be negative at stage 2, Table 4.4 includes the minimum mass mapping per pipe to achieve the expected roll/yaw frequency and Table 4.5 shows the mass distribution before and after mass shifting. Since the removed constraint violates physics, the optimal solution contains negative mass in tank 2 and tank 5. Again, it is concluded that there is no feasible mass distribution for the desired frequency. This simulation shows that the optimal mass distribution is not always found.

Table 4.4: Optimal Mass Shift Through Each Pipe for Case 2 (kg)

Pipe_12 = 4.520	Pipe_21 = -4.520
Pipe_13 = -0.335	Pipe_31 = 0.335
Pipe_15 = 4.520	Pipe_51 = -4.520
Pipe_16 = -0.335	Pipe_65 = 0.335
Pipe_23 = -4.855	Pipe_32 = 4.855
Pipe_24 = -4.520	Pipe_42 = 4.520
Pipe_26 = -4.855	Pipe_62 = 4.855
Pipe_34 = 0.335	Pipe_43 = -0.335
Pipe_35 = 4.855	Pipe_53 = -4.855
Pipe_45 = 4.520	Pipe_54 = -4.520
Pipe_46 = -0.335	Pipe_64 = 0.335
Pipe_56 = -4.855	Pipe_65 = 4.855
Total amount of mass shifted: 38.839 kg	

Table 4.5: Mass Distribution for Stage 1 and Stage 2 for Case 2 (kg)

	Stage 1	Stage 2	Mass shifted
Tank 1	10	18.371	8.371
Tank 2	10	-8.750	-18.750
Tank 3	10	20.379	10.379
Tank 4	10	8.371	8.371
Tank 5	10	-8.750	-18.750
Tank 6	10	20.379	10.379
Total Amount of Mass	60	60	0 (conserved)

Case 3 Each tank can move along each axis and the amount of masses are changing

Conditions

$m_1 = m_4,\ m_2 = m_5,\ m_3 = m_6$

Roll frequency at stage 2: $2n$

Pitch frequency at stage 2: unchanged

pitch frequency constraint (Equation (3.42))

$$\begin{aligned} &2d^2(I_r - I_y + I_p)\Delta m_1 + 2d^2(I_r - I_y - I_p)\Delta m_3 + \\ &\quad 4d(I_r - I_y + I_p)m_1\Delta x + 4d(I_r - I_y - I_p)m_3\Delta z = 0 \end{aligned} \tag{4.10}$$

roll/yaw frequency constraint (Equation (3.43))

$$4d\Delta m_2 + 8dm_2\Delta y = I_p - I_r - I_y \tag{4.11}$$

stability constraint ($I_y < I_r < I_p$)

$$\begin{aligned} &2d^2(\Delta m_1 - \Delta m_3) + 4d(m_1\Delta x - m_3\Delta z) < I_r - I_y \\ &2d^2(\Delta m_2 - \Delta m_1) + 4d(m_2\Delta y - m_1\Delta x) < I_p - I_r \end{aligned} \tag{4.12}$$

It is found that there is no applicable mass distribution to perform with the specified roll/yaw frequency from the previous simulation, case 2. Mass shift, combined with the

change of tank location, is examined to check if this design can complete the attitude transform in case 3. To develop the appropriate objective function, the objective functions for case 1 and case 2 are added and is presented in Equation (4.13).

$$\begin{aligned}\min f(x) = {} & |\text{Pipe\_12}|^2 + |\text{Pipe\_21}|^2 + |\text{Pipe\_13}|^2 + |\text{Pipe\_31}|^2 + |\text{Pipe\_15}|^2 + |\text{Pipe\_51}|^2 \\ & + |\text{Pipe\_16}|^2 + |\text{Pipe\_61}|^2 + |\text{Pipe\_23}|^2 + |\text{Pipe\_32}|^2 + |\text{Pipe\_24}|^2 + |\text{Pipe\_42}|^2 \\ & + |\text{Pipe\_26}|^2 + |\text{Pipe\_62}|^2 + |\text{Pipe\_34}|^2 + |\text{Pipe\_43}|^2 + |\text{Pipe\_35}|^2 + |\text{Pipe\_53}|^2 \\ & + |\text{Pipe\_45}|^2 + |\text{Pipe\_54}|^2 + |\text{Pipe\_46}|^2 + |\text{Pipe\_64}|^2 + |\text{Pipe\_56}|^2 + |\text{Pipe\_65}|^2 \\ & + \Big(|\text{tank 1 location change along x-axis}|^2 \\ & \quad + |\text{tank 2 location change along y-axis}|^2 \\ & \quad + |\text{tank 3 location change along z-axis}|^2 \Big)^{\frac{1}{2}}\end{aligned} \tag{4.13}$$

Tables 4.6 and 4.7 show the optimal mass mapping and the locations of each tank at stage 2 to achieve the desired roll/yaw frequency. From the results in case 1 and case 2, it may be assumed that the relocation of each tank is more dominant than the mass shift since there is no feasible mapping in case 2. It is computed that 0.05050 kg is needed to travel to change the satellite attitude thanks to the relocation of the tanks. Therefore, the mass distribution diagram at stage 2 is almost same as in Figure 4.1. Table 4.8 presents the amount of the mass per tank. Recall that one tank is connected with four pipes to transfer mass, the total amount of mass shifted for all pipes and all tanks are different. Total amount of mass in the whole system is not changed during mass redistribution, thus its value is always zero.

Table 4.6: Optimal Mass Shift Through Each Pipe for Case 3 (kg)

Pipe_12 = 0.00627	Pipe_21 = -0.00627
Pipe_13 = -0.00004	Pipe_31 = 0.00004
Pipe_15 = 0.00627	Pipe_51 = -0.00627
Pipe_16 = -0.00004	Pipe_65 = 0.00004
Pipe_23 = -0.00631	Pipe_32 = 0.00631
Pipe_24 = -0.00627	Pipe_42 = 0.00627
Pipe_26 = -0.00631	Pipe_62 = 0.00631
Pipe_34 = 0.00004	Pipe_43 = -0.00004
Pipe_35 = 0.00631	Pipe_53 = -0.00631
Pipe_45 = 0.00627	Pipe_54 = -0.00627
Pipe_46 = -0.00004	Pipe_64 = 0.00004
Pipe_56 = -0.00631	Pipe_65 = 0.00631
Total amount of mass shifted: 0.05050 kg	

Table 4.7: Tank location for Stage 1 and Stage 2 for Case 3 (m)

	Stage 1	Stage 2
Tank 1	[1, 0, 0]	[0.9996, 0, 0]
Tank 2	[0, 1, 0]	[0, 0.0638, 0]
Tank 3	[0, 0, 1]	[0, 0, 0.9997]
Tank 4	[-1, 0, 0]	[-0.9996, 0, 0]
Tank 5	[0, -1, 0]	[0, -0.0638, 0]
Tank 6	[0, 0, -1]	[0, 0, -0.9997]

Table 4.8: Mass Distribution for Stage 1 and Stage 2 for Case 3 (kg)

	Stage 1	Stage 2	Mass shifted
Tank 1	10	10.012	0.012
Tank 2	10	9.975	-0.025
Tank 3	10	10.013	0.013
Tank 4	10	10.012	0.012
Tank 5	10	9.975	-0.025
Tank 6	10	10.013	0.013
Total Amount of Mass	60	60	0 (conserved)

Since the simulation for case 3 is fairly similar to the result of case 1, the change of principal moment of inertia is also close to Equation (4.5) and computed as follows.

$$\Delta I = \begin{bmatrix} -37.485 & 0 & 0 \\ 0 & 0.027 & 0 \\ 0 & 0 & -37.488 \end{bmatrix} (\mathrm{kg} \cdot \mathrm{m}^2) \tag{4.14}$$

Figure 4.5 illustrates the moments of inertia for both stage 1 and stage 2. The amount of pitch moment is not changed compared with case 1. The other two moments are decreased similar to case 1. The roll, pitch, and yaw angles and their rates for case 3 are the same as in Figure 4.3 because the same frequency constraints are applied. Also, the ground coverage pattern is same as case 1, i.e., Figure 4.4.

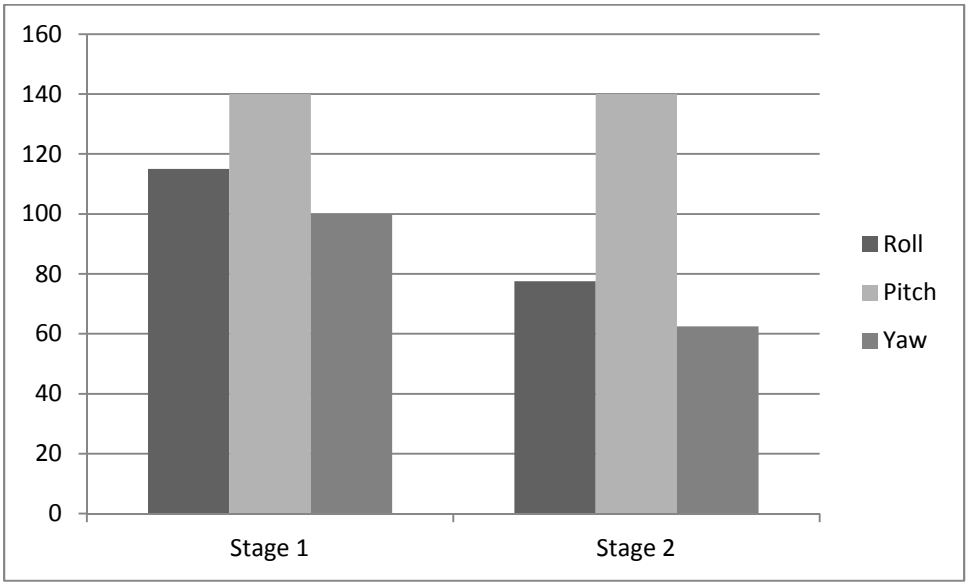

Figure 4.5: Principal Moments of Inertia for Each Stage for Case 3 ($\mathrm{kg} \cdot \mathrm{m}^2$)

Case 4 Tank locations are moving any direction and masses are changing

Conditions

$m_1 = m_4,\ m_2 = m_5,\ m_3 = m_6;\ \ \Delta x_i \neq 0,\ \Delta y_i \neq 0,\ \Delta z_i \neq 0\ (i = 1, 2, 3)$

Roll frequency at stage 2: $2n$

Pitch frequency at stage 2: unchanged

pitch frequency constraint (Equation (3.42))

$$\begin{aligned}
&(I_r - I_y)(x_1^2 + z_1^2) + I_p(x_1^2 - z_1^2)\Delta m_1 \\
&+(I_r - I_y)(x_2^2 + z_2^2) + I_p(x_2^2 - z_2^2)\Delta m_2 \\
&+(I_r - I_y)(x_3^2 + z_3^2) + I_p(x_3^2 - z_3^2)\Delta m_3 \\
&+2(I_r - I_y + I_p)m_1 x_1 \Delta x_1 + 2(I_r - I_y - I_p)m_1 z_1 \Delta z_1 \\
&+2(I_r - I_y + I_p)m_2 x_2 \Delta x_2 + 2(I_r - I_y - I_p)m_2 z_2 \Delta z_2 \\
&+2(I_r - I_y + I_p)m_3 x_3 \Delta x_3 + 2(I_r - I_y - I_p)m_3 z_3 \Delta z_3 \\
&= 0
\end{aligned} \tag{4.15}$$

roll/yaw frequency constraint (Equation (3.43))

$$\begin{aligned}
2\left(2y_1^2\Delta m_1 + 2y_2^2\Delta m_2 + 2y_3^2\Delta m_3\right) + 4(2m_1 y_1 \Delta y_1 + 2m_2 y_2 \Delta y_2 + 2m_3 y_3 \Delta y_3) \\
= I_p - I_r - I_y
\end{aligned} \tag{4.16}$$

stability constraint ($I_y < I_r < I_p$)

$$
\begin{aligned}
&2\left[(x_1^2 - z_1^2)\Delta m_1 + (x_2^2 - z_2^2)\Delta m_2 + (x_3^2 - z_3^2)\Delta m_3\right] \\
&\quad + 4(m_1 x_1 \Delta x_1 - m_1 z_1 \Delta z_1 + m_2 x_2 \Delta x_2 - m_2 z_2 \Delta z_2 + m_3 x_3 \Delta x_3 - m_3 z_3 \Delta z_3) < I_r - I_y \\
&2\left[(y_1^2 - x_1^2)\Delta m_1 + (y_2^2 - x_2^2)\Delta m_2 + (y_3^2 - x_3^2)\Delta m_3\right] \\
&\quad - 4(m_1 x_1 \Delta x_1 - m_1 y_1 \Delta y_1 + m_2 x_2 \Delta x_2 - m_2 y_2 \Delta y_2 + m_3 x_3 \Delta x_3 - m_3 y_3 \Delta y_3) < I_p - I_r
\end{aligned}
\tag{4.17}
$$

objective function

$$
\begin{aligned}
\min f(x) = {} & |\text{Pipe\_12}|^2 + |\text{Pipe\_21}|^2 + |\text{Pipe\_13}|^2 + |\text{Pipe\_31}|^2 + |\text{Pipe\_15}|^2 + |\text{Pipe\_51}|^2 \\
& + |\text{Pipe\_16}|^2 + |\text{Pipe\_61}|^2 + |\text{Pipe\_23}|^2 + |\text{Pipe\_32}|^2 + |\text{Pipe\_24}|^2 + |\text{Pipe\_42}|^2 \\
& + |\text{Pipe\_26}|^2 + |\text{Pipe\_62}|^2 + |\text{Pipe\_34}|^2 + |\text{Pipe\_43}|^2 + |\text{Pipe\_35}|^2 + |\text{Pipe\_53}|^2 \\
& + |\text{Pipe\_45}|^2 + |\text{Pipe\_54}|^2 + |\text{Pipe\_46}|^2 + |\text{Pipe\_64}|^2 + |\text{Pipe\_56}|^2 + |\text{Pipe\_65}|^2 \\
& + \Big(\big|\text{tank 1 location change along x-axis}\big|^2 \\
& \quad + |\text{tank 1 location change along y-axis}|^2 \\
& \quad + |\text{tank 1 location change along z-axis}|^2\Big)^{\frac{1}{2}} \\
& + \Big(\big|\text{tank 2 location change along x-axis}\big|^2 \\
& \quad + |\text{tank 2 location change along y-axis}|^2 \\
& \quad + |\text{tank 2 location change along z-axis}|^2\Big)^{\frac{1}{2}} \\
& + \Big(\big|\text{tank 3 location change along x-axis}\big|^2 \\
& \quad + |\text{tank 3 location change along y-axis}|^2 \\
& \quad + |\text{tank 3 location change along z-axis}|^2\Big)^{\frac{1}{2}}
\end{aligned}
\tag{4.18}
$$

As defined in Section 3.4, case 4 is the generalized design with center-of-mass fixed and three pairs of masses used to compute the mass mapping. The objective function, Equation (4.18), for case 4 is similar to case 3 except that each tank location change is not restricted to be along one axis. To compare the optimal solutions with case 3, the same frequencies and stability constraints, Equations (4.15)-(4.17), are applied. To avoid unrealistic design, each tank is limited to move outward up to $2m$ from the origin. Since each tank can be located at any place inside the system, the distance between any two tanks cannot be the same length as examined through case 1 to case 3. Therefore, a various weighting coefficients should be applied to each pipe in Equation (4.18). However, it is assumed that the mass transfer cost between any two tanks is the same, thus all weighting coefficients are set to 1.

Tables 4.9 and 4.10 present the result of the minimum mass transfer and the tank location for optimal mass distribution, respectively. A total of 0.05161 kg is required to travel for the optimal mapping at stage 2. Compared with case 3, all tank locations are located at almost same positions as in case 3. Table 4.11 contains the amount of the mass per each tank during mass mapping and a diagram of each stage is shown in Figure 4.6. As illustrated in Figure 4.1, each circle size considers the amount of mass each tank, thus all the circles have almost same size in the diagram.

Table 4.9: Optimal Mass Shift Through Each Pipe for Case 4 (kg)

Pipe_12 = 0.00613	Pipe_21 = -0.00613
Pipe_13 = -0.00046	Pipe_31 = 0.00046
Pipe_15 = 0.00615	Pipe_51 = -0.00615
Pipe_16 = -0.00039	Pipe_65 = 0.00039
Pipe_23 = -0.00635	Pipe_32 = 0.00635
Pipe_24 = -0.00611	Pipe_42 = 0.00611
Pipe_26 = -0.00641	Pipe_62 = 0.00641
Pipe_34 = 0.00040	Pipe_43 = -0.00040
Pipe_35 = 0.00637	Pipe_53 = -0.00637
Pipe_45 = 0.00608	Pipe_54 = -0.00608
Pipe_46 = -0.00036	Pipe_64 = 0.00036
Pipe_56 = -0.00641	Pipe_65 = 0.00641
Total amount of mass shifted: 0.05161 kg	

Table 4.10: Tank location for Stage 1 and Stage 2 for Case 4 (m)

	Stage 1	Stage 2
Tank 1	[1, 0, 0]	[0.999985, -0.000006, 0.000010]
Tank 2	[0, 1, 0]	[0.000221, 0.065644, 0.000220]
Tank 3	[0, 0, 1]	[-0.000003, 0.000005, 1.000012]
Tank 4	[-1, 0, 0]	[-0.999985, 0.000006, -0.000010]
Tank 5	[0, -1, 0]	[-0.000221, -0.065644, -0.000220]
Tank 6	[0, 0, -1]	[0.000003, -0.000005, -1.000012]

Table 4.11: Mass Distribution for Stage 1 and Stage 2 for Case 4 (kg)

	Stage 1	Stage 2	Mass shifted
Tank 1	10	10.0114	0.0114
Tank 2	10	9.9750	-0.0250
Tank 3	10	10.0136	0.0136
Tank 4	10	10.0114	0.0114
Tank 5	10	9.9750	-0.0250
Tank 6	10	10.0136	0.0136
Total Amount of Mass	60	60	0 (conserved)

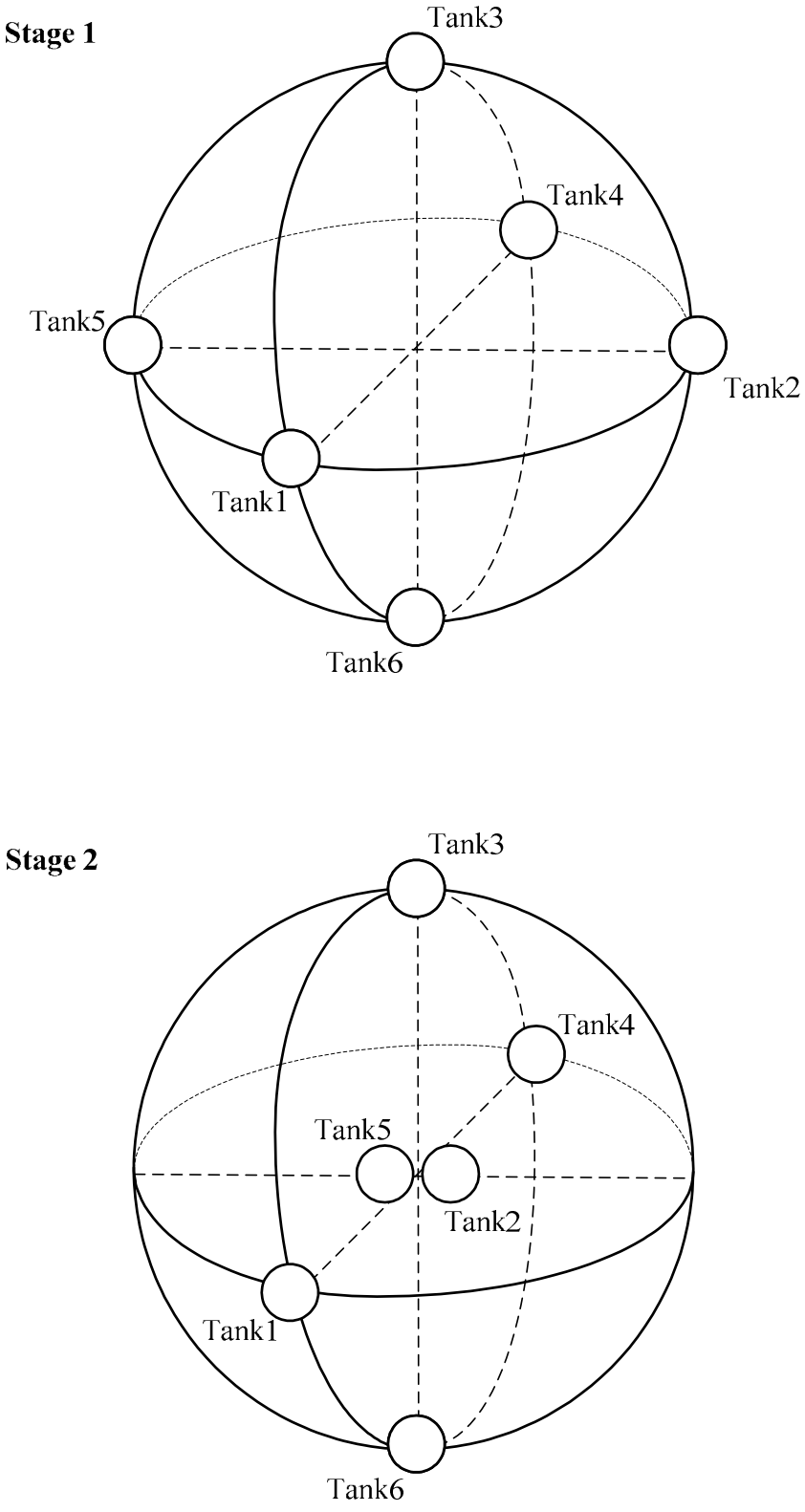

Figure 4.6: Diagram of Tank Distribution for Each Stage for Case 4

The most distinguishing property of case 4 is the appearance of product of inertia elements. Since each tank is allowed to move along each axis only for case 1, 2, and 3, the principal axes for stage 1 and stage 2 remain unchanged. If a tank is not limited to stay along the axis, off diagonal elements in the inertia matrix are not zero at stage 2 and those values cause the principal axes at stage 2 to be different from stage 1. When the roll/yaw and pitch frequency are determined to find the optimal mass transfer at stage 2, those frequencies explain the motion of the principal axes in stage 2, not stage 1. Therefore, a DCM (Direction Cosine Matrix) needs to be found to transfer data from stage 1 to stage 2 and vice versa. All data defined at stage 2 must be converted via DCM to be used at stage 1. Equation (4.19) presents the change of moment of inertia and the DCM is calculated in Equation (4.20).

$$\Delta I = \begin{bmatrix} -37.3966 & -0.0043 & -0.0001 \\ -0.0043 & 0.0499 & -0.0045 \\ -0.0001 & -0.0045 & -37.4020 \end{bmatrix} (\mathrm{kg \cdot m^2}) \tag{4.19}$$

$$\mathrm{DCM} = \begin{bmatrix} 0.99999 & 9\times10^{-6} & 5\times10^{-5} \\ 9\times10^{-6} & -0.99999 & 6\times10^{-5} \\ 5\times10^{-5} & -6\times10^{-5} & -0.99999 \end{bmatrix} \tag{4.20}$$

Since DCM in Equation (4.20) is nearly an identity matrix, both the angular velocity and rate and ground coverage area is almost same as Figure 4.2 and Figure 4.3,

respectively. Figure 4.7 illustrates the stability constraint $I_y < I_r < I_p$ for each stage is satisfied.

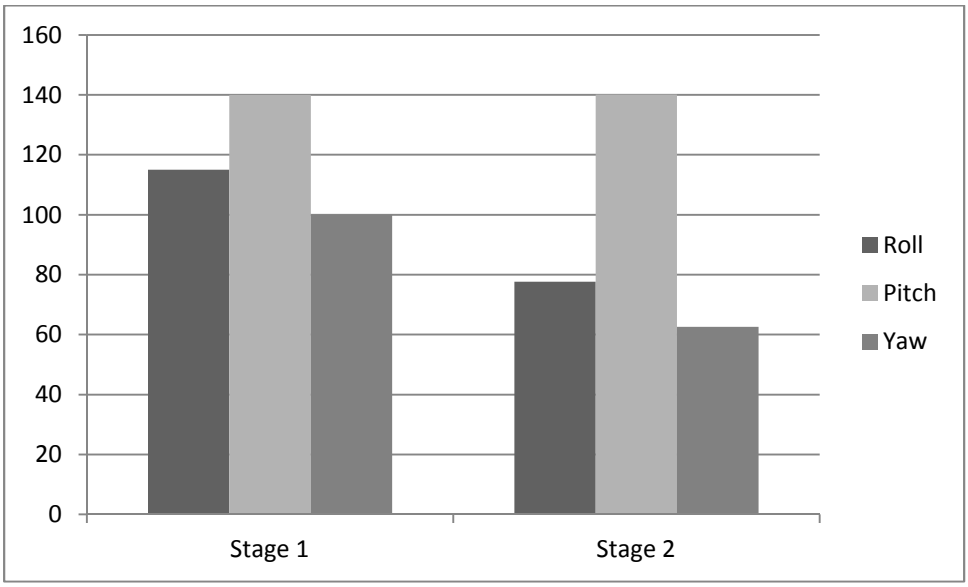

Figure 4.7: Principal Moments of Inertia for Each Stage for Case 4 ($kg \cdot m^2$)

It has been shown that the change of tank location is more effective than the mass movement to complete the attitude maneuver. This contribution can be altered by adding a relevant weighting coefficient to the objective function or boundary constraints for each tank location. More models are examined later in this chapter.

Case 5 Center-of-mass is changing due to the moving masses

Conditions

No restriction for the mass amount and the location of each tank

Roll frequency at stage 2: $2n$

Pitch frequency at stage 2: unchanged

pitch frequency constraint (Equation (3.42))

$$\begin{aligned}&(I_r - I_y + I_p)(M_{sat} + m_2 + m_3 + m_5 + m_6)\bar{d}(1)^2 + \\ &(I_r - I_y - I_p)(M_{sat} + m_1 + m_2 + m_4 + m_5)\bar{d}(3)^2 + \\ &m_1(I_r - I_y + I_p)(d - \bar{d}(1))^2 + m_4(I_r - I_y + I_p)(-d - \bar{d}(1))^2 + \\ &m_3(I_r - I_y - I_p)(d - \bar{d}(3))^2 + m_6(I_r - I_y - I_p)(-d - \bar{d}(3))^2 \\ &\quad = 0\end{aligned} \tag{4.21}$$

where $\bar{d}$ is defined in Equation (3.30) as the vector from origin to the new center-of-mass.

roll/yaw frequency constraint (Equation (3.43))

$$\begin{aligned}&\left[(M_{\text{sat}} + m_1 + m_3 + m_4 + m_6)\bar{d}(2)^2 + m_2(d - \bar{d}(2))^2 + m_5(-d - \bar{d}(2))^2\right] \\ &\qquad = \frac{1}{2}(I_p - I_r - I_y)\end{aligned} \tag{4.22}$$

stability constraint ($I_y < I_r < I_p$)

$$\begin{aligned} M_{\text{sat}}(\bar{d}(1)^2 - \bar{d}(3)^2) + m_1\left[(d-\bar{d}(1))^2 - \bar{d}(3)^2\right] + m_2\left[\bar{d}(1)^2 - \bar{d}(3)^2\right] \\ + m_3\left[\bar{d}(1)^2 - (d-\bar{d}(3))^2\right] + m_4\left[(-d-\bar{d}(1))^2 - \bar{d}(3)^2\right] \\ + m_5\left[\bar{d}(1)^2 - \bar{d}(3)^2\right] + m_6\left[\bar{d}(1)^2 - (-d-\bar{d}(3))^2\right] < I_r - I_y \\ M_{\text{sat}}(\bar{d}(2)^2 - \bar{d}(1)^2) + m_1\left[\bar{d}(2)^2 - (d-\bar{d}(1))^2\right] + m_2\left[(d-\bar{d}(2))^2 - \bar{d}(1)^2\right] \\ + m_3\left[\bar{d}(2)^2 - \bar{d}(1)^2\right] + m_4\left[\bar{d}(2)^2 - (-d-\bar{d}(1))^2\right] \\ + m_5\left[(-d-\bar{d}(2))^2 - \bar{d}(1)^2\right] + m_6\left[\bar{d}(2)^2 - \bar{d}(1)^2\right] < I_p - I_r \end{aligned} \tag{4.23}$$

objective function

$$\begin{aligned} \min f(x) = \ & |\text{Pipe\_12}|^2 + |\text{Pipe\_21}|^2 + |\text{Pipe\_13}|^2 + |\text{Pipe\_31}|^2 + |\text{Pipe\_15}|^2 + |\text{Pipe\_51}|^2 \\ & + |\text{Pipe\_16}|^2 + |\text{Pipe\_61}|^2 + |\text{Pipe\_23}|^2 + |\text{Pipe\_32}|^2 + |\text{Pipe\_24}|^2 + |\text{Pipe\_42}|^2 \\ & + |\text{Pipe\_26}|^2 + |\text{Pipe\_62}|^2 + |\text{Pipe\_34}|^2 + |\text{Pipe\_43}|^2 + |\text{Pipe\_35}|^2 + |\text{Pipe\_53}|^2 \\ & + |\text{Pipe\_45}|^2 + |\text{Pipe\_54}|^2 + |\text{Pipe\_46}|^2 + |\text{Pipe\_64}|^2 + |\text{Pipe\_56}|^2 + |\text{Pipe\_65}|^2 \end{aligned} \tag{4.24}$$

A design for case 5 is the locations of the tank are fixed, but the mass amount in each tank can be different from each other causing the change of center-of-mass. This results in the change of each tank location again. The objective function used for case 5 is given in Equation (4.24). When the objective function is minimized, the total shifted mass through pipes is the minimum mass moved and also satisfies the balanced mass distribution.

With same constraints from roll/yaw and pitch frequencies and gravity-gradient stability, it is found that there is no feasible mass distribution. This might have been

anticipated from case 1 through case 4. Among those cases, only case 2 does not have the optimal solutions since the location of each tank is not allowed to change. Also, the shift of each tank location is more effective than the mass movement in cases 3 and 4. Case 5 has a similar constraint in that the tank location is moved due to the change of center-of-mass, but the result proves that shifting mass is not enough to achieve the specified roll frequency at stage 2. Thus, the next step is to find the roll/yaw and pitch frequency range at stage 2 by trial and error with same objective function because the computation time to find the optimal solution from using MATLAB's optimization solver, *fmincon*, take less than a minute with the early version of Intel's Pentium Dual-Core processor for each case. The frequency constraints are found from Equations (3.42) and (3.43) and the stability constraints are Equation (4.23). The procedure is implemented as following.

① Try different values for roll/yaw frequency at stage 2 while the pitch frequency remains unchanged.

② Try different values for pitch frequency at stage 2 while the roll/yaw frequency remains unchanged.

The result yields,

① The available roll/yaw frequency with pitch frequency unchanged at stage 2 is from 82.3% to 108.5% of the roll/yaw frequency at stage 1.

② The available pitch frequency with roll/yaw frequency unchanged at stage 2 is from 0.1% to 166.2% of the pitch frequency at stage 1.

From the result above, the pitch frequency has a wider frequency range at stage 2 and the available frequency range satisfies all four constraints, two from frequency and two from the gravity-gradient stabilization. However, when both frequencies on boundary are applied, the feasible mass mapping is not always guaranteed.

Now that the available frequency ranges for case 5 are known, the next simulation tests a different combination of roll/yaw and pitch frequencies. For the same map-making mission, higher roll frequency is preferred to cover a larger area. The pitch frequency is not a major factor for this mission, but less frequency increases the stability of the satellite in general. Thus, the roll/yaw and pitch frequencies for stage 2 are set to 105% and 38.5% of stage 1, respectively. The pitch frequency at 38.5% is the lowest possible value when the roll/yaw frequency is 105%.

Table 4.12 shows the roll/yaw and pitch frequencies for stage 1 and stage 2. As pre-determined, pitch frequency at stage 2 is decreased to 38.5% of the pitch frequency at stage 1 while the roll/yaw frequency is increased by 5%.

Table 4.12: Roll/Yaw and Pitch Frequencies at Each Stage for Case 5 (Hz)

Parameters	Stage 1	Stage 2
Pitch frequency	0.000611	0.000234
Roll / Yaw frequency	0.001506	0.001582

Table 4.13 presents the optimal mass shift through each pipe. Since the frequency values are chosen near the boundary, more mass are shifted than the other cases. A total of 22.4874 kg of mass is shifted to achieve the required frequencies and this mapping

satisfies both minimum total mass movement and balanced mass distribution. The amount of shifted mass per each tank is presented in Table 4.14 and the diagram for each stage is illustrated in Figure 4.8. It is noticed that the size of each circle is different due to the mass shift. Case 1 through 4, the pair mass must be the same to maintain the center-of-mass unmoved but all tanks have different amount of mass. Unbalanced mass distribution causes the center-of-mass to be moved and the new center-of-mass is located at $\begin{bmatrix} -0.01657 & 0.00016 & -0.00377 \end{bmatrix}^T$ m.

Table 4.13: Optimal Mass Shift Through Each Pipe for Case 5 (kg)

Pipe_12 = 2.9966	Pipe_21 = -2.9966
Pipe_13 = 1.0373	Pipe_31 = -1.0373
Pipe_15 = 1.9135	Pipe_51 = -1.9135
Pipe_16 = 1.2530	Pipe_65 = -1.2530
Pipe_23 = -1.6617	Pipe_32 = 1.6617
Pipe_24 = -2.8073	Pipe_42 = 2.8073
Pipe_26 = -1.5866	Pipe_62 = 1.5866
Pipe_34 = -1.2517	Pipe_43 = 1.2517
Pipe_35 = 2.1459	Pipe_53 = -2.1459
Pipe_45 = 2.8804	Pipe_54 = -2.8804
Pipe_46 = 0.8406	Pipe_64 = -0.8406
Pipe_56 = -2.1128	Pipe_65 = 2.1128
Total amount of mass shifted: 22.4874 kg	

Table 4.14: Mass Distribution for Stage 1 and Stage 2 for Case 5 (kg)

	Stage 1	Stage 2	Mass shifted
Tank 1	10	17.2004	7.2004
Tank 2	10	0.9478	-9.0522
Tank 3	10	11.5186	1.5186
Tank 4	10	17.7800	7.7800
Tank 5	10	0.9475	-9.0525
Tank 6	10	11.6057	1.6057
Total Amount of Mass	60	60	0

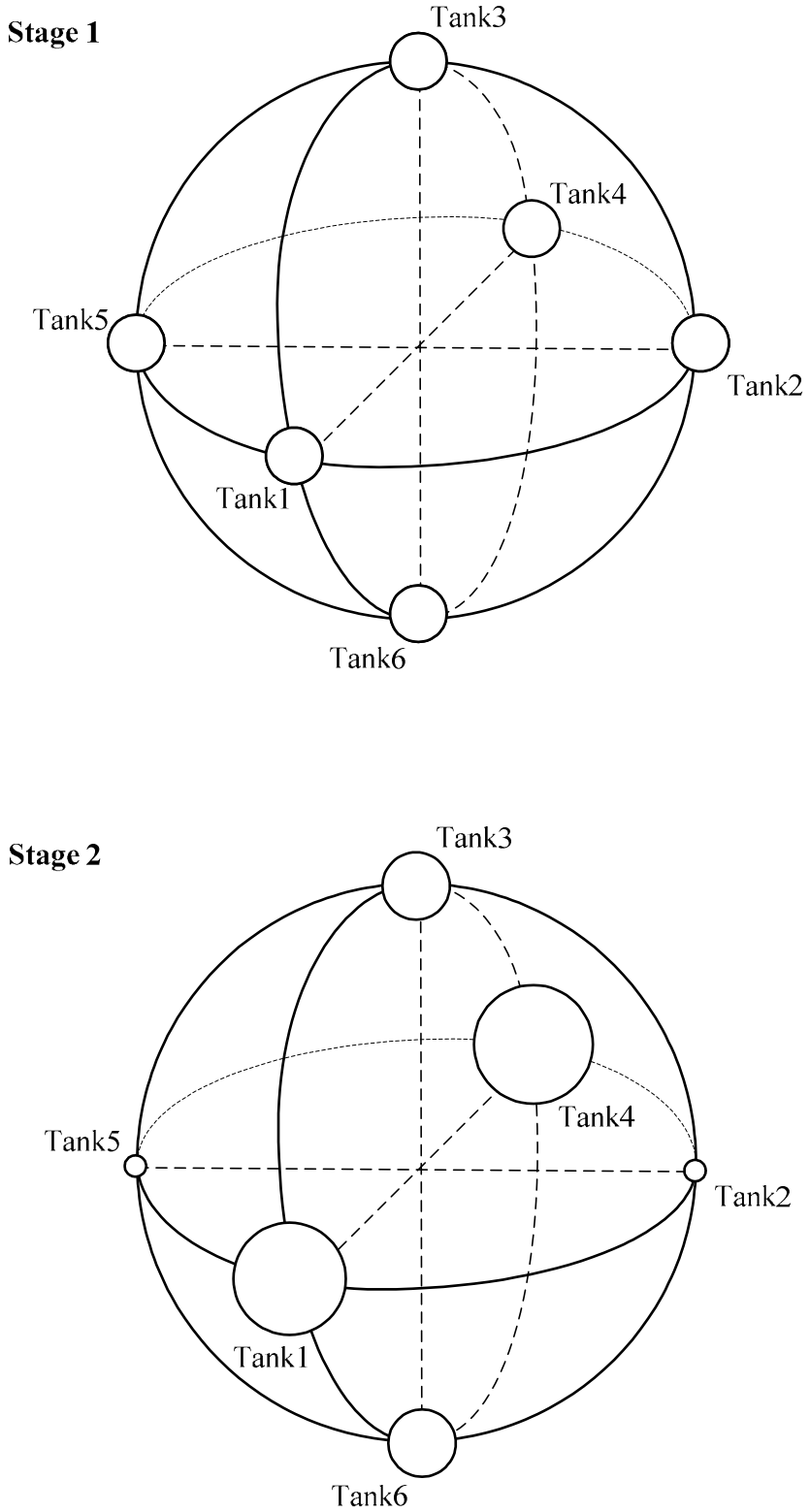

Figure 4.8: Diagram of Tank Distribution for Each Stage for Case 5 (the size of each circle is not exactly scaled)

Since the center-of-mass has been relocated, the change in moments of inertia is the summation of moment of inertia change of system mass and the satellite system. Each moments of inertia change is computed in Equations (4.25) and (4.26).

$$\Delta I_{\text{sat}} = \begin{bmatrix} 0.00142 & 0.00026 & -0.00624 \\ 0.00026 & 0.02887 & 0.00006 \\ -0.00624 & 0.00006 & 0.02745 \end{bmatrix} (\text{kg} \cdot \text{m}^2) \tag{4.25}$$

$$\Delta I_{\text{mass}} = \begin{bmatrix} 25.01976 & 0.00006 & -0.00012 \\ 0.00006 & 58.102226 & 0.00002 \\ -0.00012 & 0.00002 & 36.87293 \end{bmatrix} (\text{kg} \cdot \text{m}^2) \tag{4.26}$$

Then, the principal moments of inertia for stage 1 and stage 2 satisfy the stability constraints in Figure 4.9. Compared with previous results, all three values for the principal moments of inertia at stage 2 are increased. It is also found that the roll moment of inertia and yaw moment of inertia have almost same amount. This makes the pitch frequency a small number and longer period from Equation (2.35). As calculated in Equations (4.25) and (4.26), this simulation also creates the products of inertia. Thus, a DCM is needed to convert the data from stage 1 and stage 2 and computed as

$$\text{DCM} = \begin{bmatrix} 0.999999 & 0.002038 & -0.000001 \\ 0.002038 & -0.999999 & -0.000005 \\ -0.000001 & 0.000005 & -0.999999 \end{bmatrix} \tag{4.27}$$

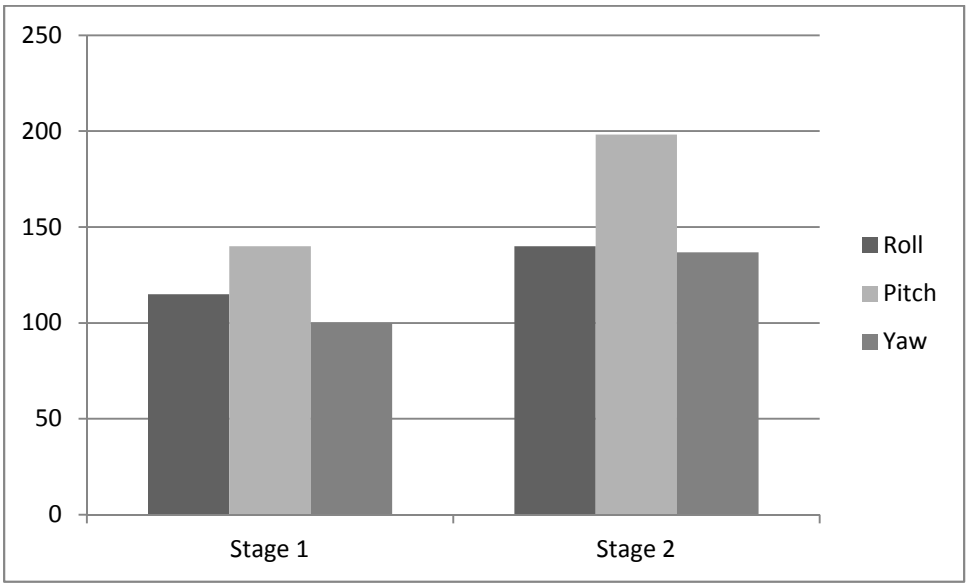

Figure 4.9: Principal Moments of Inertia for Each Stage for Case 5 ($kg \cdot m^2$)

The roll, pitch, and yaw angles and their rates for stage 1 and stage 2 are presented in Figure 4.10. To compare the attitude angles in a same coordinate system, data at stage 2 is converted into stage 1 via Equation (4.27). Since the roll/yaw frequency is increased only 5% at stage 2, frequency change is not noticeable. However, the pitch frequency change is conspicuous because the frequency is reduced to half. Figure 4.11 illustrates the ground coverage from this simulation. A 5% increase of roll/yaw frequency does not show the outstanding ground coverage change like in Figure 4.4 but the small increase is still noticed. The longitude deviation range at stage 1 is -0.061 to 0.061 degree and the deviation range at stage 2 is -0.082 to 0.082 degree.

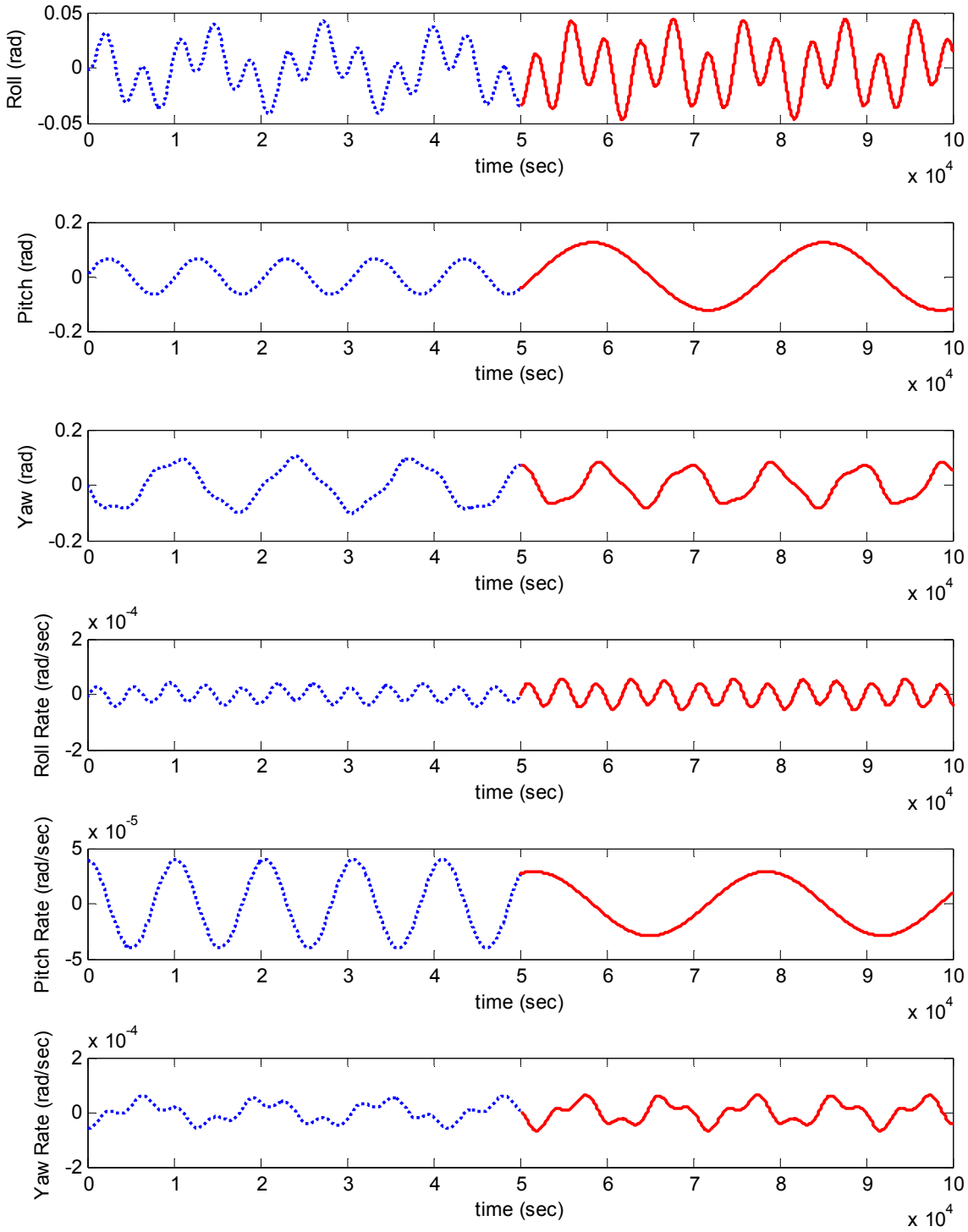

Figure 4.10: Roll, Pitch and Yaw Angles and Their Rates for Stage 1 and Stage 2 for Case 5 (stage 2 begins at 5×10^4 sec)

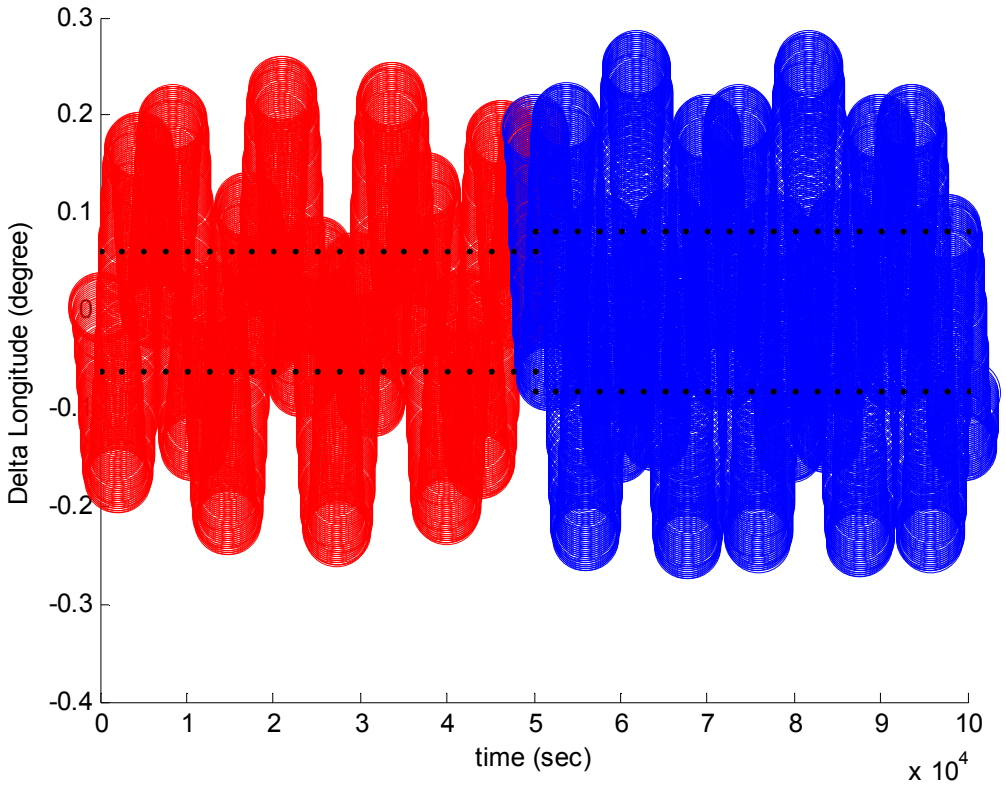

Figure 4.11: Ground Coverage Change between Stage 1 and Stage 2 for Case 5 (stage 2 begins at 5×10^4 sec)

The model for case 4 is examined to compare the optimal mass distribution subject to the same constraints. The same frequency constraints, 5% increase of roll/yaw frequency and 38.5% of pitch frequency at stage 1 are applied. Table 4.15 presents the optimal mass distribution at stage 2. Total shifted mass is still less than 0.1 kg to complete this maneuver. This means the relocation of each tank is still more dominant than the mass transfer to achieve the roll/yaw and pitch frequencies at stage 2.

Table 4.15: Optimal Mass Shift Through Each Pipe for Case 4 (kg)

Pipe_12 = 0.01250	Pipe_21 = -0.01250
Pipe_13 = 0.00985	Pipe_31 = -0.00985
Pipe_15 = 0.01250	Pipe_51 = -0.01250
Pipe_16 = 0.00985	Pipe_65 = -0.00985
Pipe_23 = -0.00264	Pipe_32 = 0.00264
Pipe_24 = -0.01250	Pipe_42 = 0.01250
Pipe_26 = -0.00264	Pipe_62 = 0.00264
Pipe_34 = -0.00986	Pipe_43 = 0.00986
Pipe_35 = 0.00264	Pipe_53 = -0.00264
Pipe_45 = 0.01250	Pipe_54 = -0.01250
Pipe_46 = 0.00986	Pipe_64 = -0.00985
Pipe_56 = -0.00264	Pipe_65 = 0.00264
Total amount of mass shifted: 0.09999 kg	

Table 4.16: Tank location for Stage 1 and Stage 2 for Case 4 (m)

	Stage 1	Stage 2
Tank 1	[1, 0, 0]	[1.311485, 0.000005, 0.000016]
Tank 2	[0, 1, 0]	[-0.000000, 0.822443, 0.000000]
Tank 3	[0, 0, 1]	[0.000000, 0.000000, 0.999998]
Tank 4	[-1, 0, 0]	[-1.311485, -0.000005, -0.000016]
Tank 5	[0, -1, 0]	[0.000000, -0.822443, -0.000000]
Tank 6	[0, 0, -1]	[-0.000000, -0.000000, -0.999998]

Table 4.17: Mass Distribution for Stage 1 and Stage 2 for Case 4 (kg)

	Stage 1	Stage 2	Mass shifted
Tank 1	10	10.0447	0.0447
Tank 2	10	9.9697	-0.0303
Tank 3	10	9.9856	-0.0144
Tank 4	10	10.0447	0.0447
Tank 5	10	9.9697	-0.0303
Tank 6	10	9.9856	-0.0144
Total Amount of Mass	60	60	0 (conserved)

Table 4.16 shows the tank location change before and after the simulation. Compared with Table 4.10, tank 1 and tank 4 move outward and tank 2 and tank 5 are shifted toward the origin. Tank 3 and tank 6 remain near their original location at stage 1. All six tanks remain near each axis even though they can be moved to any location. A diagram is illustrated in Figure 4.12. Table 4.17 contains the amount of shifted mass per each tank. Since the total mass movement shown in Table 4.15 is small, each tank also shows the small amount of mass change. In addition, the change of moment of inertia and corresponding DCM are calculated as:

$$\Delta I = \begin{bmatrix} \text{-7.19177} & \text{-0.00010} & \text{-0.00034} \\ \text{-0.00010} & 12.5199 & \text{-0.00001} \\ \text{-0.00034} & \text{-0.00001} & 5.38602 \end{bmatrix} (\text{kg} \cdot \text{m}^2) \tag{4.28}$$

$$\text{DCM} = \begin{bmatrix} 0.99999 & \text{-0.00014} & -2\times10^{-7} \\ 0.00014 & 0.99999 & -2\times10^{-6} \\ 2\times10^{-7} & 2\times10^{-6} & 0.99999 \end{bmatrix} \tag{4.29}$$

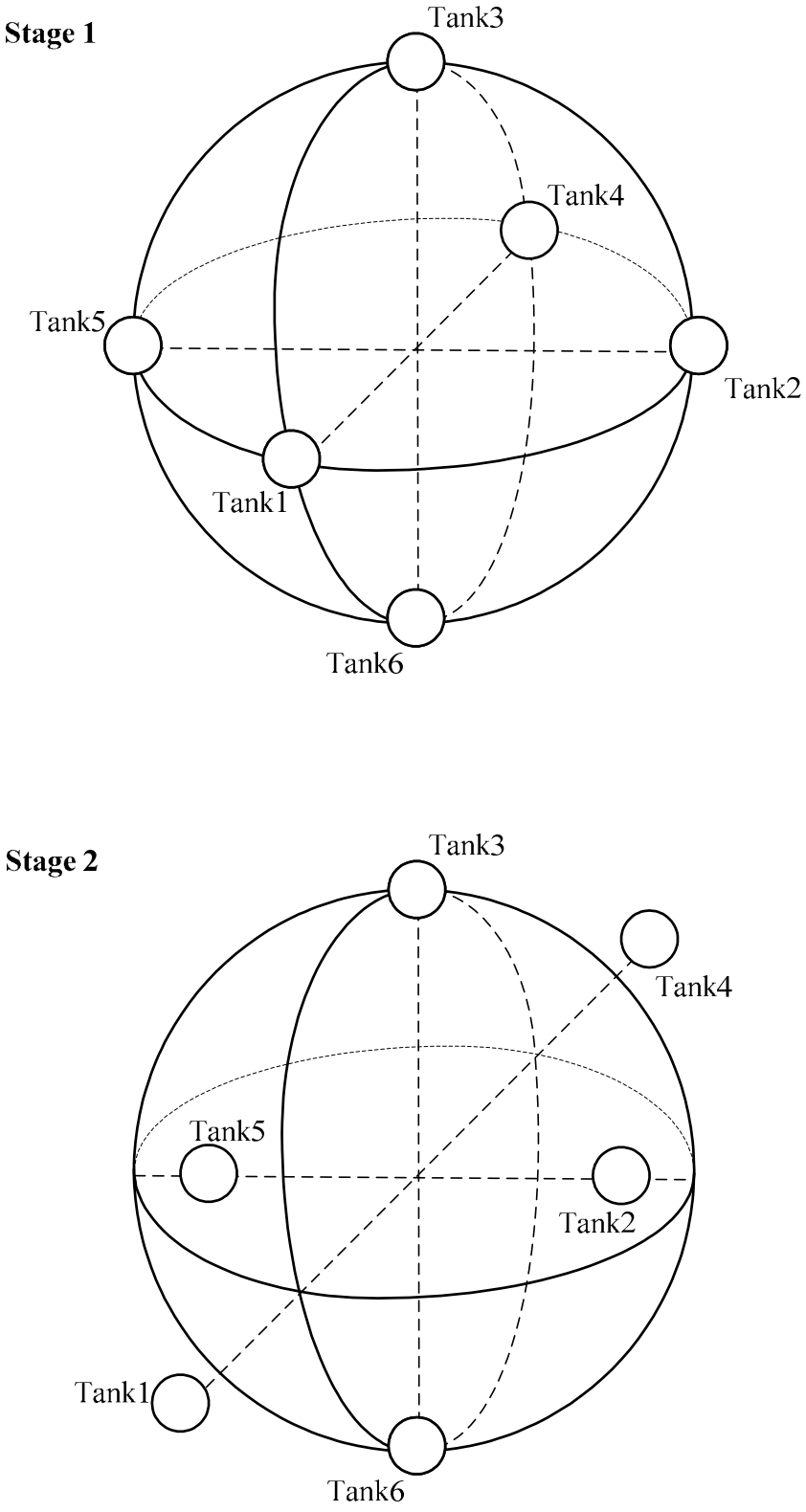

Figure 4.12: Diagram of Tank Distribution for Each Stage for Case 4

Since the DCM is near the identity matrix, angular velocity and their rates, and ground coverage are almost same as case 5. The difference is the optimal mass distribution caused by the different model. Figure 4.13 illustrates that the stability constraint $I_y < I_r < I_p$ for each stage is satisfied. As seen in Figure 4.9, the roll moment of inertia and yaw moment of inertia are pretty close each other due to the same reason, which is the pitch frequency at stage 2 is set to have low pitch frequency. On the contrary, all three values for the principal moments of inertia are not changed at stage 2 as the case 5 model presented.

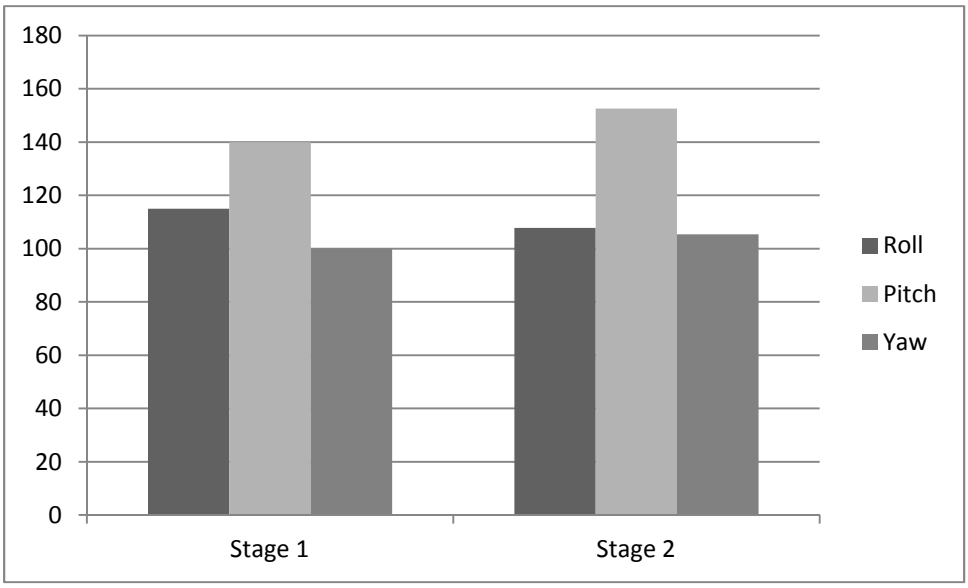

Figure 4.13: Principal Moments of Inertia for Each Stage for Case 4 ($kg \cdot m^2$)

It has been shown that two different models, case 4 and case 5, can be used to find the optimal solutions under the same frequency and stability constraints. Because each design has different characteristics, the optimal mass mapping is different for the same problem. Examples with more realistic constraints are examined for the application to the satellite.

From the result of case 4, the optimal mass distribution and the location of each tank is found. The optimal solution is acceptable mathematically, but it is not easy to place a tank only 6 cm away from the origin. Thus more realistic constraint is added which is only one pair tanks (e.g., tank 1 and tank 4) can move along one axis (e.g., x-axis) with the range of 0.9 m to 1.1 m from the origin. With the same frequency and stability constraints as above, the following results are computed.

Table 4.18 presents the mass transfer both minimizing the total mass movement and also distributing the mass mapping among tanks. The outstanding difference from the previous simulations by the case 4 model is the increase of the total shifted mass. Usually less than 1 kg is shifted with the contribution of tank relocation. Under this constraint, the advantage of tank relocation is not enough to obtain the required change in moments of inertia. Table 4.19 shows the location of each tank at stage 1 and stage 2. Case 4 model usually changes the tank location more than the mass transfer, thus the maximum movement of tank location occurs and are presented in Table 4.19. Since more mass is moved through each pipe, more mass is shifted in each tank as well. The amount of mass for each stage is found in Table 4.20. A diagram is illustrated in Figure 4.14 before and after the maneuver.

Table 4.18: Optimal Mass Shift Through Each Pipe for Case 4 (kg)

Pipe_12 = 1.281	Pipe_21 = -1.281
Pipe_13 = 0.716	Pipe_31 = -0.716
Pipe_15 = 1.281	Pipe_51 = -1.281
Pipe_16 = 0.716	Pipe_65 = -0.716
Pipe_23 = -0.565	Pipe_32 = 0.565
Pipe_24 = -1.281	Pipe_42 = 1.281
Pipe_26 = -0.565	Pipe_62 = -0.565
Pipe_34 = -0.716	Pipe_43 = 0.716
Pipe_35 = 0.565	Pipe_53 = -0.565
Pipe_45 = 1.281	Pipe_54 = -1.281
Pipe_46 = 0.716	Pipe_64 = -0.716
Pipe_56 = -0.565	Pipe_65 = 0.565
Total amount of mass shifted: 10.253 kg	

Table 4.19: Tank location for Stage 1 and Stage 2 for Case 4 (m)

	Stage 1	Stage 2
Tank 1	[1, 0, 0]	[1.1, 0, 0]
Tank 2	[0, 1, 0]	[0, 1, 0]
Tank 3	[0, 0, 1]	[0, 0, 1]
Tank 4	[-1, 0, 0]	[-1.1, 0, 0]
Tank 5	[0, -1, 0]	[0, -1, 0]
Tank 6	[0, 0, -1]	[0, 0, -1]

Table 4.20: Mass Distribution for Stage 1 and Stage 2 for Case 4 (kg)

	Stage 1	Stage 2	Mass shifted
Tank 1	10	13.996	3.996
Tank 2	10	6.306	-3.694
Tank 3	10	9.698	-0.302
Tank 4	10	13.996	3.996
Tank 5	10	6.306	-3.694
Tank 6	10	9.698	-0.302
Total Amount of Mass	60	60	0 (conserved)

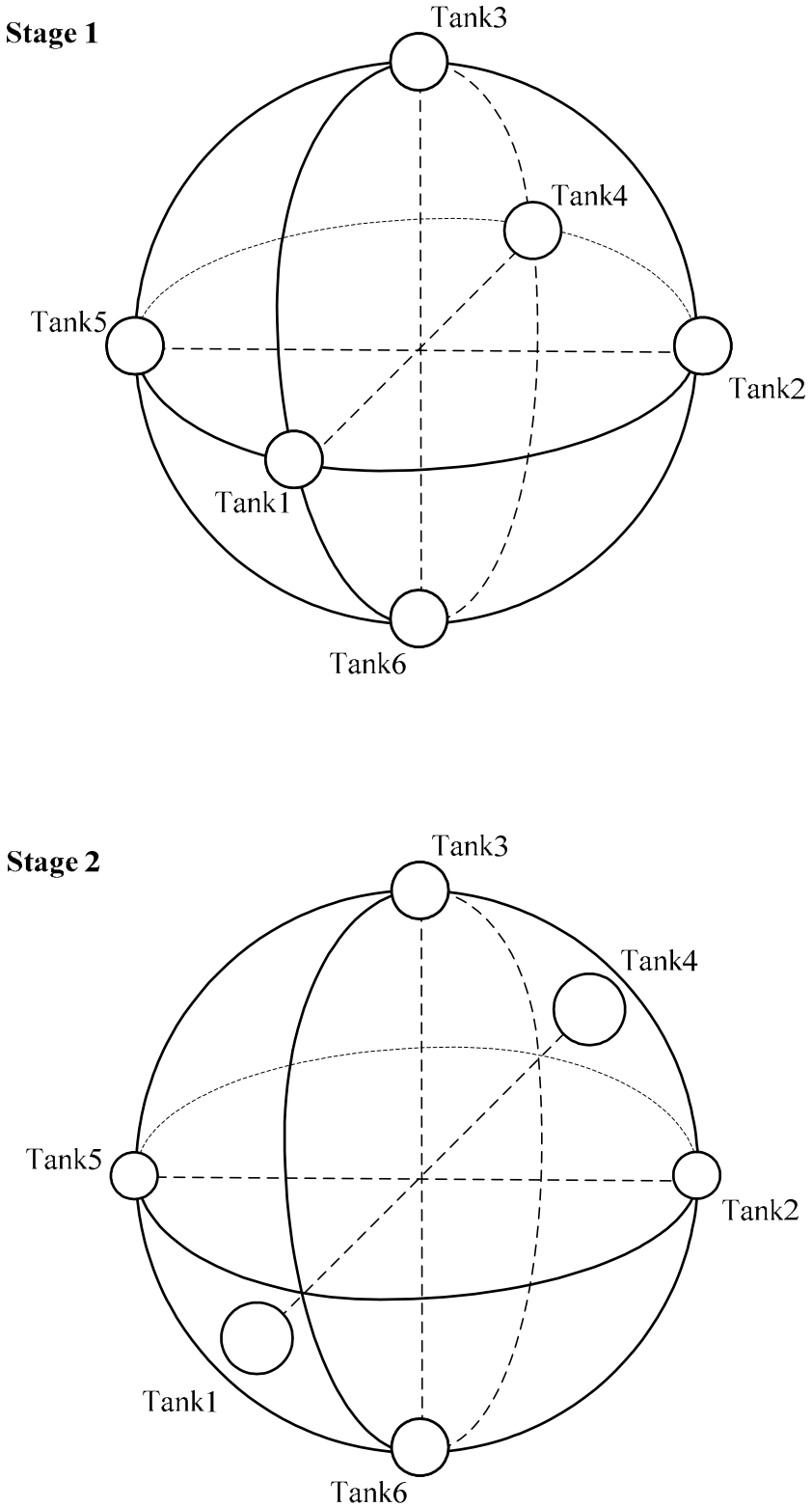

Figure 4.14: Diagram of Tank Distribution for Each Stage for Case 4

The change of the moments of inertia is computed in Equation (4.30) and the DCM becomes an identity matrix since the constraint applied for this simulation does not change the principal axes between stage 1 and stage 2. This is also verified by checking that the off diagonal terms are zero in Equation (4.30).

$$\Delta I = \begin{bmatrix} -7.9918 & 0 & 0 \\ 0 & 11.3879 & 0 \\ 0 & 0 & 4.6038 \end{bmatrix} (\mathrm{kg} \cdot \mathrm{m}^2) \tag{4.30}$$

The principal moments of inertia for both stages are presented in Figure 4.15.

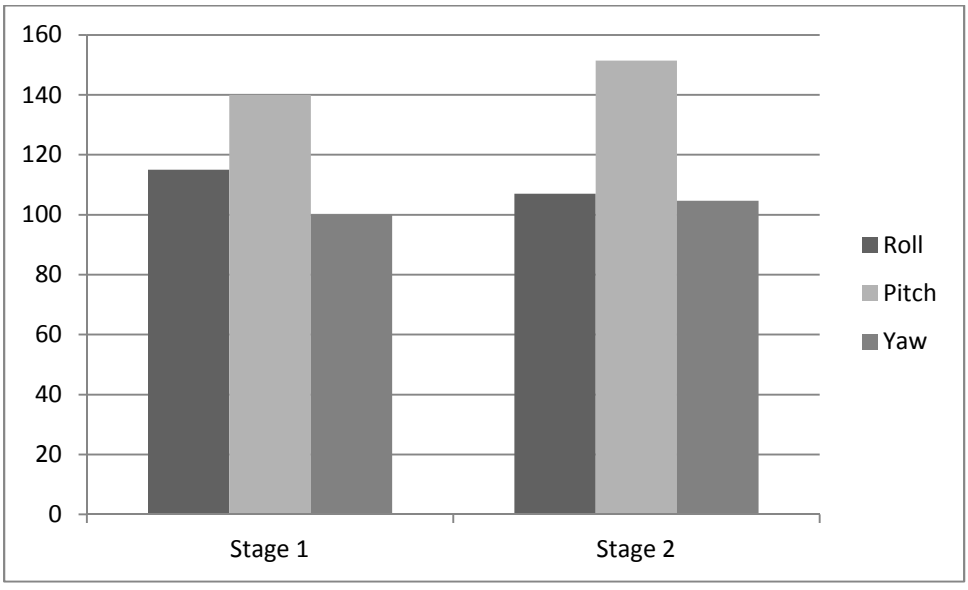

Figure 4.15: Principal Moments of Inertia for Each Stage for Case 4 ($\mathrm{kg} \cdot \mathrm{m}^2$)

A different constraint can be applied to the case 5 model such as one path (pipe) being blocked. By assuming that Pipe_12 is blocked, the optimal mass distribution is obtained as follows.

The amount of mass travelling through each pipe is presented in Table 4.21. As assumed, there is no mass transfer through Pipe_12 and Pipe_21 also has no mass movement automatically. All other pipes allow mass shift and total 23.584 kg of mass transfer satisfies both minimum total mass move and the balanced mass mapping. Table 4.22 shows the mass amount at stage 1 and stage 2. Compare with Table 4.14 containing the amount of mass with all pipes working, Table 4.22 does not show much difference. This means even one pipe fails, mass still has access through other pipes to arrive at a certain tank. When all pipes are working, the total mass amount is 22.4874 kg from Table 4.14, that is, one failed pipe does not affect finding the optimal mass distribution. Figure 4.16 illustrates the diagram when one pipe has failed. It shows similar mass distribution for the reason explained above.

Table 4.21: Optimal Mass Shift Through Each Pipe for Case 5 (kg)

Pipe_12 = 0	Pipe_21 = 0
Pipe_13 = 1.619	Pipe_31 = -1.619
Pipe_15 = 3.220	Pipe_51 = -3.220
Pipe_16 = 1.619	Pipe_65 = -1.619
Pipe_23 = -2.673	Pipe_32 = 2.673
Pipe_24 = -3.748	Pipe_42 = 3.748
Pipe_26 = -2.673	Pipe_62 = 2.673
Pipe_34 = -1.075	Pipe_43 = 1.075
Pipe_35 = 1.600	Pipe_53 = -1.600
Pipe_45 = 2.676	Pipe_54 = -2.676
Pipe_46 = 1.075	Pipe_64 = -1.075
Pipe_56 = -1.600	Pipe_65 = 1.600
Total amount of mass shifted: 23.584 kg	

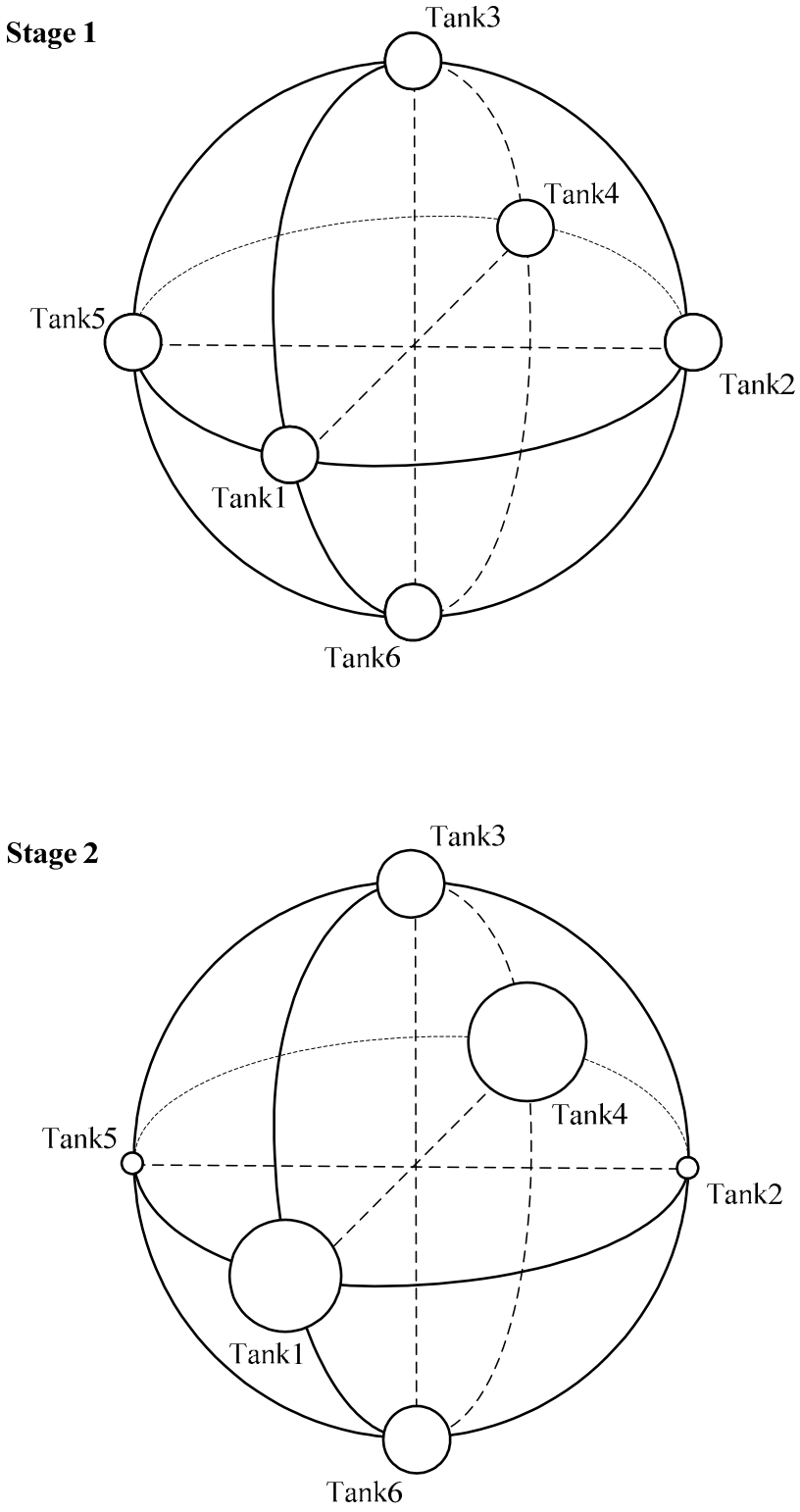

Figure 4.16: Diagram of Tank Distribution for Each Stage for Case 5 (the size of each circle is not exactly scaled)

Table 4.22: Mass Distribution for Stage 1 and Stage 2 for Case 5 (kg)

	Stage 1	Stage 2	Mass shifted
Tank 1	10	16.460	6.460
Tank 2	10	0.905	-9.095
Tank 3	10	11.578	1.578
Tank 4	10	18.576	8.576
Tank 5	10	0.900	-9.100
Tank 6	10	11.578	1.578
Total Amount of Mass	60	60	0

Equations (4.31)-(4.32) present the moment of inertia change of the satellite system and mass system due to the center-of-mass shifting. The new center-of-mass is located at $\begin{bmatrix}-0.0604 & 0.0023 & -0.0000\end{bmatrix}^T$ m and the DCM is computed in Equation (4.33).

$$\Delta I_{\text{sat}} = \begin{bmatrix} 0.00057 & 0.01444 & -0.00000 \\ 0.01444 & 0.36493 & 0.00000 \\ -0.00000 & 0.00000 & 0.36550 \end{bmatrix} (\text{kg} \cdot \text{m}^2) \tag{4.31}$$

$$\Delta I_{\text{mass}} = \begin{bmatrix} 24.96323 & 0.00334 & -0.00000 \\ 0.00334 & 58.15709 & 0.00000 \\ -0.00000 & 0.00000 & 36.80679 \end{bmatrix} (\text{kg} \cdot \text{m}^2) \tag{4.32}$$

$$\text{DCM} = \begin{bmatrix} 0.999999 & 0.000000 & -0.000000 \\ 0.000000 & -0.999999 & -0.000303 \\ -0.000000 & 0.000303 & -0.999999 \end{bmatrix} \tag{4.33}$$

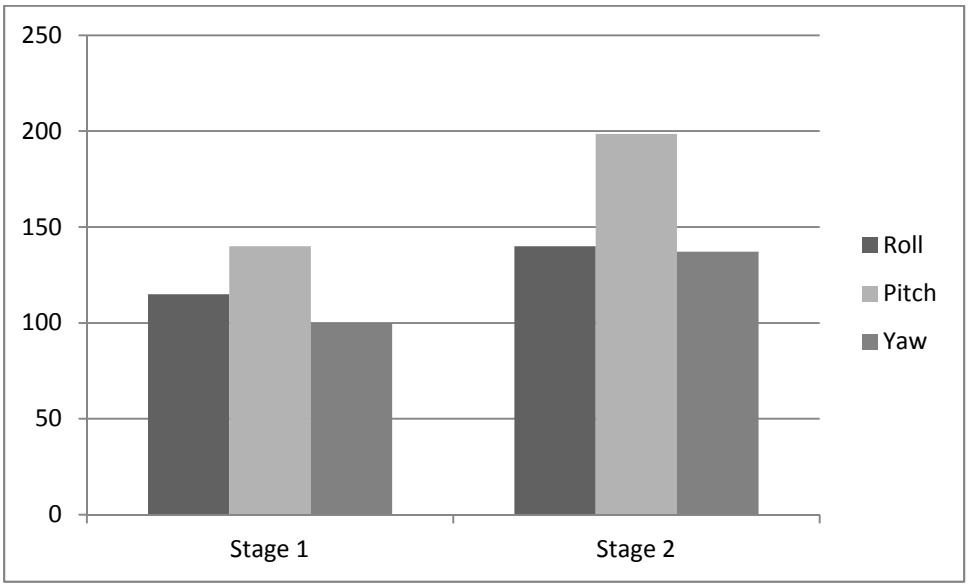

Figure 4.17: Principal Moments of Inertia for Each Stage for Case 5 ($kg \cdot m^2$)

Figure 4.17 presents the principal moments of inertia at stage 1 and stage 2. Since the mass distribution is close to the case with no failed pipe, three principal moments of inertia have similar values in Table 4.9.

It is generally known that the gravity gradient stabilization can control only two axes: roll and pitch. When Equation (3.10) is applied to Equation (2.39) for controllability check, the rank is 5 and this means the system is not fully controllable from the control vector. In Equation (3.10), it is found that one column of the 6×6 matrix is a zero vector and this column results in the rank is not full. In other words, there is no control moment applied to the yaw axis. Even optimal mass transfer does not provide the yaw control moment since the satellite at stage 2 is also assumed to be stabilized under the influence of a gravity gradient. Therefore, additional control devices are needed to control all three axes. Equation (H.9) is the governing equation with an internal rotating

device installed. The rotating device such as momentum wheel, reaction wheel, or gyro can provide the moment required along the yaw axis. Equation (H.9) does not have a zero column or row in the equation and the linearized state space form can be derived through the same way that Equation (3.10) was developed. Then, Equation (2.39) can investigate the controllability by checking the rank of the matrix with elements calculated from the state space equation.

Chapter 5

SUMMARY, CONCLUSIONS, and FUTURE WORK

The procedure of optimal reconfiguration from one mass distribution to another to accomplish attitude control has been demonstrated. Mass shifting could work as an attitude controller for fine-tuning attitude behavior in a small size satellite in LEO. To utilize the gravity gradient-torque, a system of six tanks equally distributed along an imaginary surface is introduced and two fundamental models are developed. Each system is composed of the dry satellite and the six tanks so that the configuration of the mass system can change the attitude of the satellite by changing the moments of inertia of the system from various mass distributions.

The first model is the general system such that three pairs of mass can move freely to any location. The only design restriction is that each pair of masses must have the same amount of mass to avoid the center-of-mass shifting. The optimal solution satisfies both minimal total mass movement including tank location shift and the balance of the mass mapping among all connecting pipes. Several simulations show that the optimal mass mapping is more affected by the location of each tank than the amount of mass in each tank. Since this model is too general to apply to the real system, relevant restriction may be included.

The other model is a more realistic design with the six tank locations fixed and the internal mass traveling through each pipe. Since no restriction is applied to the amount of mass per each tank, the center-of-mass change yields the location of each tank

to be changed as well. Under this situation, the location of each tank is expressed by the mass of each tank. Fewer variables results in nonlinear constraints instead.

To compute the optimal mass mapping, the roll/yaw and pitch frequencies are used because the each frequency is the function of three principal moments of inertia. The other two constraints are derived from the gravity-gradient stabilization theory. Two equality constraints from frequencies and two inequality constraints from the stability condition become the universal constraints for each simulation. Then, additional restrictions are added if necessary. No mass shift occurs between two tanks connected by a blocked pipe and the limited range of tank locations is applied to find the optimal solution.

Several examples are simulated by both models. Although the Euler angles and their rates result in almost the same model, the optimal mass distribution and the location of tank are fairly different from each other. For the free tank location model, the contribution of the tank location is much larger and the available frequency range is also wider than the changing center-of-mass model. However, more restrictions should be applied from the engineering viewpoint. The other model, changing center-of-mass, has a narrow range of roll/yaw frequency due to the limitation of the design. Since the mass reconfiguration under the gravity gradient is not designed for the major attitude controller, this model is more realistic.

Ground coverage is also introduced to guide the frequency determination. Since the frequency constraints are related to the ground coverage for a special task such as a map-making mission, higher roll frequency is selected to enlarge the coverage area on the ground. However, the feasible mass distribution is not always available. The possible

frequency range after mass distribution is found by changing one of the frequencies while the other is fixed.

Controllability is also checked for the gravity-gradient satellite. Since gravity gradient is not enough to control all three axes, the governing equation including the internal rotating device is added. That internal device generates the last axis that gravity gradient is not able to control, then control of all three axes can be fulfilled.

MATLAB's optimization solver provides a strong solver to find the optimal solution. Each process takes less than a minute even without the assistance of super computation ability. The only thing to be careful is to find the adequate frequencies; otherwise the optimization solver fails to find the answer.

Throughout various simulations, it has been demonstrated that both designs (center-of-mass fixed design and center-of-mass changing design) can work as attitude control methods for the gravity-gradient stabilized satellite. These models may use not only liquid mass but also any movable parts in any directions while the conventional gravity-gradient controller such as gravity-gradient boom has a limited design. Compared with most gravity-gradient control methods, both models provide more flexible mass distribution so that more accurate moments of inertia can be achieved. The usage of internal moving mass could be less effective than using general gravity-gradient devices, but the payload design can be more simplified since the space for the gravity-gradient devices is no longer required. Thus the new designs can be a substitute for the small size satellite in LEO requiring a high pointing accuracy.

Also, the methodology used in this simulation can be applied for a mission especially when the frequency of the roll, pitch, and yaw motion is important. It is proved that how the frequency changes affects the ground coverage changes. By increasing the ground coverage, more area can be observed while more narrow area can be observed by decreasing the coverage area. In addition, the optimization process can be added as necessary. The optimal solution with well-developed objective functions from network model theory proves that it can be applied to the various problems.

Future work may include the following ideas.

1. Both models assume that the transition occurs instantaneously without considering the continuous mass transfer. So, continuity may be the topic for the next research.
2. Even though the computation time is extremely short, there are still chances that the desired frequencies cannot be verified until the optimization solver finishes the computation. Thus, finding the safe range of frequencies based on the original mass configuration might be helpful.
3. One of the assumptions made for this dissertation is that all masses used in simulation are regarded as a point mass. If the mass in a tank is not uniformly distributed or the location of mass is not aligned with each axis may require additional calculation to find the principal axes. Consideration of the internal tank design would increase the chance to apply to the real satellite.

References

1. Studer, P., and Rodriguez, E., "High Speed Reaction Wheels for Satellite Attitude Control and Energy Storage," *Proceedings of the 20th Intersociety Energy Conversion Engineering Conference*, Vol. 2, Society of Automotive Engineers, Warrendale, PA, 1985, pp. 349-353.
2. Tsiotras, P., and Shen, H., "Satellite Attitude Control and Power Tracking with Energy/Momentum Wheels," *Journal of Guidance, Control, and Dynamics*, Vol. 24, No. 1, 2001. pp. 23-34.
3. Urakubo, T., Tsuchiya, K., and Tsujita, K., "Attitude Control of a Spacecraft with Two Reaction Wheels," *Journal of Vibration and Control*, Vol. 10, No. 9, 2004, pp. 1291-1311.
4. Krishnan, H., McClamroch, N.H., and Reyhanogle, M., "Attitude Stabilization of a Rigid Spacecraft Using Two Momentum Wheel Actuators," *Journal of Guidance, Control, and Dynamics*, Vol. 18, No. 2, 1995, pp. 256-263.
5. Mapar, J., "Innovative Approach to the Momentum Management Control for Space Station Freedom," *Journal of Guidance, Control and Dynamics*, Vol. 16, No. 1, 1993, pp. 175-181.
6. Shi, J-F., and Damaren, C. J., "Control Law for Active Structural Damping Using a Control Moment Gyro," *Journal of Guidance*, *Control, and Dynamics*, Vol. 28, No. 3, 2005, pp. 550-553.
7. Zheng, J., Banks, S. P., and Alleyne, H., "Optimal attitude control for three-axis stabilized flexible spacecraft," *Acta Astronautica* 56 (2005), pp. 519-528.

8. Shrivastava, S. K., and Modi, V. J., "Satellite Attitude Dynamics and Control in the Presence of Environmental Torques-A Brief Survey," *Journal of Guidance, Control, and Dynamics*, Vol. 6, No. 6, 1983, pp. 461-471.
9. Park, Y., "Robust and optimal attitude stabilization of spacecraft with external disturbances," *Aerospace Science and Technology* 9 (2005), pp. 253-259.
10. Lovera, M., and Astolfi, A., "Spacecraft Attitude Control Using Magnetic Actuators," *Automatica*, Vol. 40, No. 8, 2004, pp. 1405-1414.
11. Musser, K. L., and Ebert, W. L., "Autonomous Spacecraft Attitude Control Using Magnetic Torquing Only," *Proceedings of the Flight Mechanics/Estimation Theory Symposium*, NASA Goddard Space Flight Center, Greenbelt, MD, May 1989, pp. 23-38.
12. Ahsun, U., "Dynamics and Control of Eletromagnetic Satellite Formations in Low Earth Orbits," AIAA *Guidance, Navigation, and Control Conference and Exhibit*, AIAA-2006-6590, Keystone, CO, August 2006.
13. Psiaki, M. L., "Magnetic Torquer Attitude Control via Asymptotic Periodic Linear Quadratic Regulation," *Journal of Guidance, Control and Dynamics*, Vol. 24, No. 2, March-April 2001, pp. 386-394.
14. Alfriend, K. T., "Magnetic Attitude Control System for Dual-Spin Satellites," *AIAA Journal*, Vol. 13, No. 6, 1975, pp. 817-823.
15. Psiaki, M. L., "Spacecraft Attitude Stabilization Using Passive Aerodynamics and Active Magnetic Torquing," AIAA *Guidance, Navigation, and Control Conference and Exhibit*, AIAA 2003-5420, Austin, TX, August 2003.

16. Arduini, C., and Baiocco, P., "Active Magnetic Damping Attitude Control for Gravity Gradient Stabilized Spacecraft," *Journal of Guidance, Control, and Dynamics*, Vol. 20, No. 1, 1997, pp. 117-123.

17. Wisniewski, R., and Markley, L. F., "Fully Magnetic Attitude Control for Spacecraft Subject to Gravity Gradient," *Automatica*, Vol. 35, No. 7, 1999, pp. 1201-1214.

18. Martel, F., Pal, P. K., and Psiaki, M. L., "Active Magnetic Control System for Gravity Gradient Stabilized Spacecraft," *Proceedings of the 2nd Annual AIAA/USU Conference on Small Satellites*, September 1988, Logan, Utah.

19. Modi, V.J., "Attitude Dynamics of Satellites with Flexible Appendages-A Brief Review," *Journal of Spacecraft and Rockets*, Vol. 11, No. 11, 1974, pp. 743-751.

20. Lips, K. W., and Modi, V. J., "General dynamics of a Large Class of Flexible Satellite Systems," *Acta Astronautica*, Vol. 7, 1980, pp. 1349-1360.

21. Ng, A. C., and Modi, V. J., "A Formulation for Studying Dynamics of Interconnected Bodies with Application," *Proceedings AIAA/AAS Astrodynamics Conference*, August 15-17, 1988, Paper No. 88-4303-CP, pp. 660-668.

22. Kang, J-Y, and Lee, S., "Attitude Acquisition of a Satellite with a Partially Filled Liquid Tank," *Journal of Guidance, Control, and Dynamics*, Vol. 31, No. 3, 2008, pp. 790-793.

23. Kang, J-Y, and Coverstone, V. L., "Analytical Model for Momentum Transfer of Spacecraft Containing Liquid," *Journal of Guidance, Control, and Dynamics*, Vol. 33, No. 3, 2010, pp. 991-994.

24. Childs, D. W., "A Movable-Mass Attitude-Stabilization System for Artificial-g Space Stations," *Journal of Guidance, Control, and Dynamics*, Vol. 8, No. 8, August, 1971, pp. 829-834.

25. Kumar, K. D. and Zou, A. M., "Attitude Control of Miniature Satellites Using Movable Masses," AIAA-2010-1982, *Proceedings of SpaceOps 2010 Conference*, Huntsville, Alabama, April 25-30, 2010.

26. Chobotov, V. A., *Spacecraft Attitude Dynamics and Control*, Krieger Publishing Company, 1991.

27. Gregory, B. S., "Attitude Control System Design for ION, the Illinois Observing Nanosatellite," Master Thesis, University of Illinois at Urbana-Champaign, 2004.

28. Hibbeler, R. C., *Engineering Mechanics: Statics & Dynamics*, 8th Edition, Prentice-Hall, 1997.

29. Sunde, B. O., "Sensor Modeling and Attitude Determination for Micro-Satellite," Master Thesis, Norwegian University of Science and Technology, 2005.

30. Clohessy, W. H., and Wiltshire, R. S., "Terminal Guidance System for Satellite Rendezvous," *Journal of Aerospace Science*, Vol. 27, No. 9, 1960, pp. 653-658.

31. Curtis, H. D., *Orbital Mechanics for Engineering Students*, Elsevier Butterworth-Heinemann, 2005.

32. Kaplan, M. H., *Modern Spacecraft Dynamics and Control*, Wiley, 1976.

33. Kalman, R., "Contributions to the Theory of Optimal Control," *Boletin Sociedad Matematica Mexicana,* vol. 5, 1960, pp. 102–119.

34. Bowring, B. R., "Transformation from spatial to geodetic coordinates", *Survey Review*, 1976, Vol. 23, No.181, 1976, pp. 323–327.

35. Bowring, B. R., "The accuracy of geodetic latitude and height equations", *Survey Review*, Vol. 28, No. 218, 1985, pp. 202–206.

36. Jones, G. C., "New solutions for the geodetic coordinate transformation", *Bulletin Geodesique*, Vol. 76, 2002, pp. 437-446.

37. Vermeille, H., "Direct transformation from geocentric to geodetic coordinates", *Journal of Geodesy*, 2002, Vol. 76, No. 8, pp. 451–454.

38. Vermeille, H., "Computing geodetic coordinates from geocentric coordinates", *Journal of Geodesy*, 2004, Vol. 78, No.1-2, pp. 94-95.

39. Roberson, R. E., "Torques on a Satellite Vehicle from Internal Moving Mass", *Journal of Applied Mechanics*, Vol. 25, 1958, pp. 196-200.

40. Grubin, C., "Dynamics of a Vehicle Containing Moving Parts", *Journal of Applied Mechanics*, Vol. 29, 1962, pp. 486-488.

41. Kunciw, B. G. and Kaplan, M. H., "Optimal Space Station Detumbling by Internal Mass Motion", *Automatica*, Vol. 12, 1976, pp. 417-425.

42. Edwards, T. L., and Kaplan, M. H., "Automatic Space Station Detumbling by Internal Mass Motion", *AIAA Journal*, Vol. 12, No.4, 1974, pp. 496-502.

43. Sidi, M. J., *Spacecraft Dynamics and Control*, Cambridge University Press, 1997, pp. 110-111.

44. Bang, H., and Choi, H. D., "Attitude Control of a Bias Momentum Satellite Using Moment of Inertia," *IEEE Transactions on Aerospace and Electronic Systems*, Vol. 38, No.1, January 2003. pp. 243-250.

45. Larson, W. J., and Wertz, J. R., *Space Mission Analysis and Design*, 3rd Edition, Microcosm Press, 1999, pp. 110-117.

46. Cook, W. J., Cunningham, W. H., Pulleyblank, W. R., and Schrijver, A., *Combinatorial Optimization*, 1st Edition, Wiley-Interscience, 1997.

47. Dijkstra, E. W., "A Note On Two Problems In Connexion With Graphs", *Numerische Mathematik* 1, 1959. pp. 269-271.

48. MATLAB Optimization Toolbox Tutorial. http://www.mathworks.com/products/optimization, date accessed 5/10/12

Appendix A

Conversions between Coordinate Systems

There are several choices of coordinate systems for attitude control systems. It is always possible to convert from one coordinate system to another by finding the transformation matrix. Here, the various mapping matrices are calculated to complete these conversions and more details are found in [27]. With those transformations, the conversions can be performed simply by matrix multiplication.

Choose two coordinate systems **M** and **N** with base vectors $\left[\hat{\mathbf{x}}_{\mathbf{M}} \quad \hat{\mathbf{y}}_{\mathbf{M}} \quad \hat{\mathbf{z}}_{\mathbf{M}}\right]^T$ and $\left[\hat{\mathbf{x}}_{\mathbf{N}} \quad \hat{\mathbf{y}}_{\mathbf{N}} \quad \hat{\mathbf{z}}_{\mathbf{N}}\right]^T$ in each coordinate system. Then, a random vector $\bar{v}$ can be expressed in each coordinate system by a linear combination with the base:

$$\bar{v} = \left[\hat{\mathbf{x}}_{\mathbf{M}} \quad \hat{\mathbf{y}}_{\mathbf{M}} \quad \hat{\mathbf{z}}_{\mathbf{M}}\right]\bar{v}_{\mathbf{M}} = \left[\hat{\mathbf{x}}_{\mathbf{N}} \quad \hat{\mathbf{y}}_{\mathbf{N}} \quad \hat{\mathbf{z}}_{\mathbf{N}}\right]\bar{v}_{\mathbf{N}} \tag{A.1}$$

where $\bar{v}_{\mathbf{M}}$ and $\bar{v}_{\mathbf{N}}$ are the associated vectors to obtain $\bar{v}$ in each coordinate systems **M** and **N**, respectively. If $A^{\mathbf{M/N}}$ is the transformation matrix describing the orientation of coordinate system **N** to **M**, then the equations (A.2) show the conversions from $\bar{v}_{\mathbf{N}}$ to $\bar{v}_{\mathbf{M}}$. It is shown that the inverse transformation is the transpose of the same matrix in equation (A.3).

$$\bar{v}_{\mathbf{M}} = A^{\mathbf{M/N}}\bar{v}_{\mathbf{N}} \tag{A.2}$$

$$\bar{v}_{\mathbf{N}} = A^{\mathbf{N/M}}\bar{v}_{\mathbf{M}} = (A^{\mathbf{M/N}})^{T}\bar{v}_{\mathbf{M}} \tag{A.3}$$

A.1 Converting a Matrix between the Inertial and Orbital reference coordinate systems

Let $\bar{r}$ be the radius vector and $\bar{v}$ be the velocity vectors of a satellite in the inertial coordinate system. The vector $\bar{z}_C$ is defined as the unit vector in the opposite direction of the radius vector in the same coordinate system. Then the following equation holds:

$$\bar{z}_C = -\frac{\bar{r}}{r} = -\frac{1}{r}\begin{bmatrix}\mathbf{x_I} & \mathbf{y_I} & \mathbf{z_I}\end{bmatrix}\begin{bmatrix} r_x \\ r_y \\ r_z \end{bmatrix} \tag{A.4}$$

Suppose a projection of the velocity vector into the orthogonal subspace of the radius vector and let $\bar{x}_C$ be the unit vector in the direction of this projection, this can be expressed as:

$$\bar{x}_C = \frac{\bar{v} - \frac{\bar{r}\cdot\bar{v}}{r^2}\bar{r}}{\left\|\bar{v} - \frac{\bar{r}\cdot\bar{v}}{r^2}\bar{r}\right\|} = \begin{bmatrix}\mathbf{x_I} & \mathbf{y_I} & \mathbf{z_I}\end{bmatrix}\begin{bmatrix} x_x \\ y_y \\ z_z \end{bmatrix} \tag{A.5}$$

Next, $\bar{y}_C$ is defined as $\bar{z}_C \times \bar{x}_C$:

$$\overline{\mathrm{y}}_{\mathrm{C}} = \overline{\mathrm{z}}_{\mathrm{C}} \times \overline{\mathrm{x}}_{\mathrm{C}} = \begin{bmatrix} \mathbf{x_I} & \mathbf{y_I} & \mathbf{z_I} \end{bmatrix} \left(-\frac{1}{r} \begin{bmatrix} x_x \\ x_y \\ x_z \end{bmatrix} \times \begin{bmatrix} r_x \\ r_y \\ r_z \end{bmatrix} \right) = \begin{bmatrix} \mathbf{x_I} & \mathbf{y_I} & \mathbf{z_I} \end{bmatrix} \begin{bmatrix} y_x \\ y_y \\ y_z \end{bmatrix} \tag{A.6}$$

Substituting equations yields the transformation matrix from inertial to orbital reference coordinate system, $\mathrm{A}^{\mathbf{R/I}}$:

$$\begin{bmatrix} \mathbf{x_R} \\ \mathbf{y_R} \\ \mathbf{z_R} \end{bmatrix} = \begin{bmatrix} x_x & x_y & x_z \\ y_x & y_y & y_z \\ -\frac{r_x}{r} & -\frac{r_y}{r} & -\frac{r_z}{r} \end{bmatrix} \begin{bmatrix} \mathbf{x_I} \\ \mathbf{y_I} \\ \mathbf{z_I} \end{bmatrix} = \mathrm{A}^{\mathbf{R/I}} \begin{bmatrix} \mathbf{x_I} \\ \mathbf{y_I} \\ \mathbf{z_I} \end{bmatrix} \tag{A.7}$$

A.2 Converting the Angular Velocity of the Body-fixed Coordinate System with respect to the inertial Coordinate System

Equation (A.8) represents how the angular velocity of the body-fixed coordinate system is related to the inertial coordinate system. The angular velocity is the function of the radius vector $\overline{r}$ and the velocity vector $\overline{v}$ and may be computed as

$$\overline{\omega}^{\mathbf{R/I}} = -\frac{\left\| \overline{v} \times \overline{r} \right\|}{r^2} \overline{\mathrm{y}}_{\mathbf{R}} \tag{A.8}$$

If a satellite's orbit is circular, $\overline{v} \times \overline{r}$ is constant. That means the angular velocity has the same magnitude and direction at any location of the orbit.

Appendix B

Useful Properties of Direction Cosine Matrices

The first useful property of a direction cosine matrix [27] is that the $DCM^{\mathbf{M/N}}$ is a unitary rotation matrix. In other words:

$$DCM^{\mathbf{M/N}}(DCM^{\mathbf{M/N}})^{T} = I \tag{B.1}$$

As seen in Equation (B.1), the rotation matrix has its transpose matrix as its inverse matrix, which is always promised to exist. Apparently, any arbitrary vector can be expressed in either coordinate system **M** or **N**. Therefore, an arbitrary vector $\bar{v}$ can be written as

$$\bar{v} = \begin{bmatrix} \hat{\mathbf{x}}_{\mathbf{M}} & \hat{\mathbf{y}}_{\mathbf{M}} & \hat{\mathbf{z}}_{\mathbf{M}} \end{bmatrix} \bar{v}_{M} = \begin{bmatrix} \hat{\mathbf{x}}_{\mathbf{N}} & \hat{\mathbf{y}}_{\mathbf{N}} & \hat{\mathbf{z}}_{\mathbf{N}} \end{bmatrix} \bar{v}_{N} \tag{B.2}$$

where $\bar{v}_{\mathbf{M}}$ and $\bar{v}_{\mathbf{N}}$ are 3×1 column vectors. Substituting Equation (B.1) into Equation (B.2), the next equation is found:

$$\begin{bmatrix} \hat{\mathbf{x}}_{\mathbf{N}} & \hat{\mathbf{y}}_{\mathbf{N}} & \hat{\mathbf{z}}_{\mathbf{N}} \end{bmatrix} (DCM^{\mathbf{M/N}})^{T} \bar{v}_{\mathbf{M}} = \begin{bmatrix} \hat{\mathbf{x}}_{\mathbf{N}} & \hat{\mathbf{y}}_{\mathbf{N}} & \hat{\mathbf{z}}_{\mathbf{N}} \end{bmatrix} \bar{v}_{\mathbf{N}} \tag{B.3}$$

Without loss of generality, the following relationship is obtained

$$(\mathrm{DCM}^{\mathbf{M/N}})^{\mathrm{T}}\,\bar{\mathrm{v}}_{\mathbf{M}} = \bar{\mathrm{v}}_{\mathbf{N}} \tag{B.4}$$

As mentioned earlier, $\mathrm{DCM}^{\mathbf{M/N}}$ is a unitary rotation matrix. Thus multiplication of Equation (B.4) by the inverse matrix on both sides yields

$$\bar{\mathrm{v}}_{\mathbf{M}} = \mathrm{DCM}^{\mathbf{M/N}}\bar{\mathrm{v}}_{\mathbf{N}} \tag{B.5}$$

From Equation (B.5), it may be concluded the $\mathrm{DCM}^{\mathbf{M/N}}$ can work as a transformation matrix from one coordinate system to another. The matrix $\mathrm{DCM}^{\mathbf{M/N}}$ is a transformation from arbitrary system **M** to another arbitrary system **N**. Also it can be concluded that its transpose matrix $(\mathrm{DCM}^{\mathbf{M/N}})^{\mathrm{T}}$ will transform to the opposite mapping which is,

$$(\mathrm{DCM}^{\mathbf{M/N}})^{\mathrm{T}} = \mathrm{DCM}^{\mathbf{N/M}} \tag{B.6}$$

This step can be extended to more than two different coordinate systems simply applying the chain rule. Suppose a coordinate system **L** with a base unit vector, $\left[\hat{\mathbf{x}}_{\mathbf{L}} \quad \hat{\mathbf{y}}_{\mathbf{L}} \quad \hat{\mathbf{z}}_{\mathbf{L}}\right]$. Applying the same idea used for Equation (B.2) for an arbitrary vector $\bar{\mathrm{v}}$,

$$\bar{\mathrm{v}} = \left[\hat{\mathbf{x}}_{\mathbf{L}} \quad \hat{\mathbf{y}}_{\mathbf{L}} \quad \hat{\mathbf{z}}_{\mathbf{L}}\right]\bar{\mathrm{v}}_{\mathrm{L}} \tag{B.7}$$

Similarly, the following process can be led to find the mapping matrix from $\bar{v}_L$ to $\bar{v}_N$ and $\bar{v}_L$ to $\bar{v}_M$:

$$\bar{v}_N = DCM^{N/L}\bar{v}_L \tag{B.8}$$

$$\bar{v}_M = DCM^{M/L}\bar{v}_L \tag{B.9}$$

Substituting Equations (B.5) and (B.8) yields the following:

$$\bar{v}_M = DCM^{M/N}DCM^{N/L}\bar{v}_L \tag{B.10}$$

From Equations (B.8), (B.9), and (B.10), the general mapping relationship for arbitrary systems can be found.

$$DCM^{M/L} = DCM^{M/N}DCM^{N/L} \tag{B.11}$$

Appendix C

Euler Angle Rotation

To describe the rotation of a coordinate system, at most, three angles are needed to complete the rotating sequences. Those three angles are called at the Euler Angles [43] and the related transformation matrix is different for each sequence. To simplify the process, the origin of each coordinate system is assumed to be located at the same position in a space. The cycle is performed as follows

1. Rotation by the angle φ about the axis 3
2. Rotation by the angle θ about the axis 2'
3. Rotation by the angle ψ about the axis 1"

In Figure C.1, the original coordinate system, 123, is rotated around axis 3 through the Euler angle φ.

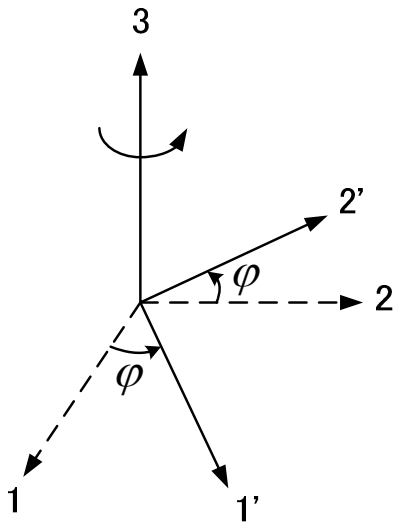

Figure C.1: Rotation by the angle φ about the axis 3

As seen, it rotates the axes 1 and 2 to 1’ and 2’ respectively and it satisfies

$$\begin{bmatrix} 1' \\ 2' \\ 3 \end{bmatrix} = \begin{bmatrix} \cos\varphi & \sin\varphi & 0 \\ -\sin\varphi & \cos\varphi & 0 \\ 0 & 0 & 1 \end{bmatrix} \begin{bmatrix} 1 \\ 2 \\ 3 \end{bmatrix} \tag{C.1}$$

The 3×3 associated rotation matrix in equation (C.1) is called the orthogonal transformation matrix, $R_3(\varphi)$, where R denotes the rotation, the subscript 3 recalls the axis and the φ is the angle of rotation.

The second rotation is illustrated in Figure C.2. The coordinate system rotates around the axis 2’ through the angle θ. The coordinate system before the rotation is 1’2’3 (used the axis 3 instead of 3’ because the axis has not been changed from the first rotation) and the coordinate system after the rotation is 1”2’3’.

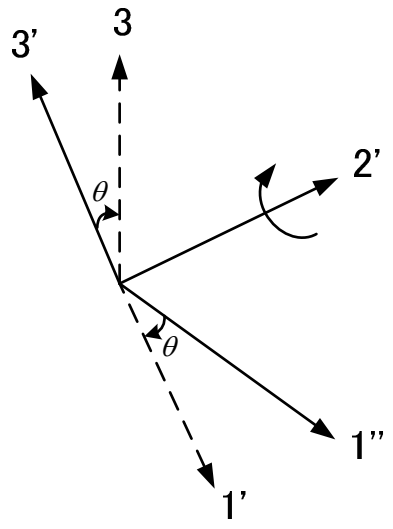

Figure C.2: Rotation by the angle θ about the axis 2’

This rotation can be expressed by the transformation matrix as:

$$\begin{bmatrix} 1'' \\ 2' \\ 3' \end{bmatrix} = \begin{bmatrix} \cos\theta & 0 & \sin\theta \\ 0 & 1 & 0 \\ -\sin\theta & 0 & \cos\theta \end{bmatrix} \begin{bmatrix} 1' \\ 2' \\ 3 \end{bmatrix} \tag{C.2}$$

The 3×3 matrix in equation (C.2) is denoted by $R_2(\theta)$, where the subscript 2 used for axis 2' and the θ is the angle of rotation.

The last rotation to complete the cycle is performed around the axis 1'' through the angle ψ. Figure C.3 shows the diagram of the final rotation.

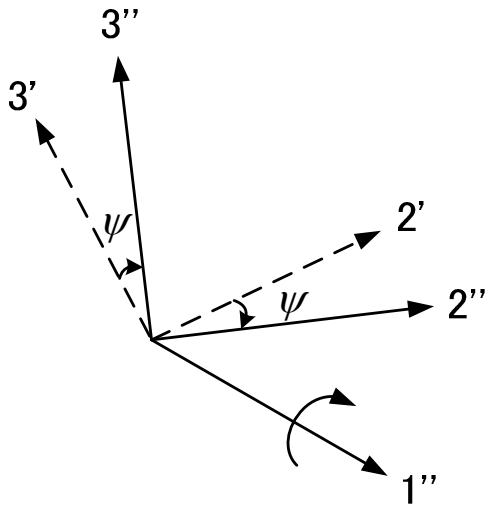

Figure C.3: Rotation by the angle ψ about the axis 1"

Similarly, the transformation matrix is calculated as:

$$\begin{bmatrix} 1'' \\ 2'' \\ 3'' \end{bmatrix} = \begin{bmatrix} 1 & 0 & 0 \\ 0 & \cos\psi & \sin\psi \\ 0 & -\sin\psi & \cos\psi \end{bmatrix} \begin{bmatrix} 1'' \\ 2' \\ 3' \end{bmatrix} \tag{C.3}$$

It is noted that the only two axes of right-hand side 2' and 3' have been changed into 2" and 3" as expected because the coordinate system rotates around the axis 1". Based on the similar notation, the 3×3 transformation matrix is called $R_1(\psi)$. Thus the transformation matrix from the one coordinate system to the other coordinate system can be found by the product of $R_3(\varphi)$, $R_2(\theta)$, and $R_1(\psi)$ in order. Thus the entire rotation transformation matrix from the coordinate system 123 to 1"2"3" is

$$\begin{bmatrix} 1'' \\ 2'' \\ 3'' \end{bmatrix} = R_1(\psi)R_2(\theta)R_3(\varphi) \begin{bmatrix} 1 \\ 2 \\ 3 \end{bmatrix} \tag{C.4}$$

Thus, the final rotation transformation matrix $R_1(\psi)R_2(\theta)R_3(\varphi)$ is

$$\begin{bmatrix} \cos\varphi\cos\theta & \sin\varphi\cos\theta & -\sin\theta \\ -\sin\varphi\cos\psi + \cos\varphi\sin\theta\sin\psi & \cos\varphi\cos\psi + \sin\varphi\sin\theta\sin\psi & \cos\theta\sin\psi \\ \sin\varphi\sin\psi + \cos\varphi\sin\theta\cos\psi & -\cos\varphi\sin\psi + \sin\varphi\sin\theta\cos\psi & \cos\theta\cos\psi \end{bmatrix} \tag{C.5}$$

As noted earlier, the inverse matrix of this matrix transforms the coordinate system 1”2”3” into 123 and is simply the transpose of Equation (C.5)

$$\begin{bmatrix} \cos\varphi\cos\theta & -\sin\varphi\cos\psi+\cos\varphi\sin\theta\sin\psi & \sin\varphi\sin\psi+\cos\varphi\sin\theta\cos\psi \\ \sin\varphi\cos\theta & \cos\varphi\cos\psi+\sin\varphi\sin\theta\sin\psi & -\cos\varphi\sin\psi+\sin\varphi\sin\theta\cos\psi \\ -\sin\theta & \cos\theta\sin\psi & \cos\theta\cos\psi \end{bmatrix} \quad \text{(C.6)}$$

Appendix D

Conversions Between Attitude Mapping Computations

Different maneuvers require different attitude representations because of its ease of use. Euler angles help understand a visual rotation while transformation matrix is pretty intuitive for a vector transformation, However, the different choice of problem solving method may delay the calculating time for the same result. Conversions between Euler angles and transformation matrix are described.

Several definitions are as following. $A^{\mathbf{M/N}}$ is the transformation matrix and ψ, θ, and φ are the Euler angles for an arbitrary coordinate system **M** with respect to the other system **N**. Let $A^{\mathbf{M/N}}$ be defined as

$$A^{\mathbf{M/N}} = \begin{bmatrix} A_{11} & A_{12} & A_{13} \\ A_{21} & A_{22} & A_{23} \\ A_{31} & A_{32} & A_{33} \end{bmatrix} \tag{D.1}$$

D.1 Conversion from the Euler Angles to the Transformation Matrix

As illustrated in Appendix B, Euler Angles represent the angles to rotate one coordinate system to align to the other system. Three successive rotations are performed to complete this maneuver and the order of the rotation about each axis results in a different rotating matrix. Total 12 different rotation matrices exist and the relationship from Euler angles to the transformation matrix is straightforward. The 3×3 rotation

matrix of the Equation (D.2) is the same matrix of Equation (B.5) which the order of rotation is $\phi-\theta-\psi$:

$$\mathrm{A}^{\mathbf{M/N}} = \begin{bmatrix} \cos\phi\cos\theta & \sin\phi\cos\theta & -\sin\theta \\ -\sin\phi\cos\psi+\cos\phi\sin\theta\sin\psi & \cos\phi\cos\psi+\sin\phi\sin\theta\sin\psi & \cos\theta\sin\psi \\ \sin\phi\sin\psi+\cos\phi\sin\theta\cos\psi & -\cos\phi\sin\psi+\sin\phi\sin\theta\cos\psi & \cos\theta\cos\psi \end{bmatrix} \quad \text{(D.2)}$$

D.2 Conversion from the Transformation Matrix to the Euler Angles

This conversion can be calculated from Equation (D.2) and inverse trigonomic functions to find the correct Euler angles. However, this method contains a problem which is caused by the quadrant ambiguities. Without full understanding of the attitude situation, it is not easy to decide the correct quadrant. If the Euler angles are assumed for reference purposes, this ambiguity may be disregarded in most cases. Then, the Euler angles ψ, θ, and φ are expressed with the elements of the transformation matrix as:

$$\psi = \tan^{-1}\left(\frac{\mathrm{A}_{32}}{\mathrm{A}_{33}}\right) \quad \text{(D.3)}$$

$$\theta = -\sin^{-1}\mathrm{A}_{13} \quad \text{(D.4)}$$

$$\varphi = \tan^{-1}\left(\frac{\mathrm{A}_{21}}{\mathrm{A}_{11}}\right) \quad \text{(D.5)}$$

Appendix E

Modified Equations of Motion of the Satellite with a Movable Mass

Equations (3.1), (3.2), and (3.3) describe the time variant attitude of a satellite with the movable mass that can be located at any place. However, the purpose of this research is to find the optimal mass distribution of the system. This means the location of the center-of-mass of the whole system is fixed when a mass transfer is completed. Also, this research concerns small angle attitude change for a nadir pointing control. Thus, the higher order terms from the multiplications of small angular velocity and their rates may be neglected. Then, the following matrix form can be applied for further computation.

$$\begin{bmatrix} \dot{\varpi}_x \\ \dot{\varpi}_y \\ \dot{\varpi}_z \end{bmatrix} = \begin{bmatrix} I_x + \mu_C(y^2+z^2) & -\mu_C xy & -\mu_C xz \\ -\mu_C yx & I_y + \mu(x^2+z^2) & -\mu_C yz \\ -\mu_C zx & -\mu_C zy & I_z + \mu_C(x^2+y^2) \end{bmatrix}^{-1} \left\{ 2 \begin{bmatrix} -(y\dot{y}+z\dot{z}) & \dot{x}y & \dot{x}z \\ \dot{y}x & -(x\dot{x}+z\dot{z}) & \dot{y}z \\ \dot{z}x & \dot{z}y & -(x\dot{x}+y\dot{y}) \end{bmatrix} \begin{bmatrix} \varpi_x \\ \varpi_y \\ \varpi_z \end{bmatrix} + \begin{bmatrix} z\ddot{y}-y\ddot{z} \\ x\ddot{z}-z\ddot{x} \\ y\ddot{x}-x\ddot{y} \end{bmatrix} \right\} \tag{E.1}$$

Appendix F

Derivation of Steady State Equation for Gravity Gradient Stabilization

The governing equations of motion including the gravity gradient are well described in Section 2.5.1 as:

$$I_y\ddot{\varphi}+(I_p-I_r)n^2\varphi+(I_p-I_r-I_y)n\dot{\psi}=0 \tag{2.29}$$

$$I_r\ddot{\psi}+(I_r-I_p+I_y)n\dot{\varphi}+4(I_p-I_y)n^2\psi=0 \tag{2.30}$$

$$I_p\ddot{\theta}+3(I_r-I_y)n^2\theta=0 \tag{2.31}$$

To develop a general state-space representation, each components of moment of inertia, Euler angles and their rates can be expressed by the summation of two terms, initial value and deviation as already defined in Equations (3.4)-(3.6)

$$I_r=I_{r_0}+\Delta I_r, \qquad I_p=I_{p_0}+\Delta I_p, \qquad I_y=I_{y_0}+\Delta I_y \tag{3.4}$$

$$\psi=\psi_0+\Delta\psi, \qquad \theta=\theta_0+\Delta\theta, \qquad \varphi=\varphi_0+\Delta\varphi \tag{3.5}$$

$$\dot{\psi}=\dot{\psi}_0+\Delta\dot{\psi}, \qquad \dot{\theta}=\dot{\theta}_0+\Delta\dot{\theta}, \qquad \dot{\varphi}=\dot{\varphi}_0+\Delta\dot{\varphi} \tag{3.6}$$

Substituting these into Equations (2.29)-(2.31) results

$$\begin{aligned}(I_{y_0}+\Delta I_y)(\ddot{\varphi}_0+\Delta\ddot{\varphi})+\left[(I_{p_0}+\Delta I_p)-(I_{r_0}+\Delta I_r)\right]n^2(\varphi_0+\Delta\varphi)\\ +\left[(I_{p_0}+\Delta I_p)-(I_{r_0}+\Delta I_r)-(I_{y_0}+\Delta I_y)\right]n(\dot{\psi}_0+\Delta\dot{\psi})=0\end{aligned} \tag{F.1}$$

$$(I_{r_0}+\Delta I_r)(\ddot{\psi}_0+\Delta\ddot{\psi})+\left[(I_{r_0}+\Delta I_r)-(I_{p_0}+\Delta I_p)+(I_{y_0}+\Delta I_y)\right]n^2(\dot{\varphi}_0+\Delta\dot{\varphi}) \\ +4\left[(I_{p_0}+\Delta I_p)-(I_{y_0}+\Delta I_y)\right]n^2(\psi_0+\Delta\psi)=0 \tag{F.2}$$

$$(I_{p_0}+\Delta I_p)(\ddot{\theta}_0+\Delta\ddot{\theta})+3\left[(I_{r_0}+\Delta I_r)-(I_{y_0}+\Delta I_y)\right]n^2(\theta_0+\Delta\theta)=0 \tag{F.3}$$

Then the Euler angles accelerations have a second order differential equations with higher order terms neglected yields

$$\Delta\ddot{\psi}=-\frac{1}{I_{r_0}+\Delta I_r}\Big[\Delta I_r\ddot{\psi}_0+4(I_{p_0}-I_{y_0})n^2\Delta\psi+4(\Delta I_p-\Delta I_y)n^2\psi_0 \\ +(I_{r_0}-I_{p_0}+I_{y_0})n\Delta\dot{\varphi}+(\Delta I_r-\Delta I_p+\Delta I_y)n\dot{\varphi}_0\Big] \tag{F.4}$$

$$\Delta\ddot{\theta}=-\frac{1}{I_{p_0}+\Delta I_p}\Big[\Delta I_p\ddot{\theta}_0+3(I_{r_0}-I_{y_0})n^2\Delta\theta+3(\Delta I_r-\Delta I_y)n^2\theta_0\Big] \tag{F.5}$$

$$\Delta\ddot{\varphi}=-\frac{1}{I_{y_0}+\Delta I_y}\Big[\Delta I_y\ddot{\varphi}_0+(I_{p_0}-I_{r_0})n^2\Delta\varphi+(\Delta I_p-\Delta I_r)n^2\varphi_0 \\ +(I_{p_0}-I_{r_0}-I_{y_0})n\Delta\dot{\psi}+(\Delta I_p-\Delta I_r-\Delta I_y)n\dot{\psi}_0\Big] \tag{F.6}$$

The following assumption can be made

$$\frac{1}{I_r}=-\frac{1}{I_{r_0}+\Delta I_r}=\frac{1}{I_{r_0}(1+\dfrac{\Delta I_r}{I_{r_0}})}=\frac{1}{I_{r_0}}\left(1+\frac{\Delta I_r}{I_{r_0}}\right)^{-1}\cong\frac{1}{I_{r_0}}\left(1-\frac{\Delta I_r}{I_{r_0}}\right) \tag{F.7}$$

Similarly,

$$\frac{1}{I_p} \cong \frac{1}{I_{p_0}}\left(1-\frac{\Delta I_p}{I_{p_0}}\right) \tag{F.8}$$

$$\frac{1}{I_y} \cong \frac{1}{I_{y_0}}\left(1-\frac{\Delta I_y}{I_{y_0}}\right) \tag{F.9}$$

Substituting into Equations (F.4)-(F.6) and neglecting higher order terms yields

$$\begin{aligned}\Delta\ddot{\psi} = -\frac{1}{I_{r_0}+\Delta I_r}\Big[&\Delta I_r\ddot{\psi}_0 + 4(I_{p_0}-I_{y_0})n^2\Delta\psi + 4(\Delta I_p-\Delta I_y)n^2\psi_0 \\ &+(I_{r_0}-I_{p_0}+I_{y_0})n\Delta\dot{\varphi}+(\Delta I_r-\Delta I_p+\Delta I_y)n\dot{\varphi}_0\Big]\end{aligned} \tag{F.10}$$

$$\Delta\ddot{\theta} = -\frac{1}{I_{p_0}+\Delta I_p}\Big[\Delta I_p\ddot{\theta}_0 + 3(I_{r_0}-I_{y_0})n^2\Delta\theta + 3(\Delta I_r-\Delta I_y)n^2\theta_0\Big] \tag{F.11}$$

$$\begin{aligned}\Delta\ddot{\varphi} = -\frac{1}{I_{y_0}+\Delta I_y}\Big[&\Delta I_y\ddot{\varphi}_0 + (I_{p_0}-I_{r_0})n^2\Delta\varphi + (\Delta I_p-\Delta I_r)n^2\varphi_0 \\ &+(I_{p_0}-I_{r_0}-I_{y_0})n\Delta\dot{\psi}+(\Delta I_p-\Delta I_r-\Delta I_y)n\dot{\psi}_0\Big]\end{aligned} \tag{F.12}$$

where the initial values for

$$\ddot{\psi}_0 = -\frac{1}{I_{r_0}}\left\{(I_{r_0}-I_{p_0}+I_{y_0})n\dot{\varphi}_0 + 4(I_{p_0}-I_{y_0})n^2\psi_0\right\} \tag{F.13}$$

$$\ddot{\theta}_0 = -\frac{3}{I_{p_0}}(I_{r_0}-I_{y_0})n^2\theta_0 \tag{F.14}$$

$$\ddot{\varphi}_0 = -\frac{1}{I_{y_0}}\Big[(I_{p_0}-I_{r_0})n^2\varphi_0 + (I_{p_0}-I_{r_0}-I_{y_0})n\dot{\psi}_0\Big] \tag{F.15}$$

Appendix G

Derivation of Steady State Equation for Gravity Gradient Stabilized Satellite with Products of Inertia Elements

Repeating the same computation as shown in Appendix F finds the Equations (G.1)-(G.3) from Equations (3.11)-(3.13).

$$\begin{aligned}\Delta\ddot{\psi} = -\frac{1}{I_{r_0}}\Big[&\Delta I_r\ddot{\psi}_0 + 4n^2(I_{p_0} - I_{y_0})\Delta\psi - 4n^2(\Delta I_p - \Delta I_y)\psi_0 - n(I_{p_0} - I_{y_0} - I_{r_0})\Delta\dot{\varphi} \\ &- n(\Delta I_p - \Delta I_y - \Delta I_r)\dot{\varphi}_0 - I_{rp_0}\Delta\ddot{\theta} - \Delta I_{rp}\ddot{\theta}_0 - I_{ry_0}\Delta\ddot{\varphi} - \Delta I_{ry}\ddot{\varphi}_0 - n^2 I_{ry_0}\Delta\varphi \\ &- n^2\Delta I_{ry}\varphi_0 - 2nI_{py_0}\Delta\dot{\theta} - 2n\Delta I_{py}\dot{\theta}_0\Big]\end{aligned} \tag{G.1}$$

$$\begin{aligned}\Delta\ddot{\theta} = -\frac{1}{I_{p_0}}\Big[&\Delta I_p\ddot{\theta}_0 + 3n^2(I_{r_0} - I_{y_0})\Delta\theta + 3n^2(\Delta I_r - \Delta I_y)\theta_0 \\ &- \Delta I_{rp}(\ddot{\psi}_0 + 2n\dot{\varphi}_0 - n^2\psi_0) - I_{rp_0}\Delta\ddot{\psi} - 2nI_{rp_0}\Delta\dot{\varphi} + n^2 I_{rp_0}\Delta\psi \\ &+ \Delta I_{py}(-\ddot{\varphi}_0 + 2n\dot{\psi}_0 + n^2\varphi_0) - I_{py_0}\Delta\ddot{\varphi} + 2nI_{py}\Delta\psi + n^2 I_{py_0}\Delta\varphi\Big]\end{aligned} \tag{G.2}$$

$$\begin{aligned}\Delta\ddot{\varphi} = -\frac{1}{I_{y_0}}\Big[&\Delta I_y\ddot{\varphi}_0 - n(I_{y_0} + I_{r_0} - I_{p_0})\Delta\dot{\psi} - n(\Delta I_y + \Delta I_r - \Delta I_p)\dot{\psi}_0 \\ &+ n^2(I_{p_0} - I_{r_0})\Delta\varphi + n^2(\Delta I_p - \Delta I_r)\varphi_0 - I_{py_0}\Delta\ddot{\theta}_0 - \Delta I_{py}\ddot{\theta}_0 \\ &- I_{ry_0}\Delta\ddot{\psi} - \Delta I_{ry}\ddot{\psi}_0 + 2nI_{rp_0}\Delta\dot{\theta} + 2n\Delta I_{rp}\dot{\theta}_0 - n^2 I_{ry_0}\Delta\psi - n^2\Delta I_{ry}\psi_0\Big]\end{aligned} \tag{G.3}$$

Define a state vector, $\bar{x} = \begin{bmatrix}\Delta\psi & \Delta\theta & \Delta\varphi & \Delta\dot{\psi} & \Delta\dot{\theta} & \Delta\dot{\varphi}\end{bmatrix}^T$, and a control vector, $\bar{u} = \begin{bmatrix}\Delta I_r & \Delta I_p & \Delta I_y & \Delta I_{rp} & \Delta I_{py} & \Delta I_{ry}\end{bmatrix}^T$, then the linearized state space equation is found as:

$$\begin{bmatrix} \Delta\ddot{\psi} \\ \Delta\dot{\theta} \\ \Delta\dot{\varphi} \\ \Delta\ddot{\psi} \\ \Delta\ddot{\theta} \\ \Delta\ddot{\varphi} \end{bmatrix} = \begin{bmatrix} A_{11} & A_{12} \\ A_{21} & A_{22} \end{bmatrix} \begin{bmatrix} \Delta\psi \\ \Delta\theta \\ \Delta\varphi \\ \Delta\dot{\psi} \\ \Delta\dot{\theta} \\ \Delta\dot{\varphi} \end{bmatrix} + \begin{bmatrix} B_{11} & B_{12} \\ B_{21} & B_{22} \end{bmatrix} \begin{bmatrix} \Delta I_r \\ \Delta I_p \\ \Delta I_y \\ \Delta I_{rp} \\ \Delta I_{py} \\ \Delta I_{ry} \end{bmatrix} + \begin{bmatrix} C_{11} \\ C_{21} \end{bmatrix} \tag{G.4}$$

where

$$A_{11} = \begin{bmatrix} 0 & 0 & 0 \\ 0 & 0 & 0 \\ 0 & 0 & 0 \end{bmatrix}, \qquad A_{12} = \begin{bmatrix} 1 & 0 & 0 \\ 0 & 1 & 0 \\ 0 & 0 & 1 \end{bmatrix}$$

$$A_{21} = \begin{bmatrix} \dfrac{4n^2\left(I_{y_0} - I_{p_0}\right)}{I_{r_0}} & 0 & \dfrac{n^2 I_{ry_0}}{I_{r_0}} \\ -\dfrac{n^2 I_{rp_0} + 2nI_{py_0}}{I_{p_0}} & \dfrac{3n^2\left(I_{y_0} - I_{r_0}\right)}{I_{p_0}} & -\dfrac{n^2 I_{py_0}}{I_{p_0}} \\ \dfrac{n^2 I_{ry_0}}{I_{y_0}} & 0 & \dfrac{n^2\left(I_{r_0} - I_{p_0}\right)}{I_{y_0}} \end{bmatrix}$$

$$A_{22} = \begin{bmatrix} 0 & -2nI_{py_0} & \dfrac{n\left(I_{p_0} - I_{y_0} - I_{r_0}\right)}{I_{r_0}} \\ 0 & 0 & \dfrac{2nI_{rp_0}}{I_{p_0}} \\ \dfrac{n\left(I_{r_0} - I_{p_0} + I_{y_0}\right)}{I_{y_0}} & -\dfrac{2nI_{rp_0}}{I_{y_0}} & 0 \end{bmatrix}$$

$$B_{11} = \begin{bmatrix} 0 & 0 & 0 \\ 0 & 0 & 0 \\ 0 & 0 & 0 \end{bmatrix}, \qquad B_{12} = \begin{bmatrix} 0 & 0 & 0 \\ 0 & 0 & 0 \\ 0 & 0 & 0 \end{bmatrix}$$

$$B_{21} = \begin{bmatrix} -\dfrac{\ddot{\psi}_0 + n\dot{\varphi}_0}{I_{r_0}} & \dfrac{4n^2\psi_0 + n\dot{\varphi}_0}{I_{r_0}} & \dfrac{4n^2\psi_0 - n\dot{\varphi}_0}{I_{r_0}} \\ -\dfrac{3n^2\theta_0}{I_{p_0}} & -\dfrac{\ddot{\theta}_0}{I_{p_0}} & \dfrac{3n^2\theta_0}{I_{p_0}} \\ \dfrac{n\dot{\psi}_0 + n^2\varphi_0}{I_{y_0}} & -\dfrac{n\dot{\psi}_0 + n^2\varphi_0}{I_{y_0}} & -\dfrac{\ddot{\varphi}_0 - n\dot{\psi}_0}{I_{y_0}} \end{bmatrix}$$

$$B_{22} = \begin{bmatrix} -\dfrac{\ddot{\theta}_0}{I_{r_0}} & \dfrac{2n\dot{\theta}_0}{I_{r_0}} & \dfrac{\ddot{\varphi}_0 + n^2\varphi_0}{I_{r_0}} \\ \dfrac{\ddot{\psi}_0 + 2n\dot{\varphi}_0 - n^2\psi_0}{I_{p_0}} & \dfrac{\ddot{\varphi}_0 - 2n\dot{\psi}_0 - n^2\varphi_0}{I_{p_0}} & 0 \\ -\dfrac{2n\dot{\theta}_0}{I_{y_0}} & \dfrac{\ddot{\theta}_0}{I_{y_0}} & \dfrac{\ddot{\psi}_0 + n^2\psi_0}{I_{y_0}} \end{bmatrix}$$

$$C_{11} = \begin{bmatrix} 0 & 0 & 0 \\ 0 & 0 & 0 \\ 0 & 0 & 0 \end{bmatrix}$$

$$C_{21} = \begin{bmatrix} \dfrac{I_{rp_0}\Delta\ddot{\theta} + I_{ry_0}\Delta\ddot{\varphi}}{I_{r_0}} \\ \dfrac{I_{rp_0}\Delta\ddot{\psi} + I_{py_0}\Delta\ddot{\varphi}}{I_{p_0}} \\ \dfrac{I_{ry_0}\Delta\ddot{\psi} + I_{py_0}\Delta\ddot{\theta}}{I_{y_0}} \end{bmatrix}$$

Note that the products of inertia appear in Equation (G.4) since the body-fixed coordinate system is not assumed to align with the principal axes. If those two axes are aligned to avoid products of inertia term, Equation (G.4) becomes the state Equation (3.10).

Appendix H

Equations of Motion for the Masses Attached Satellite with Other Actuators

The dynamics of satellite motion is given by Euler as:

$$\dot{\bar{H}} = \left[\frac{d\bar{H}}{dt}\right]_{\mathbf{I}} = \left[\frac{d\bar{H}}{dt}\right]_{\mathbf{B}} + \bar{\omega} \times \bar{H} = \bar{M}_{\text{external}} \tag{H.1}$$

where $\left[\frac{d\bar{H}}{dt}\right]_{\mathbf{I}}$, $\left[\frac{d\bar{H}}{dt}\right]_{\mathbf{B}}$ are derivatives in the inertial coordinate system and the body-fixed coordinate system respectively and $\bar{\omega}$ is the angular velocity of the body-fixed coordinate system relative to the inertial coordinate system. M_{external} is the all external moment acting on the body about its mass center. The total angular momentum, $\bar{H}$, of the satellite and internal rotating members such as momentum or reaction wheels is

$$\bar{H} = I\bar{\omega} + \bar{h} \tag{H.2}$$

where I is the moment of inertia matrix of the system and $\bar{h}$ is the angular momentum induced from internal rotating members.

The inertial angular rate of the satellite in body-fixed coordinate system is given in Equation (2.27) as $\bar{\omega} = \begin{bmatrix} \dot{\psi} + n\varphi & \dot{\theta} + n & \dot{\varphi} - n\psi \end{bmatrix}^T$ with the initial value

$\bar{\omega}_0 = \begin{bmatrix} 0 & n & 0 \end{bmatrix}^T$ for a circular orbit where *n* is mean motion. Substituting Equation (H.2) into Equation (H.1) yields

$$I\dot{\bar{\omega}} + \bar{\omega} \times I\bar{\omega} + \bar{\omega} \times \bar{h} = \bar{M}_G + \bar{M}_d - \dot{\bar{h}} \tag{H.3}$$

where $\bar{M}_G$ is the gravity gradient moment and $\bar{M}_d$ is the other environmental moment.

Each term-by-term equations of Equation (H.3) are as follows.

$$\begin{aligned} I\dot{\bar{\omega}} &= \begin{bmatrix} I_{xx} & I_{xy} & I_{xz} \\ I_{xy} & I_{yy} & I_{yz} \\ I_{xz} & I_{yz} & I_{zz} \end{bmatrix} \begin{bmatrix} \ddot{\psi} + n\dot{\varphi} \\ \ddot{\theta} \\ \ddot{\varphi} - n\dot{\psi} \end{bmatrix} \\ &= \begin{bmatrix} I_{xx} & I_{xy} & I_{xz} \\ I_{xy} & I_{yy} & I_{yz} \\ I_{xz} & I_{yz} & I_{zz} \end{bmatrix} \begin{bmatrix} \ddot{\psi} \\ \ddot{\theta} \\ \ddot{\varphi} \end{bmatrix} + \begin{bmatrix} -nI_{xz} & 0 & nI_{xx} \\ -nI_{yz} & 0 & nI_{xy} \\ -nI_{zz} & 0 & nI_{xz} \end{bmatrix} \begin{bmatrix} \dot{\psi} \\ \dot{\theta} \\ \dot{\varphi} \end{bmatrix} \end{aligned} \tag{H.4}$$

The following assumptions for the elements of $\bar{\omega}$ can be made without loss of generality.

$$\begin{aligned} \omega_x^2 &\cong 0 & \omega_y^2 &\cong 2n\dot{\theta} + \omega_0^2 \\ \omega_z^2 &\cong 0 & \omega_x\omega_y &\cong n\dot{\psi} + \omega_0^2\varphi \\ \omega_x\omega_z &\cong 0 & \omega_y\omega_z &\cong n\dot{\varphi} - n^2\psi \end{aligned} \tag{H.5}$$

Then,

$$
\begin{aligned}
&\bar{\omega}\times I\bar{\omega} \\
&= \begin{bmatrix} \hat{i} & \hat{j} & \hat{k} \\ \dot{\psi}+n\varphi & \dot{\theta}+n & \dot{\varphi}-n\psi \\ I_{xx}\omega_x+I_{xy}\omega_y+I_{xz}\omega_z & I_{xy}\omega_x+I_{yy}\omega_y+I_{yz}\omega_z & I_{xz}\omega_x+I_{yz}\omega_y+I_{zz}\omega_z \end{bmatrix} \\
&= \begin{bmatrix} nI_{xz} & 2nI_{yz} & -n(I_{yy}-I_{zz}) \\ -nI_{yz} & 0 & nI_{xy} \\ -n(I_{xx}-I_{yy}) & -2nI_{xy} & -nI_{xz} \end{bmatrix} \begin{bmatrix} \dot{\psi} \\ \dot{\theta} \\ \dot{\varphi} \end{bmatrix} \\
&+ \begin{bmatrix} n^2(I_{yy}-I_{zz}) & 0 & n^2I_{xz} \\ -n^2I_{xy} & 0 & -n^2I_{yz} \\ n^2I_{xz} & 0 & -n^2(I_{xx}-I_{yy}) \end{bmatrix} \begin{bmatrix} \psi \\ \theta \\ \varphi \end{bmatrix} + \begin{bmatrix} n^2I_{yz} \\ 0 \\ -n^2I_{xy} \end{bmatrix}
\end{aligned}
\tag{H.6}
$$

and,

$$
\begin{aligned}
\bar{\omega}\times\bar{h} &= \begin{bmatrix} \hat{i} & \hat{j} & \hat{k} \\ \dot{\psi}+n\varphi & \dot{\theta}+n & \dot{\varphi}-n\psi \\ h_x & h_y & h_z \end{bmatrix} \\
&= \begin{bmatrix} 0 & h_z & -h_y \\ -h_z & 0 & h_x \\ h_y & -h_x & 0 \end{bmatrix} \begin{bmatrix} \dot{\psi} \\ \dot{\theta} \\ \dot{\varphi} \end{bmatrix} + \begin{bmatrix} nh_y & 0 & 0 \\ -nh_x & 0 & -nh_z \\ 0 & 0 & nh_y \end{bmatrix} \begin{bmatrix} \psi \\ \theta \\ \varphi \end{bmatrix} + \begin{bmatrix} nh_z \\ 0 \\ -nh_x \end{bmatrix}
\end{aligned}
\tag{H.7}
$$

On the right hand side, the gravity gradient torque is

$$
M_G = 3n^2 \begin{bmatrix} I_{zz}-I_{yy} & I_{xy} & 0 \\ I_{xy} & I_{zz}-I_{xx} & 0 \\ -I_{xz} & -I_{yz} & 0 \end{bmatrix} \begin{bmatrix} \psi \\ \theta \\ \varphi \end{bmatrix} + 3n^2 \begin{bmatrix} -I_{yz} \\ I_{xz} \\ 0 \end{bmatrix}
\tag{H.8}
$$

Finally, substituting into Equation (H.3) yields a state equation as:

$$\begin{bmatrix} \dot{\psi} \\ \dot{\theta} \\ \dot{\varphi} \\ \ddot{\psi} \\ \ddot{\theta} \\ \ddot{\varphi} \end{bmatrix} = \begin{bmatrix} 0 & A_{12} \\ I^{-1}A_{21} & I^{-1}A_{22} \end{bmatrix} \begin{bmatrix} \psi \\ \theta \\ \varphi \\ \dot{\psi} \\ \dot{\theta} \\ \dot{\varphi} \end{bmatrix} + \begin{bmatrix} 0 \\ I^{-1}(M - \dot{\bar{h}} + A_3) \end{bmatrix} \tag{H.9}$$

where

$$A_{12} = \begin{bmatrix} 1 & 0 & 0 \\ 0 & 1 & 0 \\ 0 & 0 & 1 \end{bmatrix}$$

$$A_{21} = \begin{bmatrix} -nh_y - 4n^2(I_{yy} - I_{zz}) & 3n^2 I_{xy} & -n^2 I_{xz} \\ -nh_x + 4n^2 I_{xy} & 3n^2(I_{zz} - I_{xx}) & nh_z + n^2 I_{yz} \\ -4n^2 I_{xz} & -3n^2 I_{yz} & -nh_y - n^2(I_{yy} - I_{xx}) \end{bmatrix}$$

$$A_{22} = \begin{bmatrix} 0 & -h_z - 2nI_{yz} & h_y - n(I_{xx} - I_{yy} + I_{zz}) \\ h_z + 2nI_{yz} & 0 & -h_x - 2nI_{xy} \\ -h_y + n(I_{xx} - I_{yy} + I_{zz}) & h_x + 2nI_{xy} & 0 \end{bmatrix}$$

$$A_3 = \begin{bmatrix} -nh_z - 4n^2 I_{yz} \\ 3n^2 I_{xz} \\ nh_x + n^2 I_{xy} \end{bmatrix}$$

VITA

Young Tae Ahn

Young Tae Ahn was born in Pusan, Republic of Korea, on February 16, 1974. He attended Yonsei University from 1993-1999 where he received his Bachelor of Science degree majoring in Mathematics and minoring in Astronomy and Atmospheric Sciences. He also joined the Korea Army for 18 months during his undergraduate years. He started his master's program in Aerospace Engineering at The Pennsylvania State University in 2000. Research topic for his master's thesis was the optimal reconfiguration of a formation flying constellation. After earning his master's degree, he started his doctoral program in Aeronautical and Astronautical Engineering (currently the department name has been changed to the Department of Aerospace Engineering) at the University of Illinois at Urbana-Champaign in 2002; however, he returned to The Pennsylvania State University in 2004. He continued his doctoral program in the same major where he received his master's degree. His work developed a new control concept for a satellite attitude control system. His research interests include orbital mechanics, dynamics, and control of satellite attitude especially for formation flying constellations and the application of dynamical systems and optimization method to spacecraft dynamics and control. After completing his Ph.D. in Aerospace Engineering, he will be working as a senior research engineer in wind power generation industry in the Republic of Korea.